Scholars' Mine

Doctoral Dissertations   Student Theses and Dissertations

1975

Application of laser holographic interferometry to the analysis of ground movement above underground openings

Duk-Won Park

Recommended Citation

APPLICATION OF LASER HOLOGRAPHIC INTERFEROMETRY

TO THE ANALYSIS OF GROUND MOVEMENT

ABOVE UNDERGROUND OPENINGS

by

DUK-WON PARK, 1945-

A DISSERTATION

Presented to the Faculty of the Graduate School of the

UNIVERSITY OF MISSOURI-ROLLA

In Partial Fulfillment of the Requirements for the Degree

DOCTOR OF PHILOSOPHY

in

GEOLOGICAL ENGINEERING

1975

David R Summers

Advisor

ABSTRACT

A laser holographic interferometric technique has been recently developed and applied to research in several engineering fields. The technique has many possible applications in earth science and engineering. In this study it was shown that laser holographic interferometry can be used to study surface ground movements resulting from subsurface cavity collapse.

One of the most important advantages of the holographic interferometric technique is a rapid three dimensional displacement measurement of a surface without contact or emplacement of instruments. The surface does not have to be flat or smooth allowing deflection contours to be generated on a granular surface. These advantages were applied in a study of model subsidence.

Subsidence is a serious environmental problem, and an important factor in designing underground coal mines. This is especially true as the mining method is changed from room and pillar mining to longwall mining as is currently occurring in the U.S.A.

Subsidence models were made to simulate ground movement due to mining operations. The models were monitored using holographic interferometry to record subsidence under a variety of conditions. Room and pillar mine models using water pressure simulation successfully simulated roof movement using both double exposure and real time holographic methods. Simple cavity models provided sufficient quantitative data to analyze the effects of cavity size, depth of the cavity, cavity orientation, surface structure and some geologic factors. Gelatin and sand were used as the model materials.

Sequential cavity development models were developed which provided consistent results of continuous subsidence development.

The investigation proved subsidence modelling techniques using laser holographic interferometry are practical. This method can be used for more complex subsidence studies to evaluate the influence of geometry, materials and time.

ACKNOWLEDGMENTS

The author wishes to express thanks to his major advisor Dr. David A. Summers for his valued advice and continued encouragement in the work leading to his dissertation and also for his assistance in the final working of the text.

Sincere appreciation and gratitude is extended to Dr. Nolan B. Aughenbaugh, Chairman of Mining, Petroleum and Geological Engineering Department, for his wisdom, advice and financial support throughout the graduate work.

The author also wishes to acknowledge the assistance of Dr. Ron L. Reisbig and Dr. Peter G. Hansen. They not only gave valuable advice but also contributed equipment and facilities for the research.

A special thanks is extended to Mr. Roy P. Barton, the department mechanic, who constructed the models and equipment.

Finally, great appreciation is extended to the author's wife, Sunny, whose love, partnership and patience accelerated the finish of the concluding part of the research.

TABLE OF CONTENTS

TABLE OF CONTENTS (cont.)

TABLE OF CONTENTS (cont.)

TABLE OF CONTENTS (cont.)

LIST OF ILLUSTRATIONS

LIST OF ILLUSTRATIONS (cont.)

LIST OF ILLUSTRATIONS (cont.)

LIST OF ILLUSTRATIONS (cont.)

LIST OF TABLES

I. INTRODUCTION

In recent years there has been an increase both in federal and public interest concerning the development of coal as a major American fuel resource. Present forecasts (1)* predict coal will be the major energy source until the turn of this century because of its abundance, economics and state of technology for competing sources of energy.

Although much attention currently is being given to the problems associated with strip mining, the vast majority of the North American coal reserves lie under sufficient depth of rock that underground mining techniques must be employed for their extraction. It is necessary to mine deeper and deeper as the mineral resources near the surface are mined out and surface mining becomes less popular. Greater development of the underground mining techniques can therefore be predicted. The problem is how to extract the greatest volume of mineral with minimum cost and minimum risk.

There are two ways in which underground coal seams may be mined. The first method, by far, the most popular in the U.S. is known as "room and pillar" mining. The second method is "longwall" mining, a technique little used in the U.S. but very popular in Europe.

At the present time, most of the coal that is mined underground in the U.S. is extracted by the room and pillar method of mining (Figure I.1).

In room and pillar operations, the mining machine, which is generally around 12 feet wide, drives a system of tunnels or entries

---

*Numbers in parenthesis refer to references in the bibliography.

forward into the coal. It does this by grinding off the coal from the free surface and loading it onto a conveyor belt or shuttle car for transport out of the mine (Figure I.1). After the tunnels have been advanced, the machine pulls back and drives interconnecting tunnels, known as crosscuts, between the entries. This operation isolates pillars, which are left to support the mine roof (Figure I.2). These pillars must continue to support the roof after the machine has moved on, because men and material must pass through the entries to the working areas, and coal must be carried back through them for transport to the surface. In some mines, these pillars are later extracted as the seam is worked out, but where this is not possible, up to 58 percent of the coal may be left as an unavailable asset (2).

The size of the pillars left between the entries and crosscuts is a function of coal strength and seam depth (3). With increasing seam depth, a greater percentage of the coal must be left in place to hold the increased weight of overlying roof rock. As the depth increases, it is advantageous to change to a method of mining referred to as longwall mining.

Longwall mining overcomes the roof stability problem in a different way. Two tunnels are initially driven some 400 to 600 feet apart and then connected at their furthest ends. Within this end connection, a set of supports is established. A mining machine then moves through the connection between the tunnels and peels off a slice of coal on the inner face (Figure I.3). This coal is loaded onto a conveyor belt that is located under the supports, and is carried to one of the side tunnels (entries) through which it is carried to the surface. As the
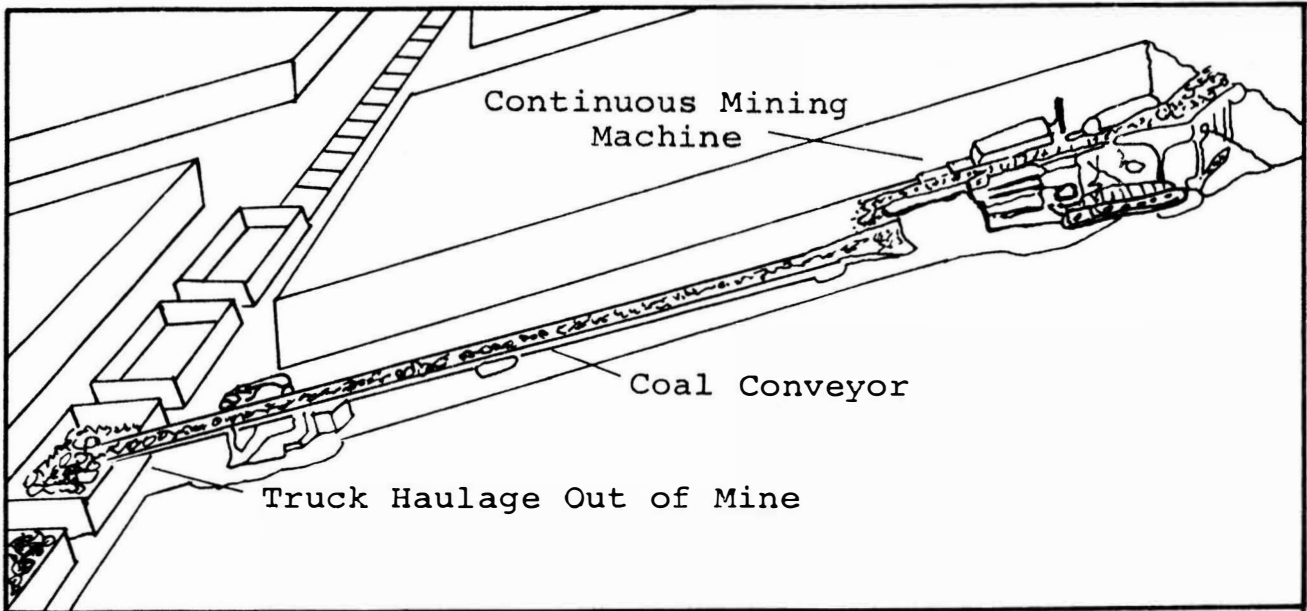
Figure I.1. Room and Pillar Mining Operation Using
a Continuous Miner (4).

A - Undercut Coal
B - Drill Holes for
    Explosives
C - Blast Coal Down
D - Load Out Coal
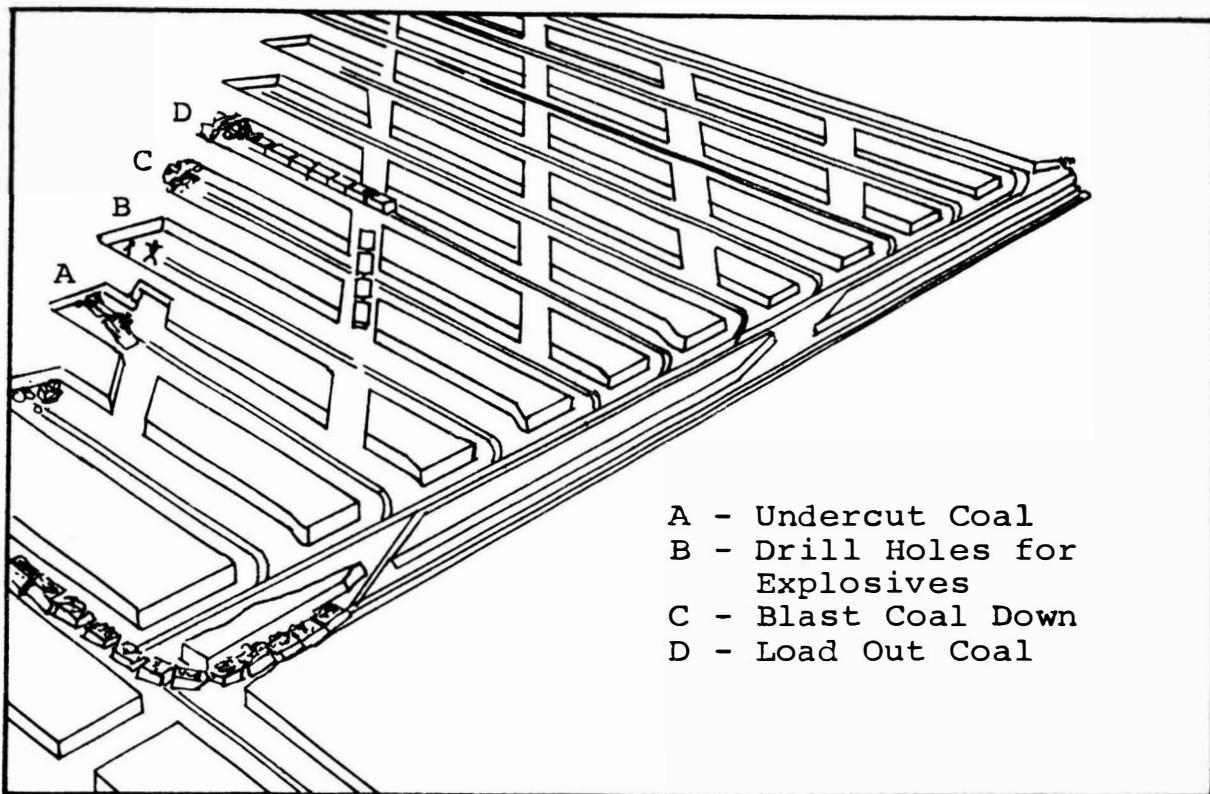
Figure I.2. Layout of a Room and Pillar Mine
Using Conventional Techniques (4).

Solid Coal

Mining
Machine

400 yards

Conveyor

Roof Bolted
Entry

Roof Bolted
Entry

Gob
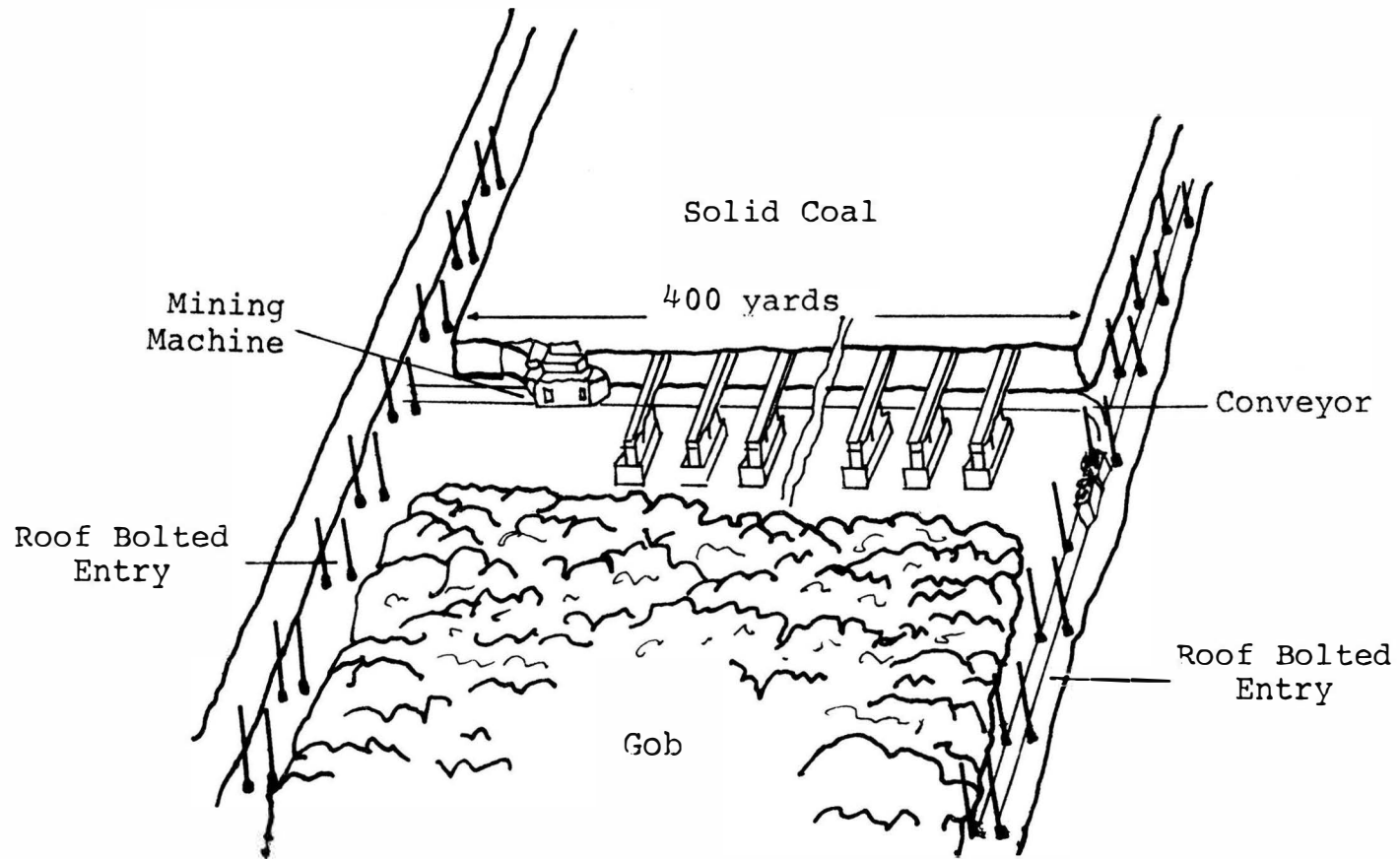
Figure I.3.   Simplified Equipment Layout for a Longwall Face (5).

coal is removed, the support system is moved forward into the space created in such a manner as to keep a ten-foot wide area of support open in front of the coal face. Behind the supports, the roof is allowed to collapse because access to the working face is maintained through the entries which lie ahead of the working face.

Longwall mining eliminates most of the danger from roof falls that kill or injure the miners and has the added advantages of allowing almost total recovery of the available coal. It has one drawback. The collapse of the mine roof behind the face eventually stopes to the surface and can damage any buildings which are located over the worked areas. Surface subsidence, however, is not confined to areas over longwall operations. Some eastern and midwestern U.S. cities (6) are located over abandoned room and pillar operations which have gradually deteriorated with time, with the result that subsidence is taking place 20 to 50 years after mining has ceased. The resulting subsidence is causing extensive damage to the buildings in the city.

Surface ground movement due to subsurface mining can be a major problem in the latter case. Subsidence due to underground mining has often been a serious problem in Europe where the longwall mining method is used. To reduce expense and to extract more coal, longwall mining is currently being introduced in the U.S. The ground control problem therefore is real, since subsidence can be a problem environmentally and possibly economically. Subsidence causes distortion of overlying structures and underground structures.

Very little of the subsidence phenomena in the U.S. has been studied until recently. The reason is that, since room and pillar

mining is the main method of mining, subsidence has not been that common in comparison with European countries. However, while European subsidence studies are well advanced, American conditions have proven different to the extent that European analysis do·not hold on this continent (7). For example the subsidence profile obtained from the Illinois coal mines (93) did not agree with those from the United Kingdom (88,92) and U.S.S.R. (89).

In the past, methods of analysis and model measurements of subsidence have been based mainly on the relative displacement of individual points on a model surface. In the study herein reported, a laser holographic interferometer is used to give a picture of total roof displacement over the surface subsidence area, generating displacement contour lines which allow a more accurate analysis of the total subsidence development. Holographic interferometry gives a three dimensional record from which it is possible to measure displacement over the area with an accuracy of several micro-inches. Sand was used as the modelling material. It was found that contour lines could be generated on the granular surface of the sand without any preparation. Data of the desired accuracy was achieved using models 8 by 8 inches square. Once the equipment was set up and the models fabricated more than ten subsidence holograms were taken in a day.

The main object of the study was to determine the applicability of holographic interferometry to model studies of subsidence, and to investigate subsidence phenomena above the underground opening under varying geometric conditions. Subsidence profiles have been constructed and controlling factors of subsidence analyzed. The factors considered

were the depth to the cavity, cavity geometry, cavity orientation, material strength, simple geologic factors and time.

It is intended that this study will assist engineers in understanding subsidence phenomena and in the application of the new technique to the field of rock and soil mechanics.

II. REVIEW OF LITERATURE

A comprehensive literature review has been undertaken, covering published articles in the fields of mine subsidence, mine model studies and the use of holographic interferometry, particularly, in the application to the rock mechanics area. Although some of the literature reviewed was not directly related to the project, nevertheless, it is included since it is considered relevant to future investigations.

A. Subsidence Due to Underground Openings

   1. Mechanism of Subsidence

      A proposed restricted definition for subsidence is "the lowering of the ground surface due to underground mining operations. The surface movements may be separated into two components, viz. 1) a vertical movement or subsidence and 2) a lateral horizontal movement (sometimes called 'draw') which is recorded in the form of tensional and compressive strain (8)."

      However, subsidence can be caused not only by the collapse of underground openings but also by groundwater withdrawal or by geotechnical forces generated by earthquakes and tectonic movements. The area of interest for this project is subsidence generated by failure over underground openings, especially coal mining operations.

      Subsidence can be divided into two categories, subsurface

subsidence and surface subsidence. Subsurface subsidence is a convergence of local failures in the rock surrounding the opening and surface subsidence is the depression created at ground level as a result of subsurface subsidence. The two categories are therefore interrelated.

The cause of subsidence is, obviously, the movement of adjacent material into the excavated cavity. There are theories which seek to explain the phenomena of strata movement (9,10).

a. Dome or Arch Theories

The first one is the pressure arch theory. The major factors which control development of a pressure arch are the sagging and separation of the beds immediately above an opening. As the superincumbent beds fail the span of failure is reduced (Figure II.1) so that ultimately, should the opening be deep enough, the bed is reached which has sufficient strength to stand. The load from this and overlying beds is transferred through the solid remnants of the underlying rock and adds to the major abutment pressures. This results in a stress concentration in the roof in the vicinity of the abutments or coal face and generates a dome shaped pressure arch above the opening. The relative movement within the broken material is opposed by shearing resistance along the zone of contact between the yielding and stationary masses. Since the shearing resistance tends to support failed rock it increases the pressure on the adjoining stationary part (11).

Support
Arch

Broken Rock

Support
Arch
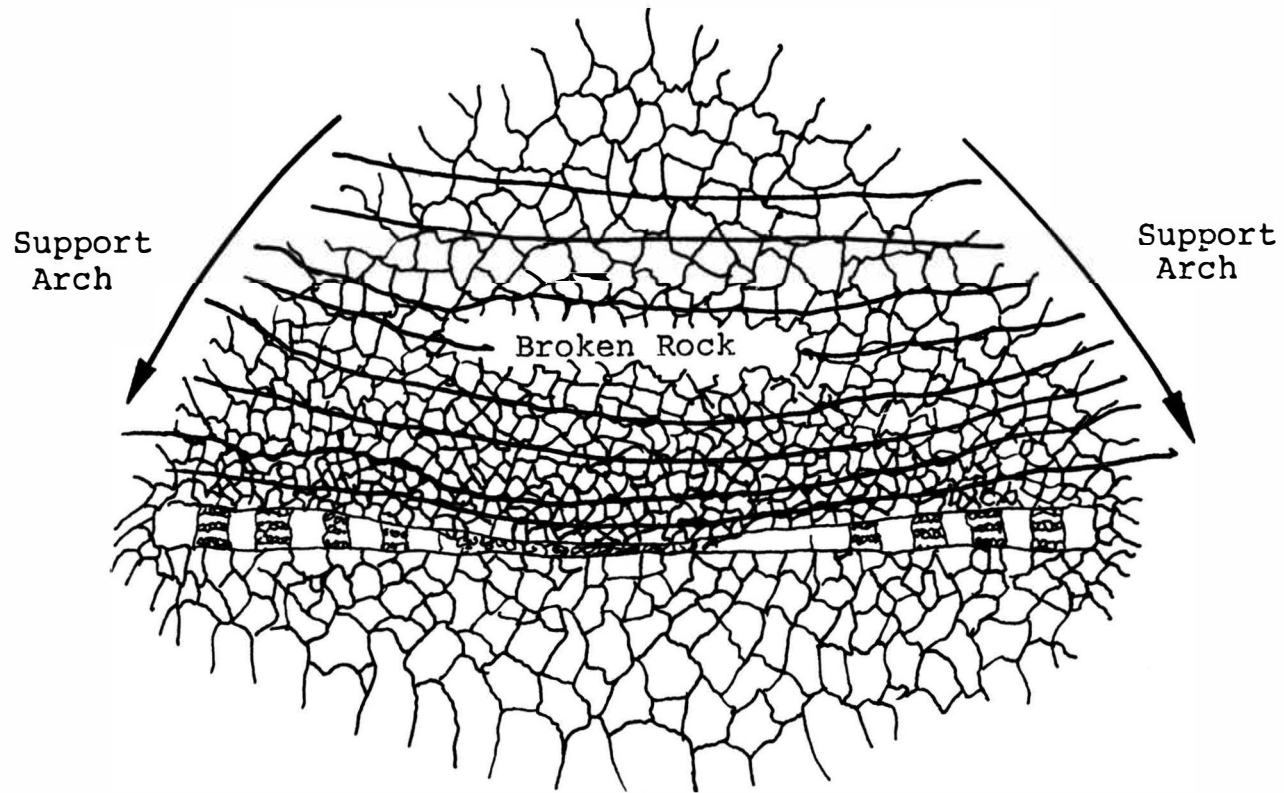
Figure II.1. Pressure Arch Dome.

As the broken rocks fall they increase in volume due to the creation of voids in the pile (called bulking) and this reduces the height of the cavity. The rock increase in volume to equal the volume of the cavity as the hole moves upward and roof falls will stop. When such failure reaches the surface, subsidence usually is at maximum much smaller than the cavity height. Kim (12) evaluated several theories on failure dome growth and the methods to define the limiting height of roof falls.

b. Trough Theories

Denkhaus (10) discussed the development of the trough theory of subsidence. A zone of influence is postulated, in which movement occurs and which spreads from the excavation to the surface, and this can be considered as a movement trough. This concept considers the ground to act as loose granular matter. In this case the internal friction angle of the ground is an important factor since it is used in describing the failure theories of granular materials. Denkhaus (10) covered the concept as follows;

When ground movement extends to the surface the vertically magnified subsidence profile usually forms the shape shown a vertical cross section (Figure III.2). The typical lateral strain on the ground surface is also shown.

It is assumed that the limit plane of influence, which the edge of ground movement by the opening, is straight (AB). The angle between the vertical line from the abut of the cavity and the limit plane of influence is called the angle of draw (θ).
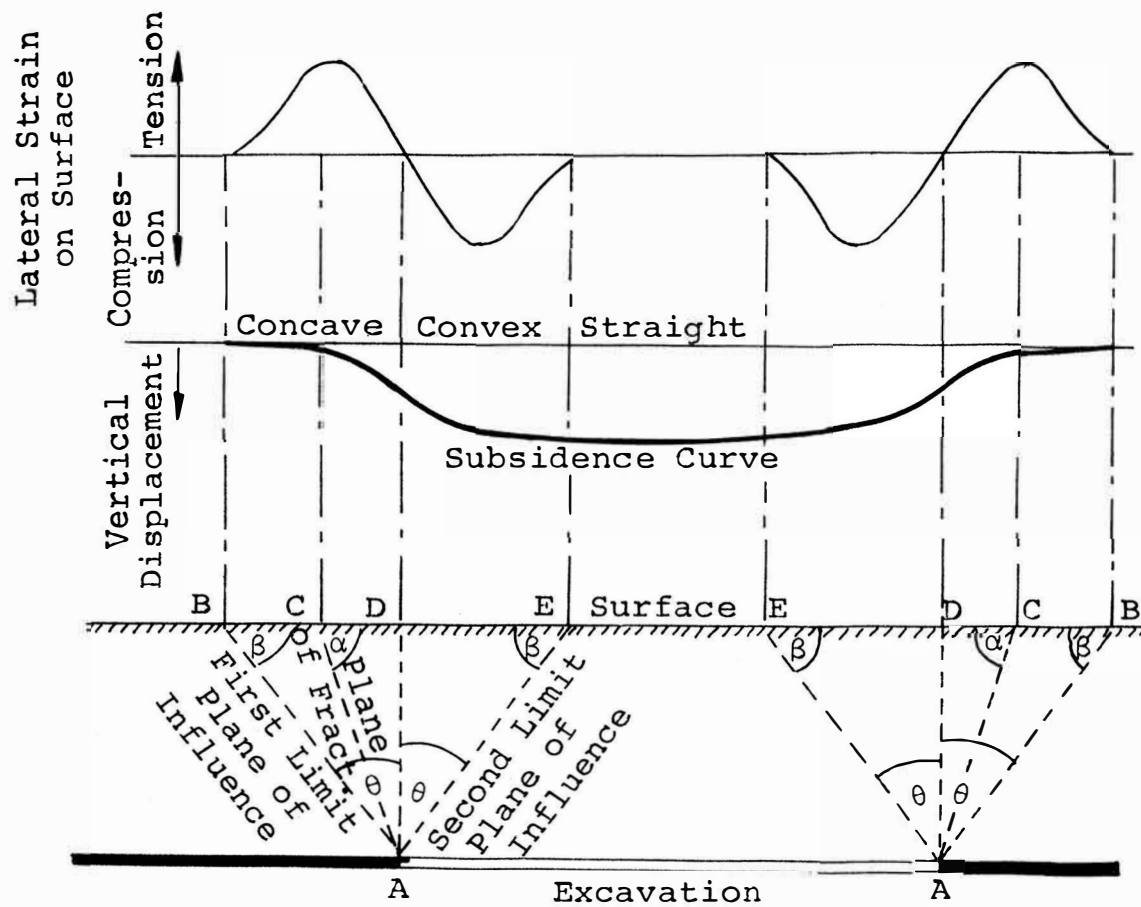
Figure II.2.   Subsidence Profile and Lateral
Strain Distribution (10).

From B to C the vertical displacement increases gradually and the lateral movement, which causes a tensile strain, also increases. At the point C the vertical displacement increases sharply and the lateral strain reaches its maximum and begins to decrease. It is assumed that this is due to downward sliding of the ground along CA, call the plane fracture, with a dip (α) called the angle of slide.

At point D vertically above the face A, the curvature of the subsidence line is assumed to change from concave to convex downward. The point is called the point of inflection.

There are three categories of subsidence trough. To explain them, line AE, which makes the same angle with the angle of draw from AD, is drawn. At the point E the subsidence has attained its maximum value. If EA planes on the opposite faces intersect below the ground surface, the stage is called subcritical (Figure II.3(a). The ground subsidence will increase with increasing opening span.

If the EA planes intersect at the ground surface, the critical subsidence has been reached and the maximum attainable subsidence occurs at this point (Figure II.3(b)). If the EA planes meet above the ground surface then there is supercritical subsidence and maximum subsidence is attained at more than one point (Figure II.3(c)).

These stages develop in the order subcritical, critical and supercritical according to the increase in the width/depth ratio of the cavity.

c. Continuum Theories

The dome theories and trough theories deal with the relative
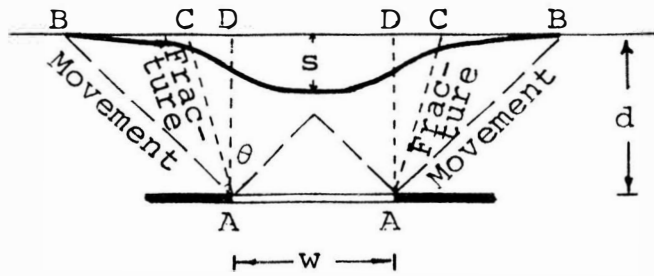
(a)
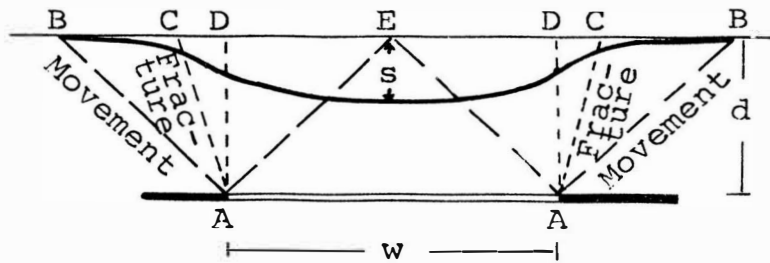
(b)
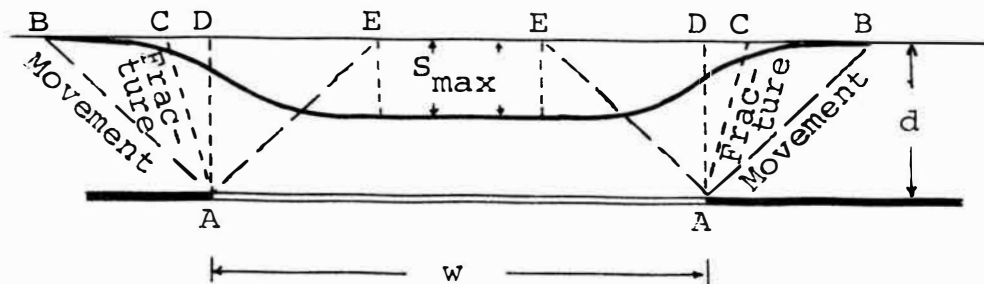
(c)

Figure II.3.   (a)   Subcritical Subsidence
                (b)   Critical Subsidence
                (c)   Supercritical Subsidence

movement and fracture patterns rather than with magnitude of the movement. The earth is considered as a continuous elastic body in continuum theories of subsidence phenomena. General elastic theories and finite element methods are typical analyzing methods.

In actuality there is no single theory which describes real strata movements around an underground cavity, but theories can be combined. Wiggil (13) suggested a theory combining dome theory and the trough theory as shown in Figure II.4. Near the cavity a fracture dome is formed and trough subsidence is developed above the dome.

2. Angle of Draw

The angle of draw in mine subsidence is an important parameter defining the area of subsidence. It is defined as the angle between the vertical line from the abutment and the limit point of the surface subsidence (the angle θ in Figure II.2). Singh, et al. (14) concluded that the angle of draw is based on movement of fractured rock mass, bending of beams or cantilevers, or in extreme cases, bending followed by flow of the rock mass.

Usually the subsidence area is larger than that of cavity (positive draw angle), but some cases report a negative draw angle (15,16). A theory is not established for a negative angle of draw.

Generally a draw angle 30-50° is common in the various coal-fields (14,17). The width/depth ratio of the opening has also been found to affect the angle of draw. As the width/depth value increases the angle of draw also increases to a value between 30°
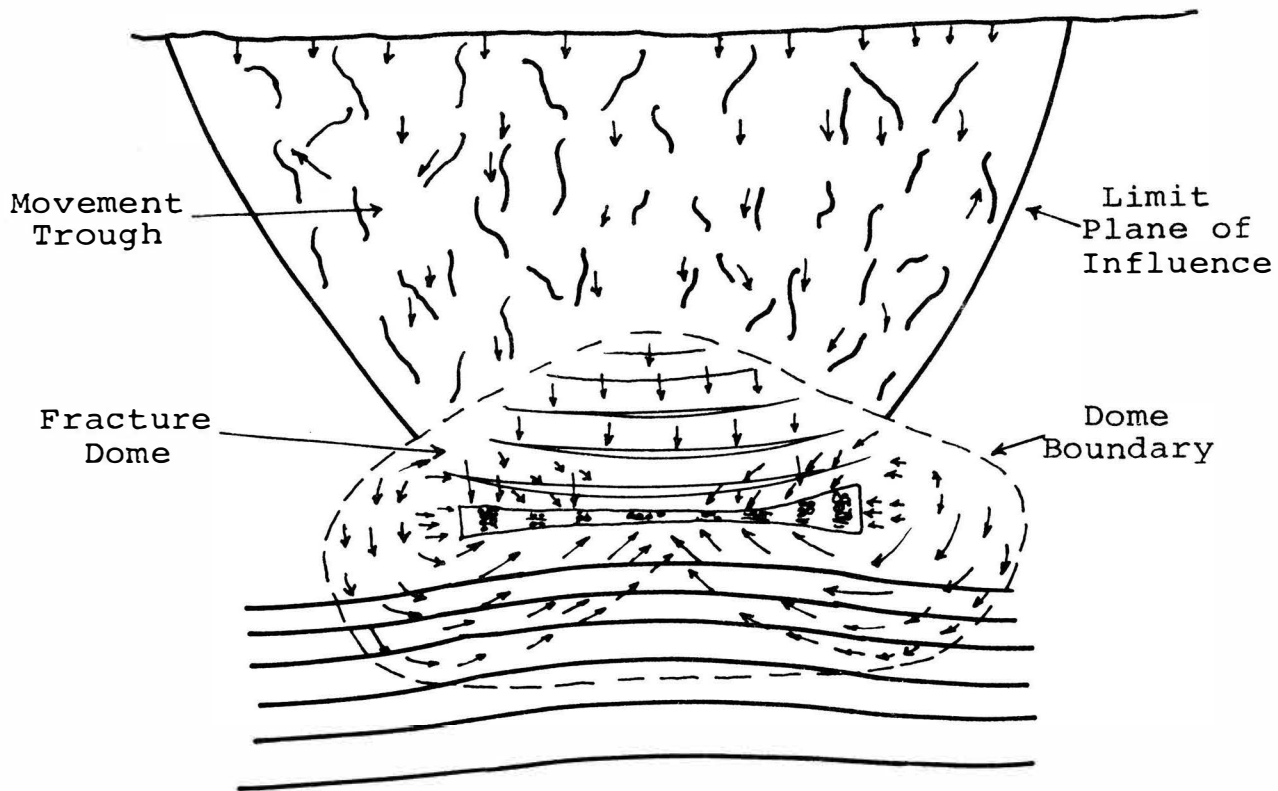
Figure II.4. Dome and Movement Trough (13).
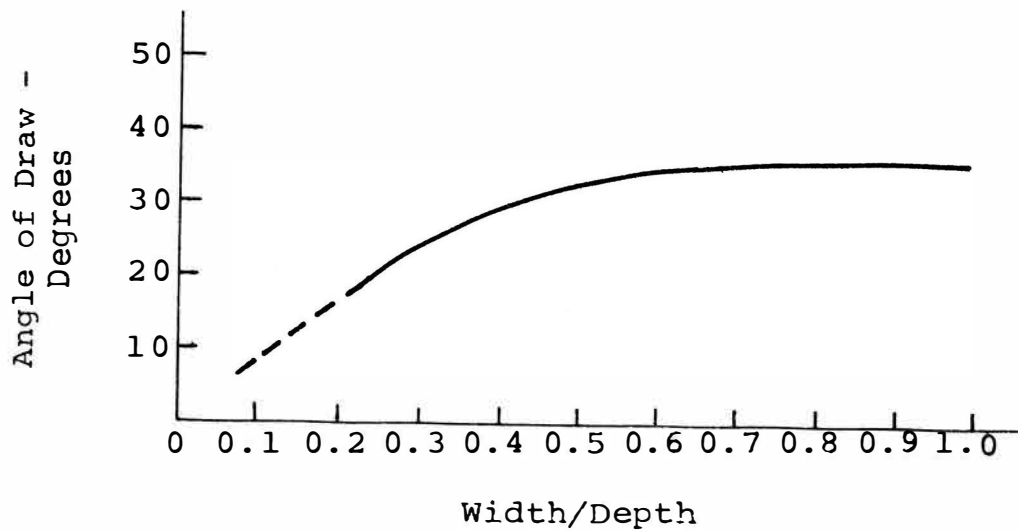
Figure II.5. Angle of Draw vs. Cavity Width/Depth (15).

and 40° (15), beyond which it stabilizes, shown in Figure II.5.

3. Subsidence - Cavity Width - Cavity Depth

As explained in the Section A-l-b, critical subsidence at a particular width/depth ratio of the cavity. Figure II.6 shows the development of subsidence by sequential cavity development. The critical width is the cavity width when maximum attainable subsidence is first developed.

A critical width can be approximately determined by projecting lines from the edges of the collapsed area inward at the angle of draw and when these two lines intersect the ground surface, the critical width has been attained (18). Thus the critical width (Wc) in nearly horizontally bedded stratigraphy is approximately,

$$Wc = 2D \tan \theta \qquad\qquad (II.1)$$

where D is the depth of the cavity,

θ is the angle of draw.

The National Coal Board's examination of subsidence activity produced empirical relationships between the maximum subsidence and the thickness, depth and width of a collapsed coal seam and the volume of subsidence (Figure II.7). In Figure II.7 maximum subsidence increase with cavity width. When an underground mine advances the working face maximum subsidence should increase for the same cavity height and depth.

The results of a study from the northern coalfield of England
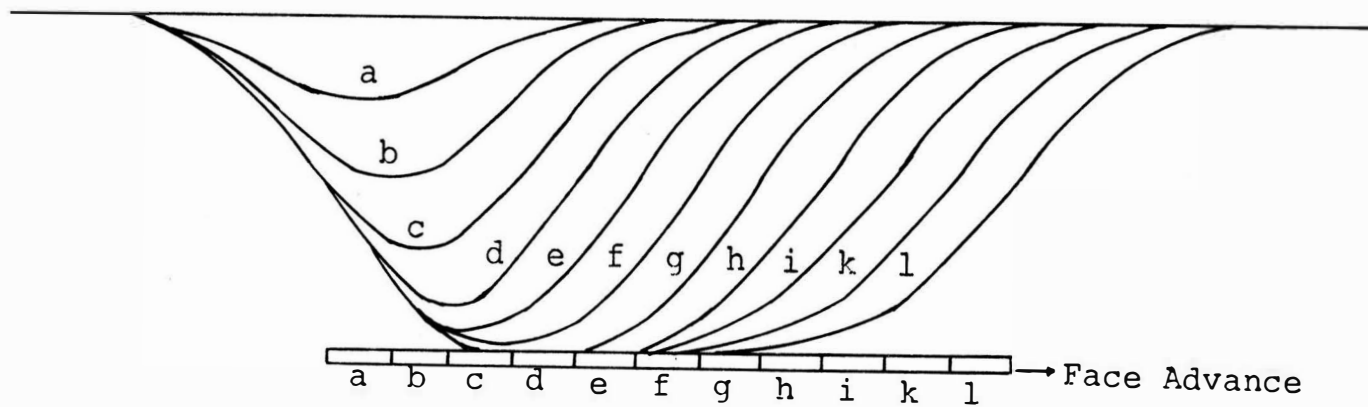
Figure II.6. Sequential Subsidence Development.
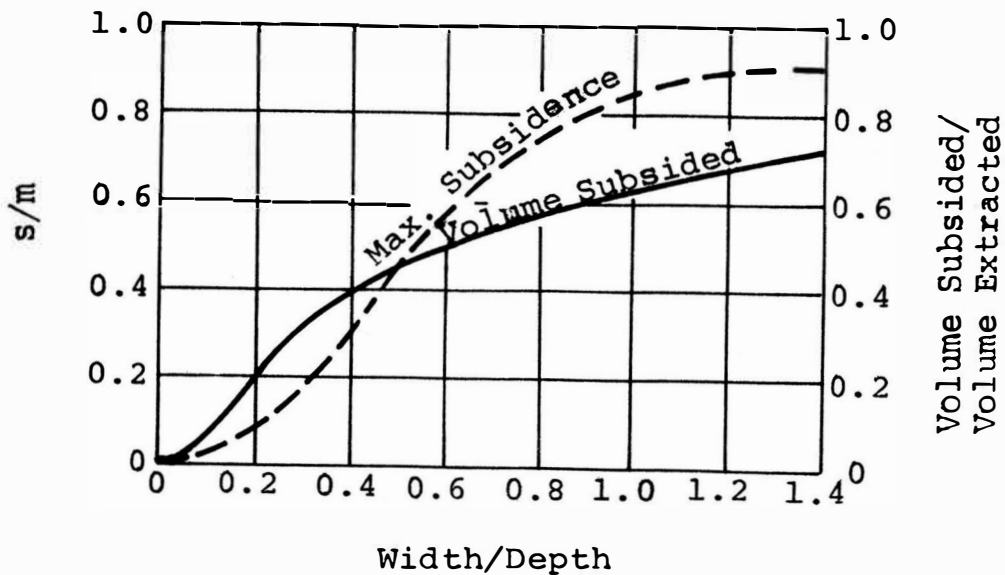
Figure II.7.   Cavity Width/Depth Ratio vs.
              Subsidence Factor (s/m) and Sub-
              sidence Volume/Extracted Volume (4).
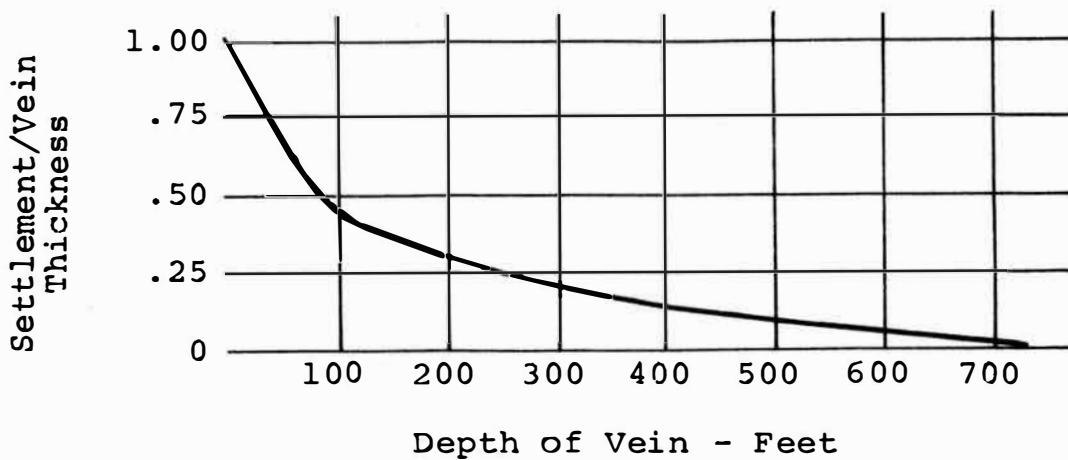
Figure II.8.   Depth of the Cavity vs. Sub-
              sidence Factor (s/m) (19).

were reported (18) Orchard, et al. (19) showed the relationship of subsidence (s/m) to width and depth (Figure II.8).

The typical relationship of subsidence to face advance vs. depth is shown in Figure II.9. Practical examples of sequential observations are discussed by Rellensman, et al. (20).

4. Time Dependent Subsidence Study

It is very important to know how long subsidence development takes from underground initiation until it develops at the surface and also the time taken for surface movement to cease.

When a longwall working face advances subsidence will increase until the critical subsidence is reached. After critical subsidence occurs the area affected by subsidence will continue to grow with the advance of the working face, but the maximum subsidence will remain constant.

The time taken by total ground movement to reach the surface is primarily dependent upon the depth and size of working. The other factors are the method of working, rate of face advance, nature of strata, degree of extraction, seam thickness and the presence of old workings and water, if any (21).

Duration of subsidence effects can be expressed as (22),

$$\text{Time of Travel (days)} = d (\tan \alpha_1 - \tan \alpha_2)/r \qquad \text{(II.2)}$$

where

d is the depth of the seam in ft.,

α_1 is the stationary angle of draw,
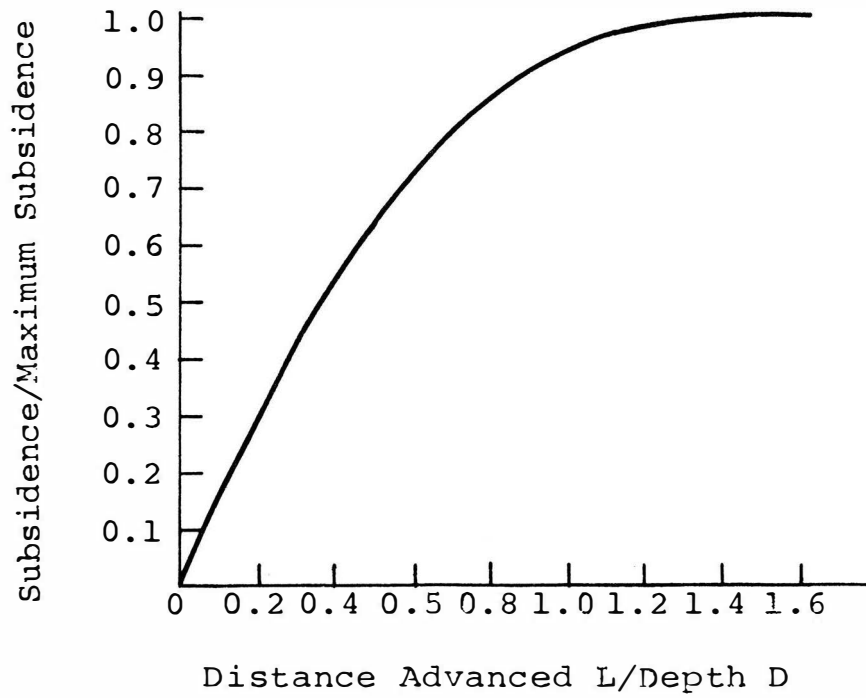
Figure II.9. Face Advance/Depth vs.
Subsidence/Maximum Subsidence (14).

α_2 is the travelling angle of draw,

r is the average rate of advance of the face in ft. per day.

From use of a similar equation, Wardell (23) concluded that for a given angle of draw, development of subsidence was a function of depth and rate of advance, being directly proportional to depth and inversely proportional to the rate of advance. Wardell gave the following expression for determination of the time factor,

$$t = 2d \tan \theta / s \tag{II.3}$$

where

t is the time of movement in weeks

d is the depth

s is the rate of face advance per week

θ is the angle of draw.

Terzaghi does not quantify the value for the time of subsidence but his value is given indirectly by Deere (24) as

$$t = RL^{-1} \tag{II.4}$$

where

L is the tunnel width

R is constant concerning with the character of rock (the values are defined in 24)

Examples of the relationship between time and subsidence in

Great Britain (22) and India (21) are shown in Figure II.10. The rate of subsidence increases with time to a maximum in the middle of the subsidence period and decreases toward the end of the period.

Whetton (22) concluded that aspect of time subsidence of room and pillar mines as it affects the post mining movements of the coal measure strata of Great Britain, would seem to be;

1) The depth of the workings

2) The area of the workings

3) The percentage extraction within the area extracted within the area worked, and arising from this, the dispersion of pillars of support (if any).

5. Subsidence Study Through Profile Functions

a. Horizontal Seams

There are two main methods for analysis of mine subsidence profiles. The first method is profile functions of surface subsidence measured from models (7,25) and field observations (15,21,26) and the second is the profile functions from superposition method (23,27) which uses influence functions (17).

In the most cases, a subsidence profile is calculated relative to maximum possible subsidence based on the following equation,

$$s = K_x S_{max} \qquad \text{(II.5)}$$

where
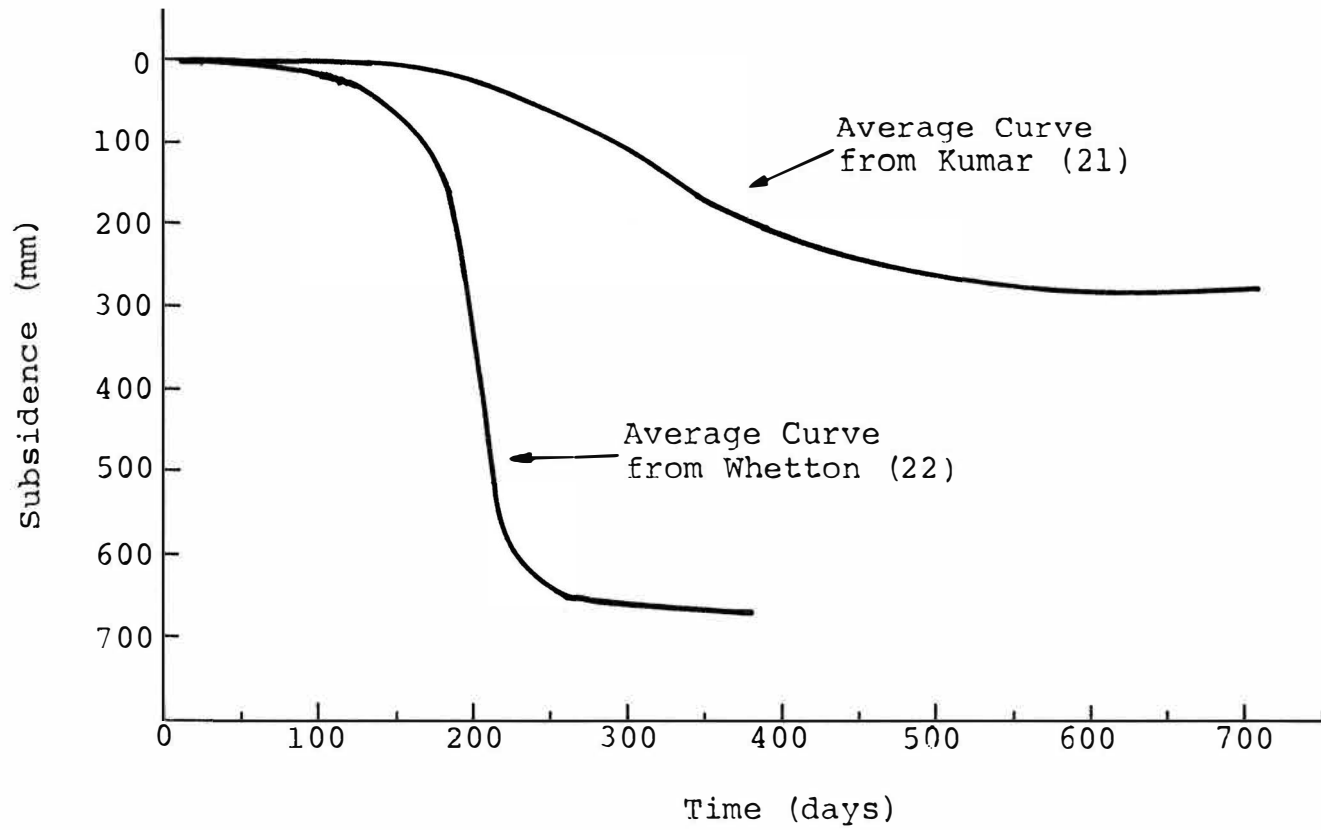
Figure II.10. Subsidence Development vs. Time.

s is subsidence

K_x is coefficient at x in Figure II.11

S_{max} is maximum subsidence

i. Profile Functions

Hyperbolic functions have been suggested based on model and theoretical investigations (17,28) expressed by

$$s = \frac{1}{2} S_{max} \left\{ 1 - \tanh\left(\frac{2x}{B}\right) \right\} \qquad (II.6)$$

where

s is subsidence at the position of x

S_{max} is maximum subsidence

B is half of the subsidence width (see Figure II.11)

Hoffman (29) suggested a trigonometric equation obtained from model investigation expressed by

$$s = S_{max} \sin^2\left\{ \frac{\pi}{4}\left(\frac{x}{B} - 1\right) \right\} \qquad (II.7)$$

These equations were derived from measurements of the vertical surface displacement profile of dimensional models. In the past two dimensional models have generally been used because considerable difficulty and expense is required to make a three dimensional model suitable for analysis. Sand, gelatin, granulated glass, granulated metal and plastic layers are the usual material for models. But, generally, the material properties have not been considered in subsidence studies.
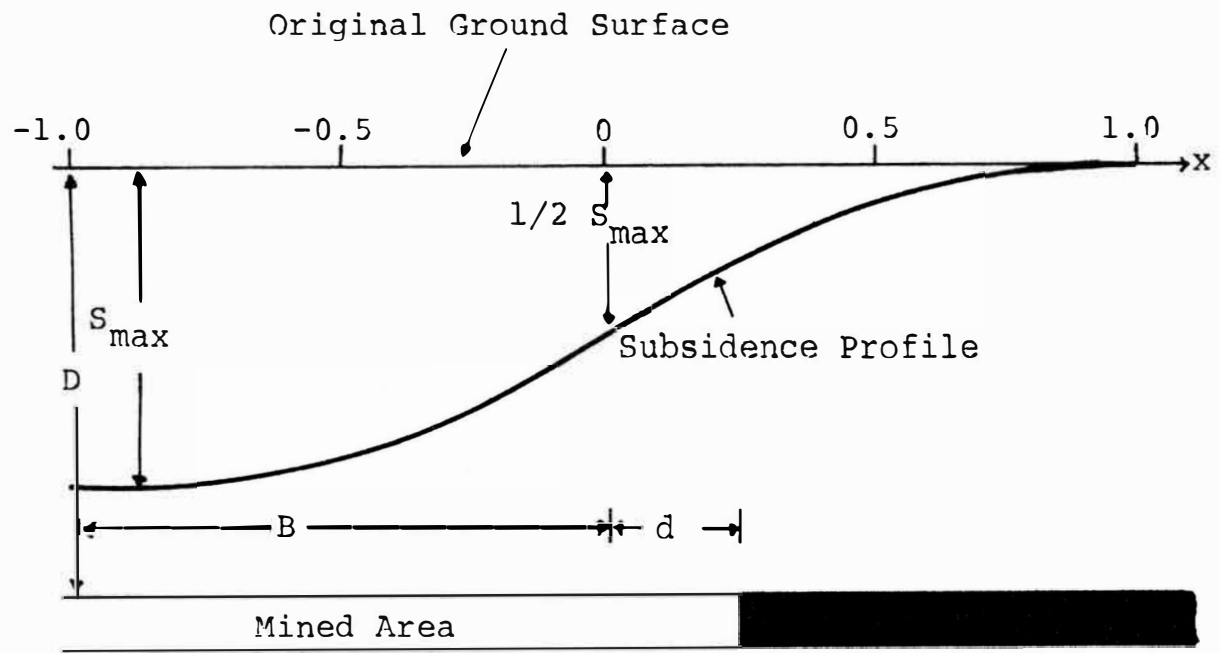
Figure II.11.   Subsidence Profile.

A model equation for two dimensional profiles based on the field observation in Donet coalfield (22,23) has been defined as

$$s = S_{max} \sqrt{n_1 n_2} \left\{ n^2 (1 - x + \frac{\sin 2x}{2}) + \frac{1 - n^2}{4} (1 + \cos x)^2 \right\} \qquad (II.8)$$

where $\qquad n_1 = 0.9 \frac{w_1}{h}, \; n_2 = 0.9 \frac{x_2}{h}, \; n = n_1,$

w_1 is the cavity width parallel to the subsidence
   profile plane

w_2 is the cavity width perpendicular to the subsidence
   profile plane

Equation II.8 applies when $n > 1/3$. In case of $n < 1/3$, it is replaced by the uniform expression

$$s = \frac{1}{4} S_{max} (1 + \cos \pi x_o)^2 \qquad (II.9)$$

Kumar and Singh (21) used a simpler form of profile equation obtained based on data from the Indian coalfields (Refer to Figure VI.16)

$$s = S_{max} (1 - \frac{x^2}{r^2}) \qquad (II.10)$$

Another expression from the field observation of British coalfield (15) is

$$s = S_{max} \exp(- \frac{x^{2n}}{b - cx^2}) \qquad (II.11)$$

where

b,c are constant

n is l or 2

b, c and n values are not set for different conditions.

Schmidt (30) suggested an equation, which is similar to the Gaussian error function, to describe the slope of subsidence trough due to a circular shaped tunnel opening as follows,

$$s = S_{max} \exp(-x^2/2B^2) \qquad (II.12)$$

In Figure II.12 a complete critical profile s_1 would occur if there is no ribside at A_2 and if A_1 were the edge of a semi-infinite extraction area. Reestablishing the seam with its other edge at A_2 would create an inverse critical profile s_2. According to the principle of superposition (17,23,27), the difference $s_1 - s_2$ would remain as the profile resulting from the subcritical area between A_1 and A_2.

From the Equation II.6

$$s_1 = \frac{1}{2} S_{max}(1 - \tanh \frac{2x}{B}) \qquad (II.13)$$

$$s_2 = \frac{1}{2} S_{max}(1 - \tanh \frac{2x + W}{B}) \qquad (II.14)$$

so,

$$s = s_1 - s_2 = \frac{1}{2} S_{max}(\tanh \frac{2x + W}{B} - \tanh \frac{2x}{B}) \qquad (II.15)$$

Borecki and Chudek (31) introduced several subsidence profile
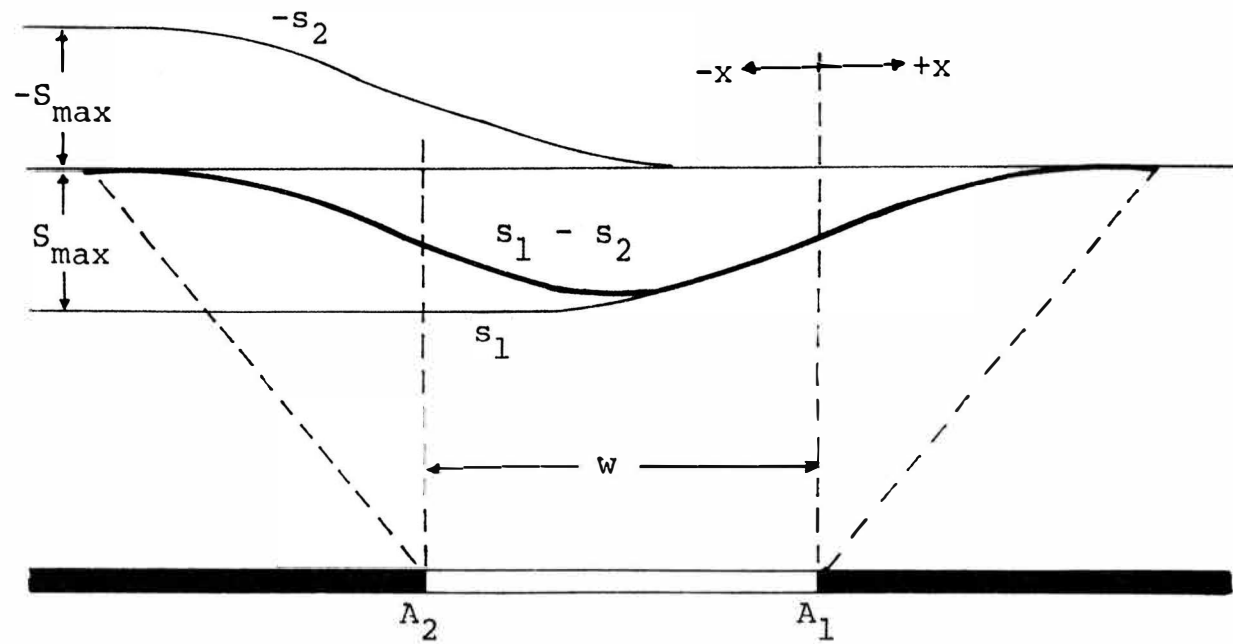
Figure II.12. Superposition of Two Critical Profiles (17).

functions as follows;

The first one is assumed that subsidence profile curve can be expressed as Gaussian Curve from the Error Function,

$$s = S_{max} \exp(-\pi x^2/r^2) \tag{II.16}$$

where

r is subsidence width

The second equation is derived from the Theory of Salustowicz. He derived the profile equation based on Winklera's medium theory, which is a beam deflection theory with part of the beam located on an elastic body. The equation is derived from the solution of the momentum equation,

$$EJ \frac{d^2 w'}{dx^2} = -M \tag{II.17}$$

where

M is the bending moment in vertical cross section

w' is the subsidence of the overburden in vertical cross section

J is the moment of inertia

E' is E (Young's modulus)/$(1 - \nu^2)$

The solution is made

when $x \geqq 0$

$$s = S_{max} - \frac{1}{2} S_{max} \exp(-\sqrt{\pi}\ x'/r)\cos \frac{\sqrt{\pi}}{r} x' \qquad (II.18)$$

when $x \leqq 0$

$$s = \frac{1}{2} S_{max} \exp(\sqrt{\pi}\ x'/r)\cos \frac{\sqrt{\pi}}{r} x' \qquad (II.19)$$

where

   x' is the horizontal distance from the maximum slope

      of the profile curve

The third equation is derived from the Theory of Awierszyna based on average field measurements taken in Russian coalfields,

$$s = S_{max}(1 - \frac{x}{2.13 \cdot 1})^{4.54}\ e^{2.13\ x/\ell} \qquad (II.20)$$

where

   ℓ is horizontal distance between the center and the

      point of maximum slope

ii. Profile Functions from Superposition Method

A subsidence trough can be assumed to be constructed from a series of infinitesimal trough which are produced by individual small extraction elements of area dA. P can be expressed in terms of its magnitude of influence r, which is the horizontal distance between point P and element dA. There are several

equations expressed for P (17). S_{max} is expressed by P(r) as

$$S_{max} = 2\pi \int_0^B r \, P(r) \, dr \qquad (II.21)$$

And infinitesimal subsidence P dA of the surface point P at the horizontal distance r makes the relationship

$$s = \iint_A P(r) \, dA \qquad (II.22)$$

The resultant formula by Brauner (17) is

$$s = \frac{S_{max}}{\pi} \left\{ \frac{\pi}{12} - \frac{x}{15} \sqrt{1 - x^2} \, (8x^4 - 26x^2 + 33) - \arcsin x \right\}$$

$$(II.23)$$

Knothe's and Bal's methods are based on similar influence functions, while Zenc (29) introduced the methods and the differences between them, and calculated values for K_s.

b. Inclined Seams

Opening an inclined seam will create an unsymmetrical subsidence trough profile. With increasing inclination of the beds the limit angle to the rise increases and the limit angle of the dip decreases the area to the dip therefore increases and the area to the rise decreases.

The subsidence profile based on equation II.11 was used for an example (17), from which Marr (15) introduced the equation,

$$s = S_{max} \exp\left(- \frac{x^{2n}}{b + cx^{2n}}\right) \qquad \text{(II.24)}$$

where

x is distance from the position of maximum subsidence

b and c are constants

n is 1 or 2

For inclined seams the angle of draw on the rise side and that on the dip side can be calculated by the following equations (14)

1) O'Donohue's Formula;

This is on the basis of 8° angle of draw for horizontal strata.

$$\theta_d = a + (1/3)d \qquad \text{(II.25)}$$

$$\theta_r = a - (1/3)d \qquad \text{(II.26)}$$

where

θ_r and θ_d are the angle of draw on rise and dip side, respectively

a is the angle of draw in horizontal bed

b is the inclination of seam

2) Statham's Formula;

$$\theta_r = a + ((24 - a)/24 \cdot d) \qquad (II.27)$$

$$\theta_d = a - (a/24 \cdot d) \qquad (II.28)$$

3) Luise's Formula;

$$\theta_r = 10 - 40 \tan(a - 5) \qquad (II.29)$$

$$\theta_d = 10 - 20 \tan(a - 5) \qquad (II.30)$$

Luise's formula is applicable to the coal measure strata
of inclination more than 30°.

The angles of draw of inclined coal seams of the various
British coalfields are plotted in Figure II.13.

B. Holographic Interferometry and Its Applications

There are many applications of laser holography in engineering.
This literature review stressed the possible applications of
holographic interferometry to the earth science area.

1. Laser Holography

Gabor (32) first demonstrated the feasibility of the
holographic method in 1948 using white light to devise a three
dimensional object recording method. In 1963 Leith and Upatnieks
(33) found that a laser was capable of producing very intense
monochromatic coherent radiation in regions of the spectrum that
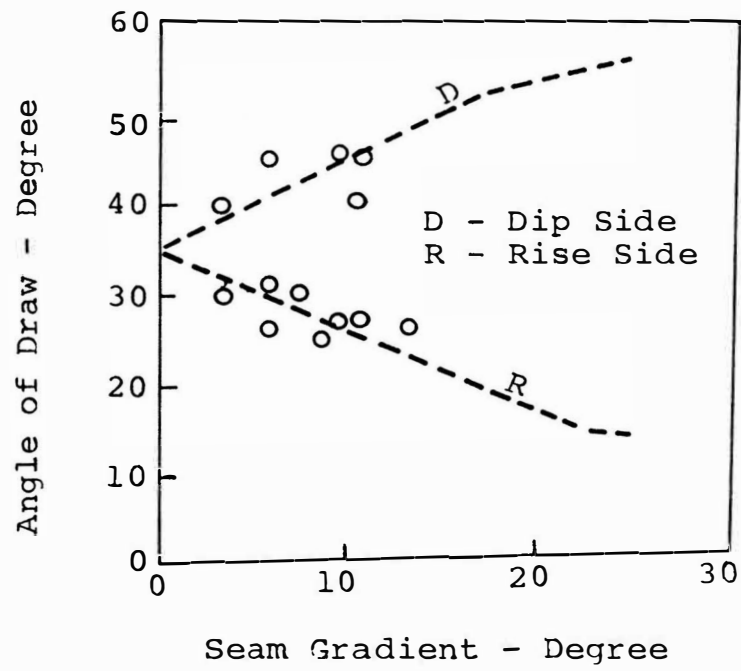
Figure II.13.   Seam Gradient vs. Angle of Draw (14).

can be recorded photographically. (Laser is an acronym for light
amplification by stimulated emission of radiation.) Lasers
generate energy by use of the electrons bound to an atom rather
than by use of the free electrons created from a heated cathode.
Atoms are excited by the additional pumping of radiation raising
the energy level. When the level drops there is an emission of
electrons. There are two different kinds of laser, continuous
laser and pulsed laser. Most of the gas lasers (He-Ne, Cd, CO_2,
etc.) generate continuous laser light, while ruby lasers generate
pulsed laser emission with a duration of several nanoseconds.

Holography has been rapidly developed due to the improved
quality of the image and simplification of technique allowed by
use of the laser. There has been great deal of interest generated
in the last few years in the application of holography to the
field of engineering.

A hologram is the photographic record of the interference
pattern formed at the photographic plate when two sets of
coherent light (laser) waves interfere. When this photographic
record is developed, and illuminated with the laser light
reference beam, the original scene is represented to the viewer
as a reconstructed image. A theory of wave front reconstruction
was described by Meyer-Arendt (34).

Use of the holographic method allows measurements of surface
strain, the sum of the principal stresses of photoelastic
material, surface roughness, and thermal distribution without
physical contact with the specimen, and flaws can also be detected

by means of interferometric methods.

2. Holographic Interferometry

Holographic interferometry is concerned with the formation and interpretation of the fringe patterns which appear when a wave, generated at some earlier time and stored in a hologram, is later reconstructed and caused to interfere with a comparison wave. There are several interferometric methods, namely, double exposure, real time and time average.

The double exposure method entails making two exposures of the subject on the holographic plate. The first exposure records the initial or base condition of the surface and the second exposure records the disturbed condition. The two images interfere and produce fringes visible when the holographic plate is developed and illuminated by the reference beam of expanded laser light. Disturbed condition here means displacement of the illuminated surface and the change of refractive indices through the path of the object beam.

Real time holograms are made by taking one exposure of the original specimen condition. The hologram plate is developed while clamped in its original position. When the distorted specimen is viewed through the holographic plate the displacement fringes will be seen. A double exposure hologram shows only one fringe system set, but a real time hologram can show a series of changing fringe systems. However, a permanent record of fringe patterns for real time holograms must be obtained using

conventional photographic techniques. Real time holograms are
more difficult to make, but are more economical and yield better
data for time dependent changing fringe systems (35).

Time average holographic interferometry is the method for
forming a time average hologram of a vibrating surface.
Illumination of the hologram yields an image of the surface on
which is superimposed a number of observable interference fringes.
The contour fringes are contour lines of equal displacement of
the vibrating surface. By this method vibration analysis can be
conducted (36).

3. Displacement Measurement

Wilson, et al (37) have shown that a deflection of the subject
surface sufficient to generate a fringe can be calculated from the
relationship shown in Figure II.14. The unit vector acting in
the direction of light receiving is $\hat{i}$, and that in the direction
of reflecting light is $\hat{r}$. Should the point (P) at which the beam
is reflected move to the location P' then a phase change will
occur in the beam at the receiver. This change ($\Delta\phi$) is given by

$$\Delta\phi = \frac{2\pi}{\lambda} d(\hat{i} + \hat{r}) \tag{II.31}$$

where

λ is the wave length (6328 nano-meters for He-Ne laser),

d is the amount of displacement
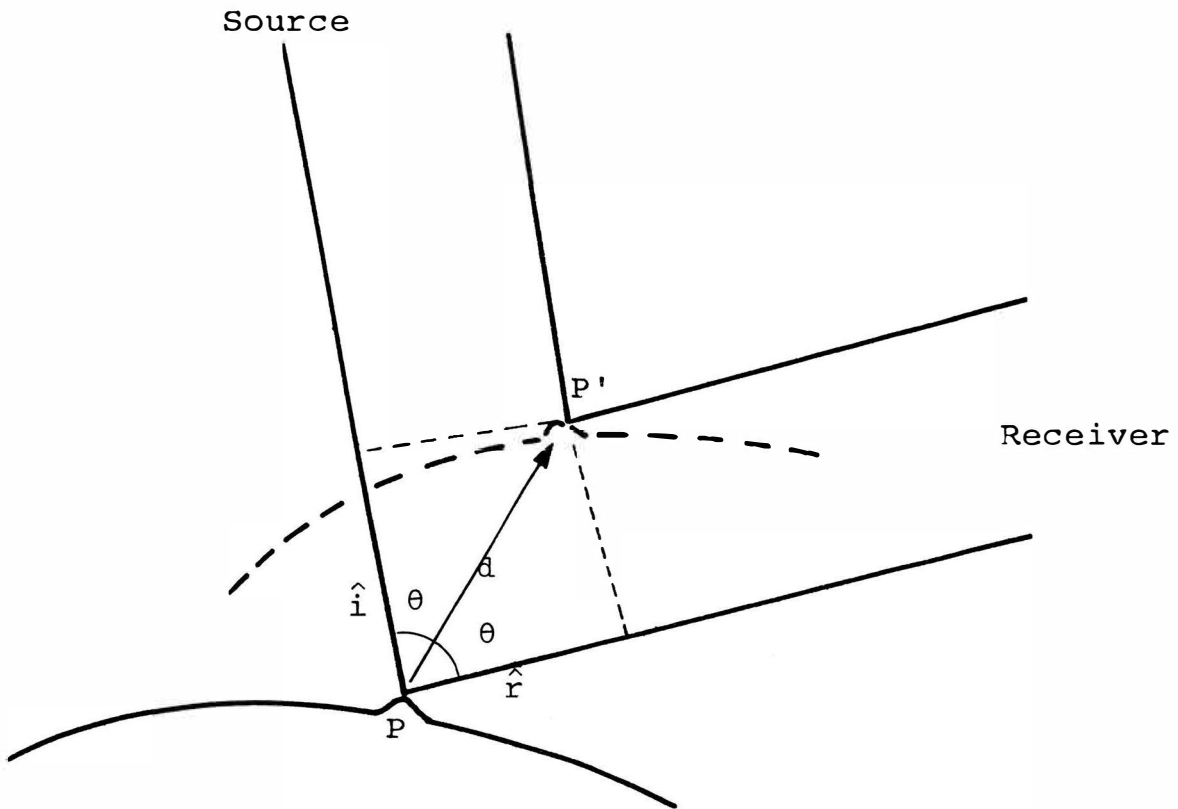
Figure II.14.   The Path of the Laser Light on
                the Displaced Surfaces.

When the phase change is from one fringe to a second ($\Delta\phi = 2\pi$) then

$$d = \frac{\lambda}{(\hat{i} + \hat{r})} = \frac{\lambda}{2 \cos \theta} \qquad (II.32)$$

where

θ is the incident angle of the laser light beam on the model.

Wilson, et al. (37) measured deflection of a uniformly loaded semi-clamped rectangular plate supported by struts using the double exposure method. Sampson (38) explained the general theories of holographic interferometry and fringe interpretation, and measured deflection of a cantilever beam and a uniformly pressurized plate. Dudderar (39) has applied the deflection measurement method to measure the deflection around the crack tip of a forked specimen under tensile loading with consequent crack opening.

Burchett and Irwin (40) have detected radial displacement of internally pressurized hollow cylinders. Microscopic radial deflections of cylinders under small expansive loads predict at the points of strain anomalies the location of the final fractures when the cylinders are later tested to construction. This method of analysis of radial displacement can be also used for measuring thermal expansion cylindrical samples.

Yamaguchi, et al. (41) introduced the method of measuring Poisson's ratio from the measurement of deflection on a

rectangular plate.

Aprahamian,et al.(42) used the pulsed laser double exposure method for recording a transverse wave propagating down a long beam. Because of the short exposure time of a pulsed laser, dynamic movement of the specimen could be detected.

4. Photoelastic Holography

Several papers (37-40) have discussed the combination of photoelasticity and holography. On the image of the hologram, there are two families of fringe patterns. One family represents the isochromatic fringe pattern normally associated with photoelasticity which yields the difference between the principal stresses. The other family represents the isopachic fringe pattern associated with interferometry which yields the sum of the principal stresses. From these complementary patterns, the magnitudes of the principal stresses can readily be determined throughout the field of observation. Unfortunately, these fringe patterns are not completely independent but interact in such a way as to make interpretation difficult in critical regions of the model.

Holloway (45) obtained single- and double-exposure photoelastic holograms of stress waves using a pulsed ruby laser. The clarity of the reconstructed images is comparable with photographs taken using a standard polariscope. Nishida,et al. (47) gave an analytical interpretation of the relation between the stress-strain state of a transparent elastic plate and the

light intensity of the plate observed through a Mach-Zender interferometer.

As mentioned before, the two sets of fringe systems, isochromatic fringes and isopachic fringes, are not independent. O'Regan,et al.(43) developed a new system which readily permits simultaneous acquisition of these fringe patterns without their undesirable material interactions as well as providing increased sensitivity. The new interferometer uses a double-pass object beam and an optical rotator to eliminate the isochromatic fringe pattern and effect from the isopachic interferogram.

Hovanesian,et al.(48) developed a simple method to determine the isopachic- and isochromatic-stress fringe material values using a calibration method. The application of interferometry together with a photoelastic coating method was suggested. In this case, the hologram apparatus is simply rearranged so that the object beam can be reflected from the coating-prototype interface and directed to the hologram plates.

5. Acoustical Holography

Apart from laser holography, there are other types of holography ranging from X-ray to far infrared and the microwave region. By means of acoustical waves acoustical holograms can be produced.

Acoustical holography is a technique of imaging that records the pattern formed by the interference of two sets of sound waves. One set of waves (often the ultrasonic reference wave)

is characterized by a simple acoustic wave front of one frequency. The other wave (object wave) passes through the object and interacts with the reference wave. The acoustic waves are generated by transducers located in a liquid media. The waves are coherent because they are produced by the same oscillator. The interaction makes the form of a very fine ripple on the liquid surface. This surface irregularity is a phase hologram, by reflecting coherent light from it, the observer views the reconstructed acoustical image. Electronic scanning can also be used instead of liquid media.

Real time holograms can be made to allow real time acoustical imaging, providing the operator with an instantaneous view of all internal structures.

Acoustical holography provides a completely new and unique approach to visualization, resolution and proper interpretation of flaws in the material. This method is far superior to standard ultrasonic testing techniques since it provides a true optical image of the flaw with high resolution.

When compared with other nondestructive testing techniques, acoustic holography seems to offer some important advantages, which are listed as follows (49-52). Because sound can penetrate deeply into most materials without losing much energy, images can be produced through thick iron castings or welded joints. And because even a small flaw or discontinuity will cause a rapid energy loss, testers can obtain data that is impossible to obtain with other techniques. For example minor disbonding of honeycomb

panels can be detected by acoustic holography. The exact location of the flaw or disbonding can be established. Ultrasonic imaging has also proved effective in medical research and diagnosis because it differentiates between various kinds of tissues-tendons, muscles, bones and arteries.

Through use of low frequency sound waves, it may be possible to make holograms of strata deep under the earth's surface. A form of seismic holography would be useful in searching for oil and mineral deposits (49).

Brenden,et al.(53) discussed an application of acoustical holography to geologic investigations. Acoustical transducers are used to convert electrical signals into acoustical signals. These signals are reflected from anomalies in the surrounding rocks. The reflected sound energy is reconverted to electrical signals by the same transducers or a second transducer mounted close to it. Both the amplitude of the received signal and the elapsed time between the generation and the time of return of the echo received is accurately measured. This information is further processed by the equipment to produce the raw data needed for mapping anomalies in the rock. This mapping may be interpreted to indicate fault structures and mineralized zone. An example of the method and necessary computer analysis is given in this references.

6. Conclusions

There are several alternative applications of holographic methods to the earth sciences. Thermal stress measurement (54),

detecting temperature variation near the surface (42), microwave hologram radar imagery (55) and mapping systems (56,57) are examples. But the most important and common methods are discussed in the previous section.

For three particular categories, deflection measurement, photoelastic holography, and acoustical holography, there have been few investigations relating earth materials to date due to the novelty of the holographic method. It is believed that the holographic method can be used successfully to solve problems in soils engineering, rocks engineering and geological engineering in various ways as the technique is refined and developed.

In summary, the important advantages and disadvantages in the applications of holography to engineering are listed.

Advantages:

1) the ability to obtain a three dimensional record of events relating to a particular object.

2) the ability to remotely sense change which does not require surface attachment or special preparation of the specimen.

3) the ability to measure displacement with a high degree of accuracy (measured in micro-inches).

4) the ability to observe deflection as it occurs by using real time holography.

5) the ability to facilitate stress analysis when combined with the photoelastic method.

6) stress analysis can be carried out using photoelastic coating method.

7) the ability to generate elevation contours.

8) the ability to detect flaws, cavities and internal structures using acoustic holography.

9. relatively inexpensiveness of this system compared to most other methods.

10. the ability to produce quantitative results.

Disadvantages:

1) very sensitive to vibration and displacement, requiring specially stable and vibration free environment for the system.

2) the maximum measurable displacement is smaller than other methods.

C. Model Studies

Model analysis is an alternative to mathematical strain and stress analysis in the determination of the behavior of structures. Through model analysis the effects of physical properties, dimensions and loading can be simulated and analyzed more easily and economically. Model studies allow combination of different factors; for instance, strength and physical properties, inhomogeneities, and geologic structures. So model studies may be carried out in order to obtain the interrelationships between factors.

In order to decide what kind of modelling method, material and method of analysis to use for the subsidence study, a literature

review of model studies previously applied in soil and rock mechanics was undertaken.

Model studies covering room and pillar mine model studies and longwall mine model studies were examined.

In model studies, there are true models, mathematical model, distorted models, strain gage models, photoelastic models, stress coating models, holographic models and centrifugal models for soil and rock mechanics.

1. Mine Structure Models and Foundation Models

Hobbs and Adler (58,59) have observed strata movement around mine roadways using scale models. Factors studied included applied pressure, roof and floor strength, roadway shape and the size and strength of ribside supports. Similar studies also have been made in Germany.

Harris (60) used a sand box to examine the possible distribution of stress in the region of coal-mine face working; the floor of the box represents the top of a coal seam, and strips of the floor can be lowered successively through a distance equivalent to the seam thickness to represent an advancing longwall face. The effects of depth, seam thickness, arching and two types of sand were considered. Possible distortional errors of this technique have been discussed by Daws (61).

The Bureau of Mines (62) presented a method for reducing the complexity of designing room and pillar mining systems by treating the openings as anisotropic soft inclusions in the surrounding

ore or host rock. The effective Young's moduli for the systems were calculated by use of theoretical models. A stress coating method was used to determine the directions of principal stresses, and finite element analysis was used to determine strain distributions. The field stress around the inclusion was then applied to the actual opening shape to determine the stress distribution within the mining region.

Serata (63) has developed a time-dependent mathematical model of underground openings and support systems. The triaxial properties of visco-elastic rocks and the nature of the underground stress field were studied in order to establish a theoretical basis for the models. The theoretical conclusions were tested by using analog models of the structures.

The time dependent laboratory testing has been criticized by Barr (64). He indicated that rapid laboratory time testing disregards the time dependence of creep under mining conditions, and also strain hardening under laboratory testing conditions alters the creep behavior of the rock.

Stephanson (65) obtained the mathematical solutions of deflections, bending moments, and longitudinal deformations of single and multilayer roofs in horizontally bedded rocks. The theories for single and double layer roofs were verified by model experiment, taking into consideration the deflection of the pillar. The theories developed for single and multi-layered roofs have been verified using models with uniform load distribution on the top surface of the model and centrifugal model loading. The

results from the model experiments and the theories thus verified were applied to a prototype and found to agree with the real condition.

Besides true models and mathematical models, instrumented models and photoelastic models are being used to study design. Zelonka,et al.(66) have encased strain gage networks in epoxy to evaluate the advantages of the system. They found that any number of gages, in any configuration could be used with this method. It will give consistent results when the model is constructed properly.

Haas,et al.(67) determined the behavior of rock like model structures simulating lined and unlined tunnels by use of strain and displacement gages. Major problems solved were the design of rock like materials and embedment of strain gages.

The photoelastic technique is one of the most popular current mine modelling technique. The fundamental principles of photoelasticity were established many years ago, but the application in engineering has mostly been in the last decade following the development of suitable birefringent materials. The accuracy of the three dimensional frozen stress method has been improved, and a photoelastic coating technique is applicable for non-birefringent material.

Scott (68) used three dimensional photoelastic techniques to determine the stress distribution in pillars and roof of a room and pillar mine model. The stress freezing technique was used and stresses were calculated using the shear difference method.

A photoelastic model of an underground opening was loaded in the centrifuge to determine the effect of boding loading. Stress distribution and concentration within a rock bench, due to the presence of the opening, were examined (69).

Agarwal (70) has developed a new technique to analyze two dimensional non-homogeneous models. A simple three layered medium with a circular hole centrally located in the intermediate layer was considered. The Young's modulus of the intermediate layer was lower than that of the other layers. His studies showed that the stress distribution around the circle hole in a stratified medium was significantly different when compared to the case of a continuous homogeneous medium. A comparison of stress distribution and procedures for preparation and testing of the model is given in the paper. The excavation openings in coal and frequently in bedded or vein-type deposits are examples of mine structures in nonhomogeneous materials. The composite model technique may provide a powerful tool for stress analysis.

Wilson and Bohidar (71) evaluated the internal stress distribution in pillars based on photoelastic studies and destructive testing of models, showin that pillar failure is a function of the internal stress distribution and that stability can be improved by altering the internal stress pattern.

Theocaris,et al.(72) investigated the internal stress distribution with change in volume created by restrained shrinkage of cement paste due to hydration of cement at early ages, using a

photoelastic technique. The model consisted of a square array of circular inclusions made of pure epoxy polymer embedded in a matrix made of plasticized epoxy resin. The stresses, affected by microcracks which were caused by tensile stressed developing at the interface between the aggregate and cement paste, were analyzed. The effect of the ratio of the average diameter of aggregates to the average distance between surface and surface of aggregates was studied upon the stress distribution.

Ergün has studied the stress distribution in two dimensional discontinuous plate models with regular orthogonal joint sets (73). It was demonstrated photoelastically that the stress distribution in a jointed rock mass was affected by

1) The presence of voids along joints

2) The ratio of the applied pressures

3) The combination of joints to the direction of the applied pressures

4) The matter in which the pressures were applied (stress history).

Bricic and Nesovic (74) investigated the discontinuous foundation soil at the abutments of the Dam Grancarevo. The foundation soil of the dam is full of cracks in different directions and the goal of the investigation was the analysis of the influence of cracks in rock on the state of stress in both dam and foundation rock. A two dimensional model of the dam was examined by classical photoelasticity. The influence of cracks on the redistribution of stresses in both dam and foundation was the subject of the analysis, especially the change of the point

of application and the direction of the resulting force transferred from the dam to the foundation soil. The location of cracks was determined from the geological map of the existing rock. All data necessary to the determination of the stress field were obtained.

2. Mine Subsidence Models

To obtain fundamental relations describing the subsidence phenomena, most previous model studies have been two dimensional because three dimensional models require more effort, expense and time.

There are two approaches to subsidence; the empirical approach and the phenomenological approach. Voight and Pariseau (75) has reviewed both techniques.

In the empirical approach, the stochastic model can be a typical model. A conceptual model for stochastic media offered by Litwiniszin (76) and Sweet (77) consists of a layered sequence of small cubical cells, each containing a ball. If a ball is removed from a lower cell, it can be replaced with equal probability by the ball from either of the two cells directly above. In this way upward movement of the void will occur and develop to the surface. This approach can be used to define the development of the bell shaped subsidence profile. Several laboratory experiments (78,79) involving the moment of a sand mass have been performed in order to check the validity of the stochastic model theories.

In the phenomenological approach, elastic, viscoelastic, plastic and time dependent studies can be included. In the classical elastic solution, Berry (80,82), Berry and Sales (82) and Hackett (84,85) have solved the problem using existing elastic theories. Whetton and King (22) used gelatin to model elastic behavior. Polyurethene rubber has been adopted to bind multi-layered strata, while remaining sensitive enough to allow the model to be actuated by gravity alone (86).

Inman (87) made a viscoelastic approach in an attempt to introduce time as a variable in the description of mine subsidence.

Dahl (88) used numerical analytical techniques, considering two and three dimensional elasto-elastoplastic analysis of mine subsidence. The results were compared with the field data from the coal mines in South East Pennsylvania, West Virginia and Great Britain.

III.   THE HOLOGRAPHIC SYSTEMS AND CALIBRATION

A.   The Holographic Systems

The principles of holographic interferometry, as a means of displacement measurement, were introduced in the literature review (Chapter II).   There are several different systems used for the investigation.   The principles basically are the same for each.

All the systems employed both a reference and an object beam. The beam from the laser was divided into these two beams by a beam splitter (Figure III.1).   The divided beams were expanded by the beam expanders and pinholes to illuminate the area of the model and the recording plate.   Pinholes were used to filter laser light.   When a focused laser beam passes through a narrow hole (pinhole) the intensity of light expanded by the convex lenses becomes homogeneous across the beam.   The combined unit of beam expander and pinhole is called a spacial filter.

A variable beam splitter was used to control the ratio of intensities of the divided laser beams.   The beam splitter was coated with aluminum and the density of coating was continuously yet regularly varied so that the reflectivity can be adjusted to the required level.   From the experiment it was found that an intensity ratio between the reference and the object beam from 6:1 to 8:1 gave the best results.

The holographic equipment was mounted on a granite slab, size 4 ft. x 6 ft. x 6 inches.   Granite has a low thermal expansion and provides an optically flat mounting surface.   The granite slab was

mounted on four automobile tires, a layer of styrofoam and a layer of timber to eliminate transmission of ground vibrations which might induce relative movement of the components of the equipment.

A simple holographic system is shown in Figure III.1. Most displacement measuring holographic systems are similar to this, but some variations in layout can be made. The incident angle of the light beam as it strikes the model surface is an important factor in data interpretation (refer to Chapter II, Section B-3). The incident angle must therefore be measured whenever the system changes.

The holographic system used for the calibration procedure, the water pressure room and pillar mine models and electromagnetic models are shown in Figure III.2. This system uses collimators, which are 7.75 inch diameter convex lenses placed in front of the pinhole to make the expanded beam parallel.

Figure III.3 shows the holographic system used with the longwall mine models. The object beam illuminated the surface of the model obliquely, and was not therefore parallel to the table surface as in Figure III.2.

A 25 milliwatt He-Ne laser manufactured by Jodon Engineering Associates, Inc.* was used as the light source. The beam expander has 40 X magnification and the pinhole size 7.5 micro-meters. Front surface mirrors were used to improve reflection. These were purchased from Gaertner Scientific Corporation.

---

*The use of manufacturers names is for the purposes of identification only and should not be construed as an endorsement of any product by either the U.S. Bureau of Mines or the University of Missouri-Rolla.
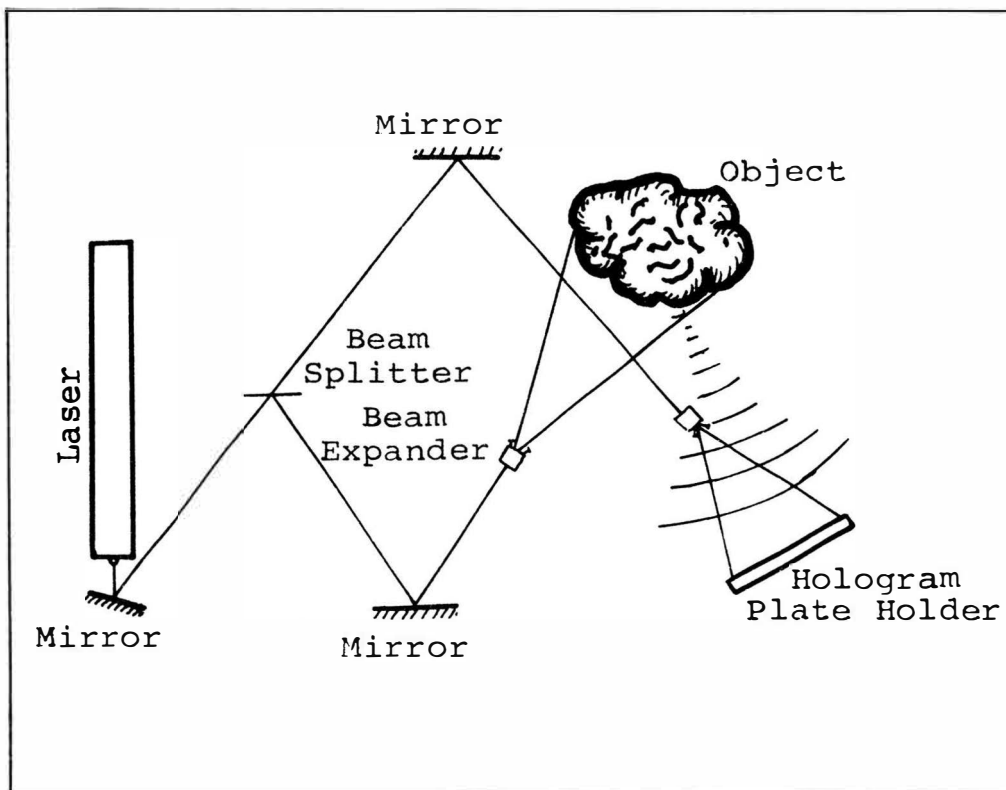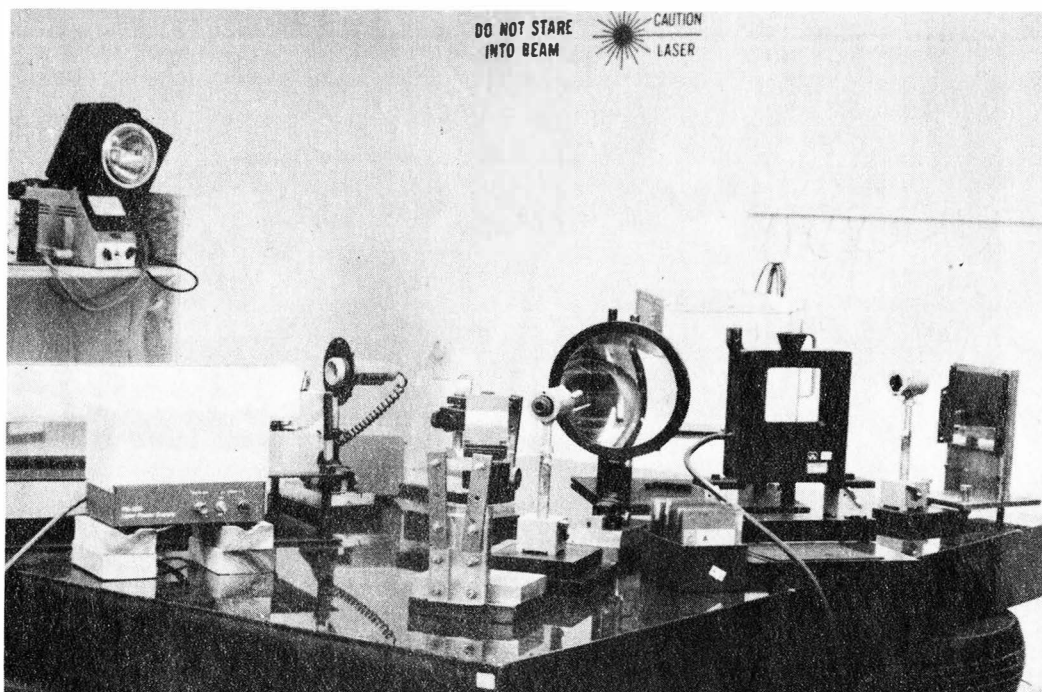
Figure III.1. Simple Holographic System.

(a)
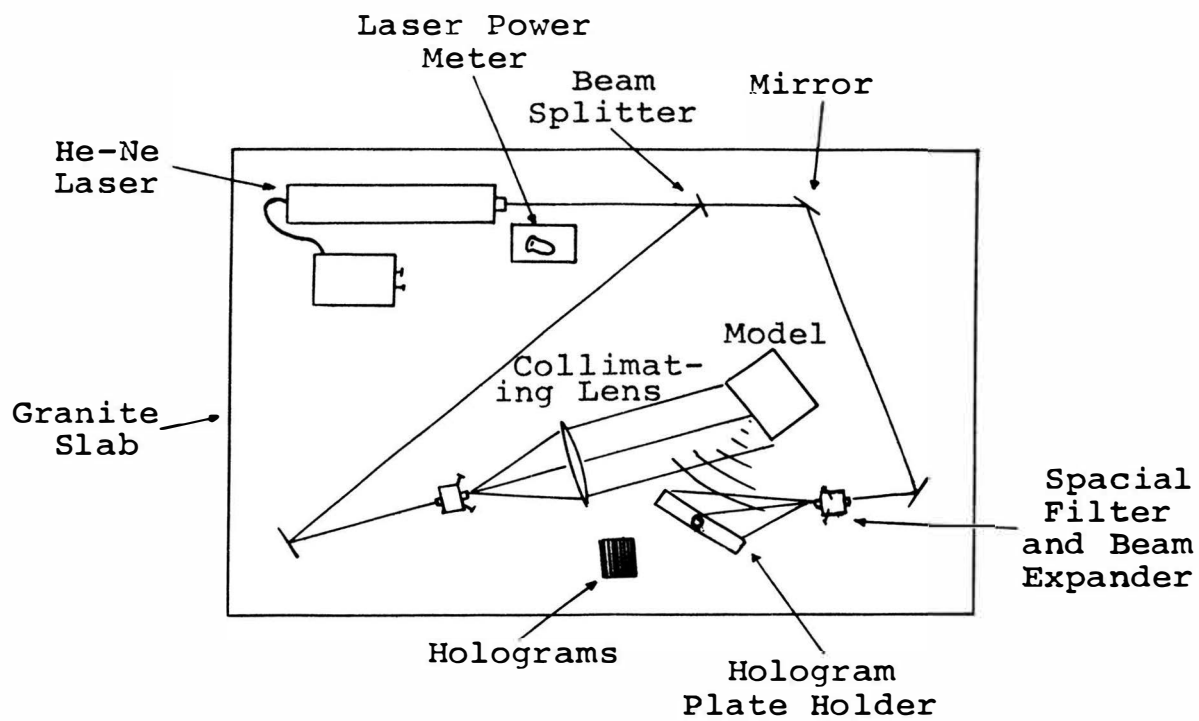
(b)

Figure III.2. Holographic System I.
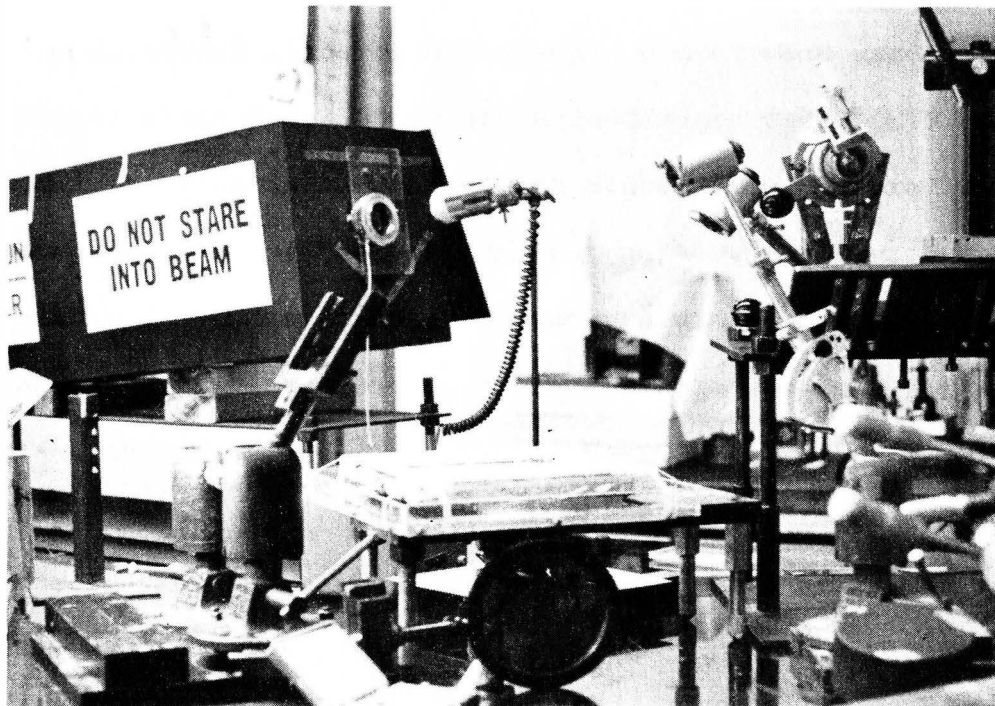
(a)
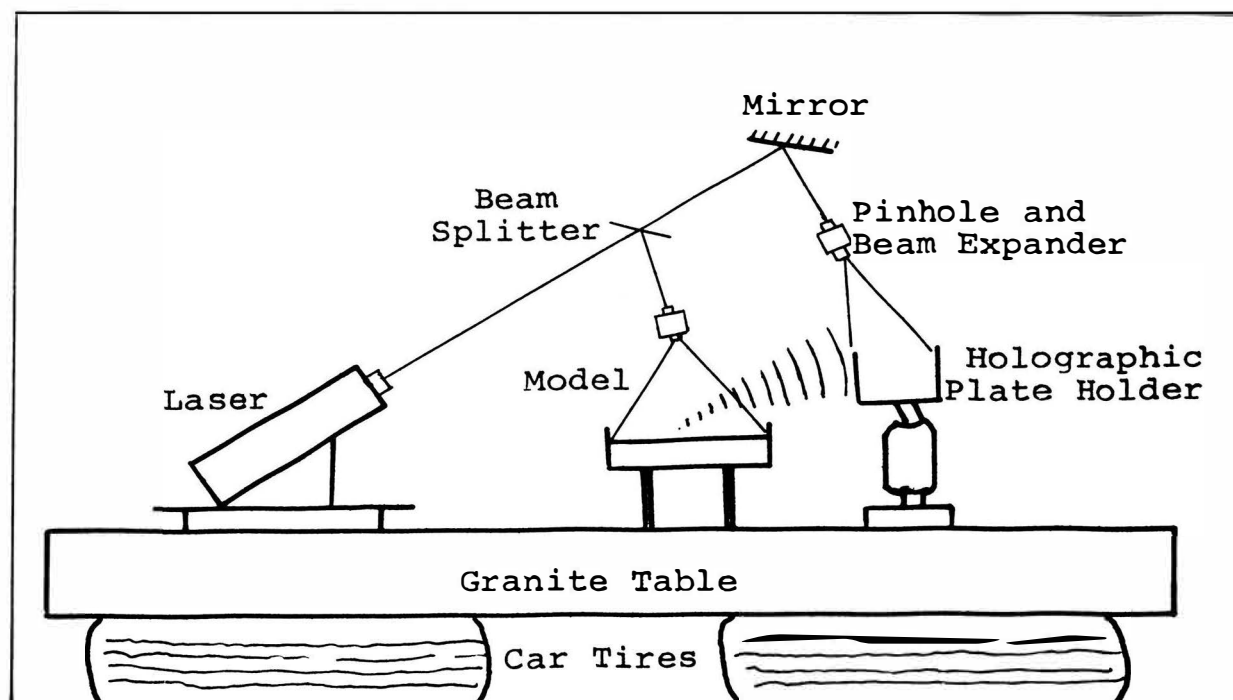
(b)

Figure III.3. Holographic System II.

Two different kinds of holographic plates were used: KODAK

Holographic Plate Type 120-02 and Agfa-Gevaert Type 10E75 Holographic

Plate manufactured in Belgium. Both plate sizes measured 4 x 5 inches,

and were adequate for the project, but Agfa-Gevaert type was faster

in sensitivity and required less exposure time, the plates were also

thicker. For these reasons Agfa-Gevaert type was used for most of

the research.

Equation II.32 was used to interpret the contour fringes obtained

from the subsidence models. A calibration test, described in the next

section, was run to verify that the theory is applicable for data

interpretation.

B.   The Calibration Test

In order to verify the calculation relating fringe density to

model displacement a calibration model was constructed. A dial gage

was connected with a micrometer feed to which a needle was attached

(Figure III.4). The incremental unit of the dial gage was 100

micro-inches. The needle rested on the center of a circular aluminum

plate which was clamped at its edges. The size of the aluminim plate

was 3 1/4 inches in diameter.

Two holograms were made at 100 micro-inches deflection and 300

micro-inches deflection respectively (Figures III.5 and III.6). The

computed fringe number and experimentally measured fringe numbers

were compared (Table 1). The results show that the measured and

computed values were within an accuracy of three percent. Error is

probably due to inaccuracies in turning the micrometer, measuring the
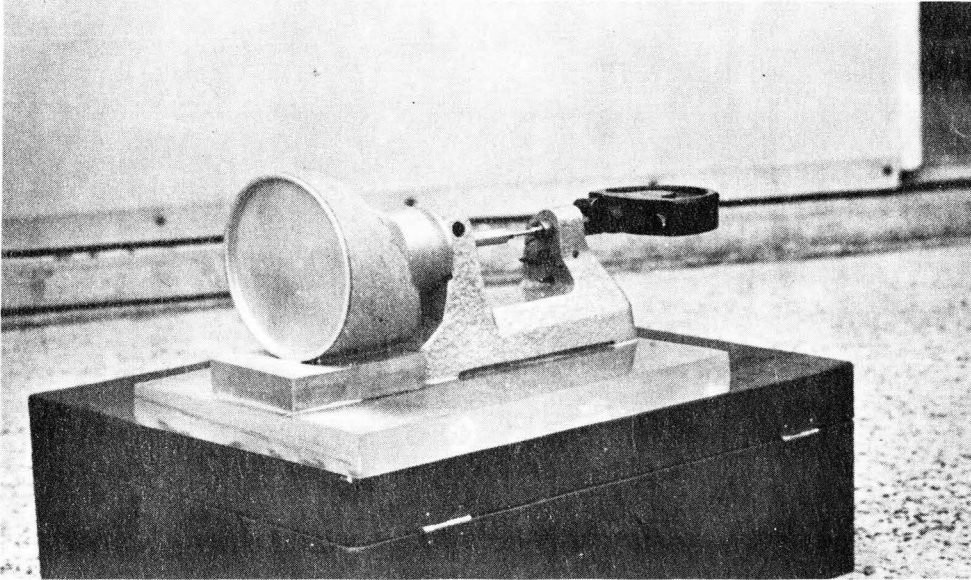
Figure III.4. Calibration Model.
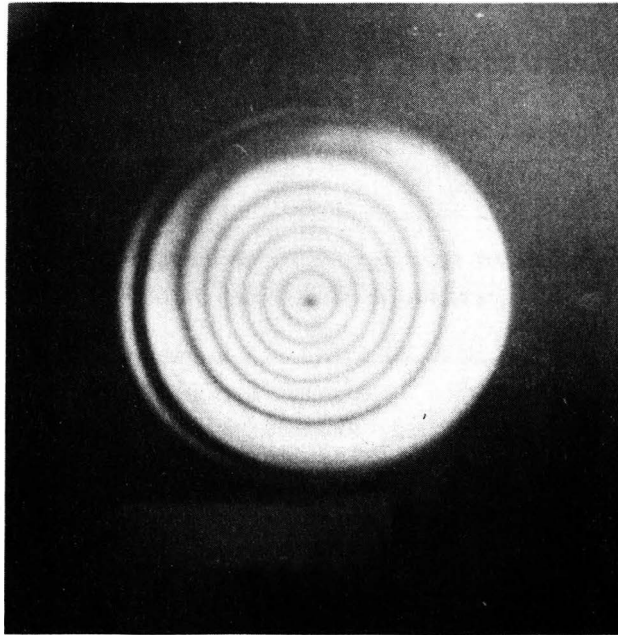
Figure III.5.   100 Micro-inches Deflection.
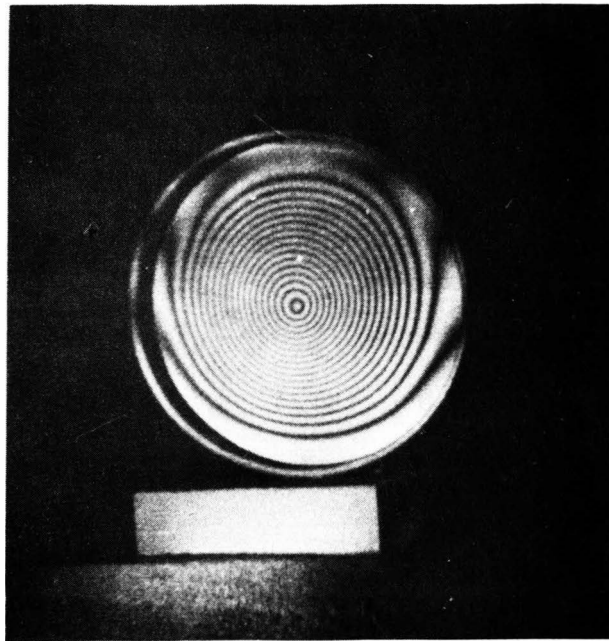
Figure III.6.   300 Micro-inches Deflection.

incidental angle and boundary conditions affecting plate displacement. The results thus indicate that the system is sufficiently accurate provided care is taken in carrying out the experiment.

Table 1. Comparison of the Fringe Numbers from Experiment and Calculation.

Deflection (micro-inches)	Fringe Number from Experiment	Calculated Fringe Number
100	6.5	6.5
300	19.0	19.5

IV.   ELECTROMAGNET ROOM AND PILLAR MINE MODELS

Electromagnetic models simulating the room and pillar mining method were developed in the first stage of the program. The models were also used while the author familiarized himself with the holographic technique. The first successful hologram for the project was taken from these models. The 20 milliwatt laser covered an area of approximately 10 x 10 inches of the model surface with sufficient light to make holograms. An aluminum spray coating improved reflectivity from the model surface. It was an undercoating material, Tens-Lac, normally used with the stress coating produced by Photolastic Inc.

Two types of electromagnetic model were designed. The results obtained did not provide sufficient data for a subsidence study and the model technique was discontinued due to the length of time required to make each model. Improvements can be made to utilize the model and the experimental method is described.

A. Models

A thin plate was used to simulate a mine roof. The plate was supported by four aluminum rings or cubes (Figure IV.1). The gravitational force was modeled by a magnetic field generated by an underlying electromagnet. The size of the plate was 5.5 x 4 x 1/64 inches. The ring pillars were 3/4 inches in diameter.

Figure **IV.2** shows the improved electromagnet and model layout for a room and pillar intersection. A low carbon steel was used for all parts of the model. A threaded location hole was tapped in the base of the steel box to hold the electromagnetic coil. The coil was
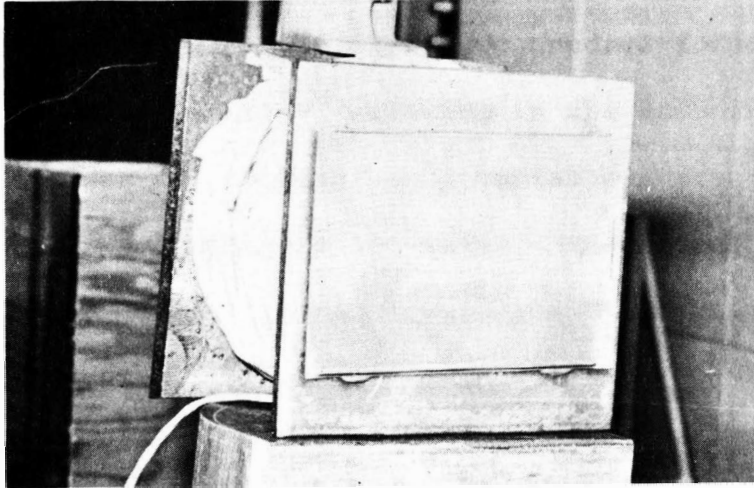
Figure IV.1. Electromagnet Model.
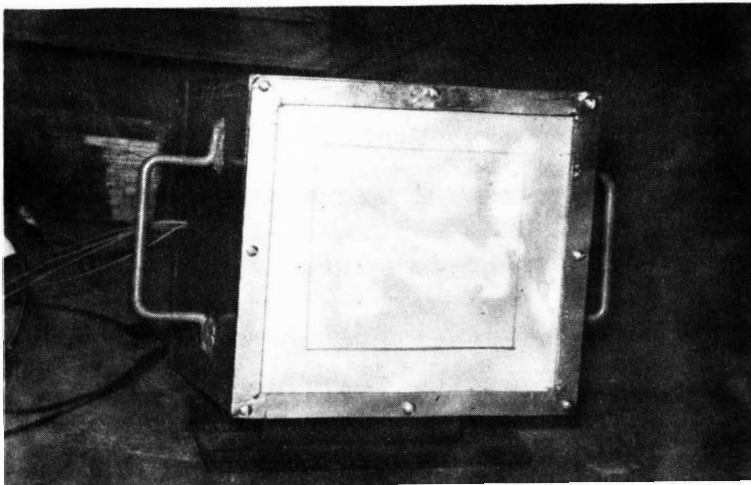
(a)

Figure IV.2. Improved Electromagnet Model. (a,b)
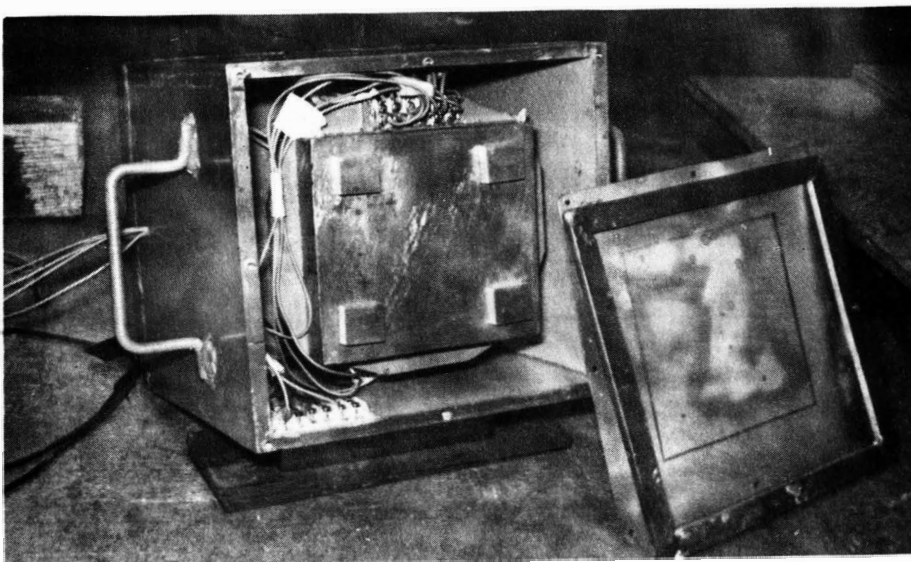
(b)

wound with a terminal at every two hundred turns up to six hundred turns in order to allow variation in the strength of the magnetic field. Power was supplied by a variable current D.C. power supply with a maximum output of 900 watts. The desired magnetic force was obtained by controlling the current and selecting the required terminals. The size of the plate was 10 x 10 x 1/16 inches, and the modulus of elasticity of the steel was 63.3 x 10^6 psi and Poisson's ratio was 0.31. Various sizes of pillars were used, 0.5 x 0.5 inches, 1 x 1 inches, 1.5 x 1.5 inches and 2 x 2 inches.

The strength of the magnetic field was measured using a Gauss meter, and a calibration test was made to relate magnetic force to the current and number of coils. The magnetic force is directly related to the flux density between the core and the plate. Several holes were made on the test plate of the model, and the flux density was measured for each hole at a certain and number of turns of coil.

Difficulties were experienced in making the models, particularly the aluminum pillars. This is because holographic interferometry will measure deflections of micro-inches, and the surface of the plate and the pillars must be therefore parallel and flat. When the number of pillars was increased it became more difficult to ensure that all the pillar surfaces touched the plate concurrently since very high accuracies were required in construction of the parts and their assembly.

B. Testing Procedures and Results

The double exposure method was used to make holograms of the

electromagnetic models. The first exposure was taken before the magnetic force was applied. The second exposure was taken after the desired magnetic force had been applied. In some cases, with the improved electromagnet, the first exposure was taken after a low level of magnetic force had been applied. In this way the plate was initially in contact with the pillar surfaces and this removed some errors.

Four holograms were taken with the first simple electromagnetic model. Figure IV.3 shows one of these images taken using an ordinary camera and 35 mm Plus-X Pan film (KODAK). This was the first hologram taken in the project. The fringe show the deflection which occurs over the plate. There was no deflection around the area where the pillars were located. Deflection increased toward the center of the model, and both sides of the pillars show that there was deflection toward the electromagnet.

The limiting number of fringes which can be detected in a unit area is a function of the resolution of holographic plate and that of the recording film. Magnetic force was not measured for this model.

Three holograms were taken using the improved electromagnetic model with 4 pillars (Figure IV.4), and the data of current and fringe numbers is listed in Table 2.

The results were not sufficiently consistent for analysis as the number of pillars was increased. The source of error was traced to inaccuracy of model preparation. A second problem was created by the boundary of the model. Unless some flexible device was used, boundary problems provided complications. The ability to simulate a gravity force using electromagnets and the holographic technique was
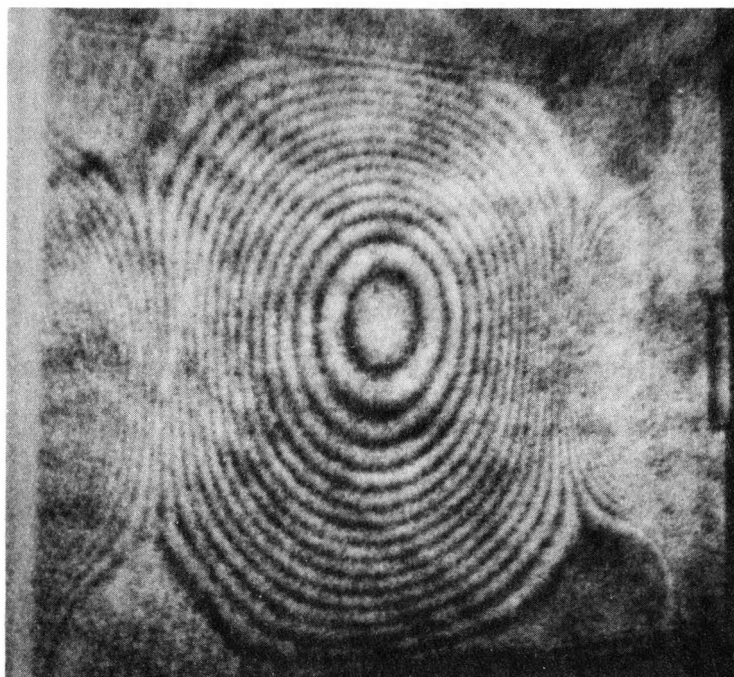
Figure IV.3. Deflection Pattern of the Electromagnet Model.
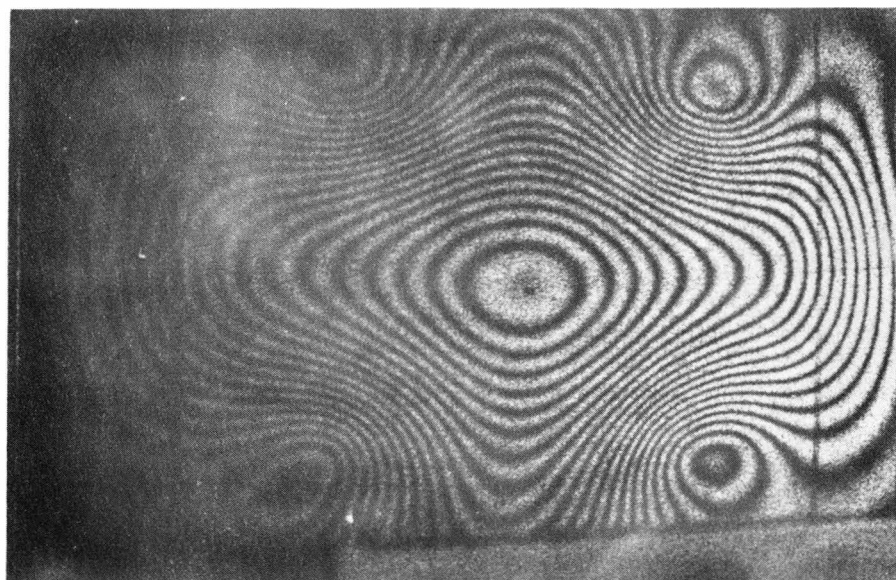
Figure IV.4. Deflection Pattern of the
Improved Electromagnet Model.

successfully demonstrated, but the technique was considered inferior to
the water pressure room and pillar modelling method because of the
amount of time required for model preparation.

Table 2. The Relationship Between Current
and Deflection (Fringe Number).

Current (Amperes)	Fringes
7	10
14	22
22	30

V. WATER PRESSURE ROOM AND PILLAR MINE MODELS

Rocks do not behave completely as elastic materials. Especially, when the rocks above underground openings are thick, there are factors controlling movement beyond the simple elastic response, plasticity, arching effects, creep and geologic structures are examples. But where overlying layers are relatively thin and there are few geologic irregularities, elastic response can be taken to govern most of the roof movement including deflection and subsidence phenomena.

A water loaded room and pillar mine model was constructed using plexiglass which behaved elastically in the range of the applied load for the test. Double exposure and real time holographic methods were used to measure deflection of the model, and self consistent results were obtained.

A. Water Pressure Models and Testing Procedures

Three water pressure models were constructed containing 4, 9 and 16 pillars respectively. Each model consisted of two plates between which the pillars were cemented by use of a structural adhesives manufactured by Minnesota Mining and Manufacturing Company. A hard plexiglass was used to simulate the pillars, the rib and the roof. A piece of plastic, 1 x 5 x 3/4 inches, was attached to each side of the plates to make a square room, and pillars were distributed in a square pattern (Figure V.1). The inner dimensions of the retaining frame were 5 x 5 x 3/4 inches, those of the pillars were 1/2 x 1/2 x 3/4 inches and the thickness of the plexiglass was 3/32 inches. The modulus of elasticity of the plexiglass was measured and found to be
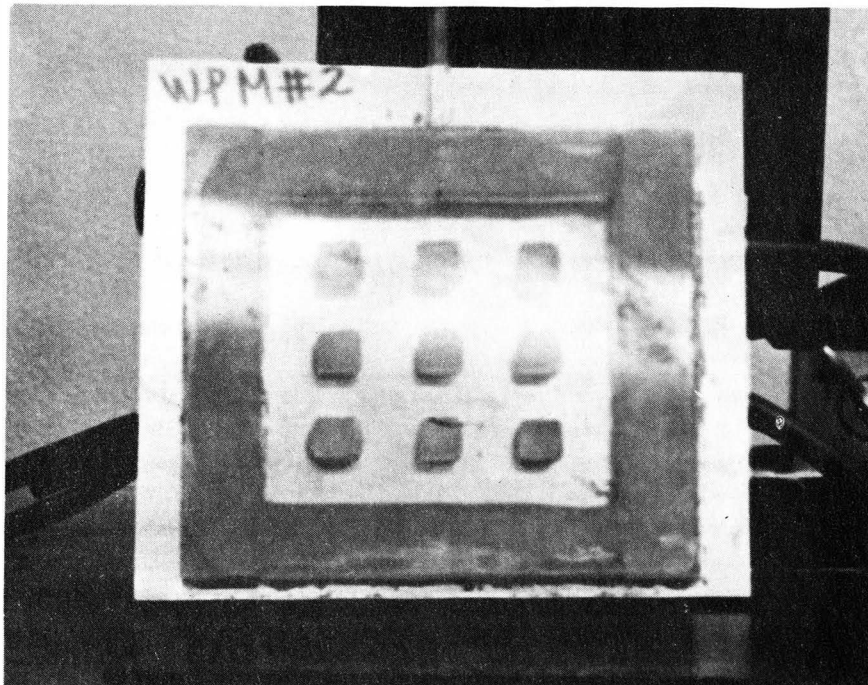
Figure V.1. Water Pressure Room and Pillar
Mine Model (9 pillars).

2.46×10^{6} psi and Poisson's ratio was 0.37.

The model was filled with water and connected to the reservoir and loaded by raising the reservoir relative to the models. The model deflection was measured holographically.

In order to obtain a better reflection, the plates of the water pressure models and that of the electromagnetic models were coated with the aluminum spray.

The deflection patterns for the roof obtained from both electromagnetic and water pressure models for various applied loading conditions were considered as a simulation of roof deflection and the subsidence pattern of thin overlying strata. Load was applied at values below 2 psi, and the deflection caused by compression of pillars was so small as to be neglected (The compression strain is of the order of 0.8×10^{-6} inches).

The specimen was held with the roof and floor plates vertical to facilitate measurement of deflection.

Fourteen holograms were taken using this model and the double exposure method and different loading conditions for each test (Figures V.2-V.7).

Real time holographic techniques were also used for the four pillar system to produce a series of pictures of changing fringes as the load changed over the period that one of the pillars failed. Using a real time plate holder a hologram was taken before the model was loaded. The holographic plate was then developed in place. The pillar on the upper left side became disconnected from the model floor due to failure of the adhesive and as the pressure was increased
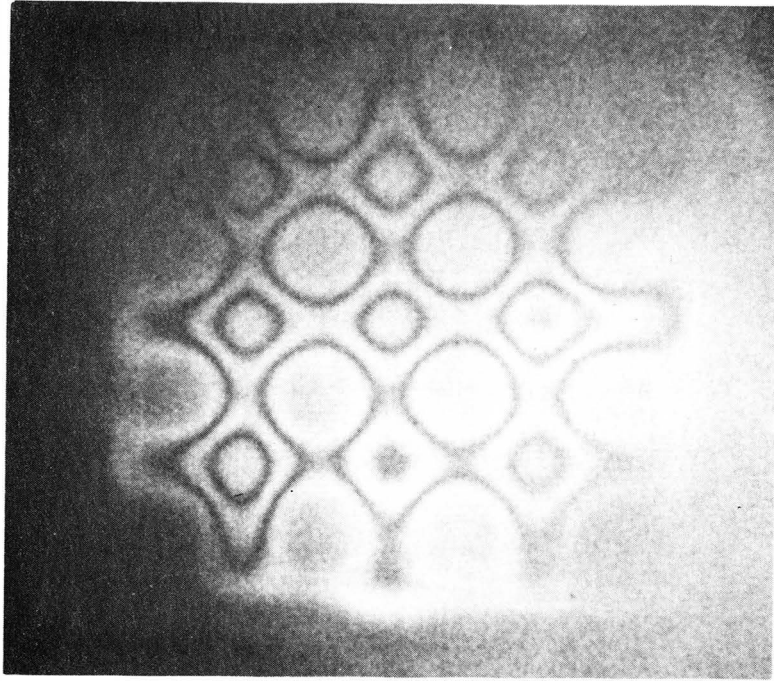
Figure V.2. 16 Pillar Model - 0.433 psi Applied.
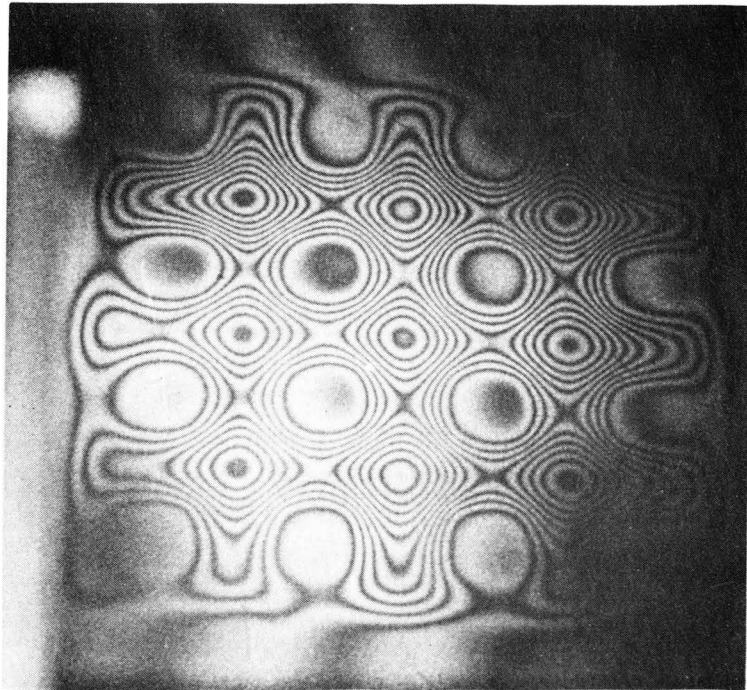
Figure V.3. 16 Pillar Model - 1.732 psi Applied.
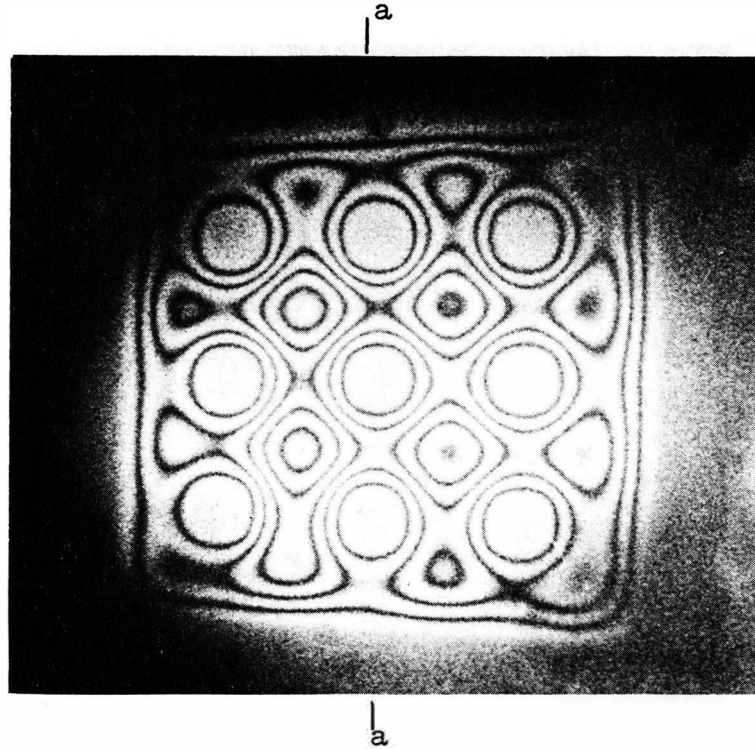
Figure V.4. 9 Pillar Model - 0.433 psi Applied.
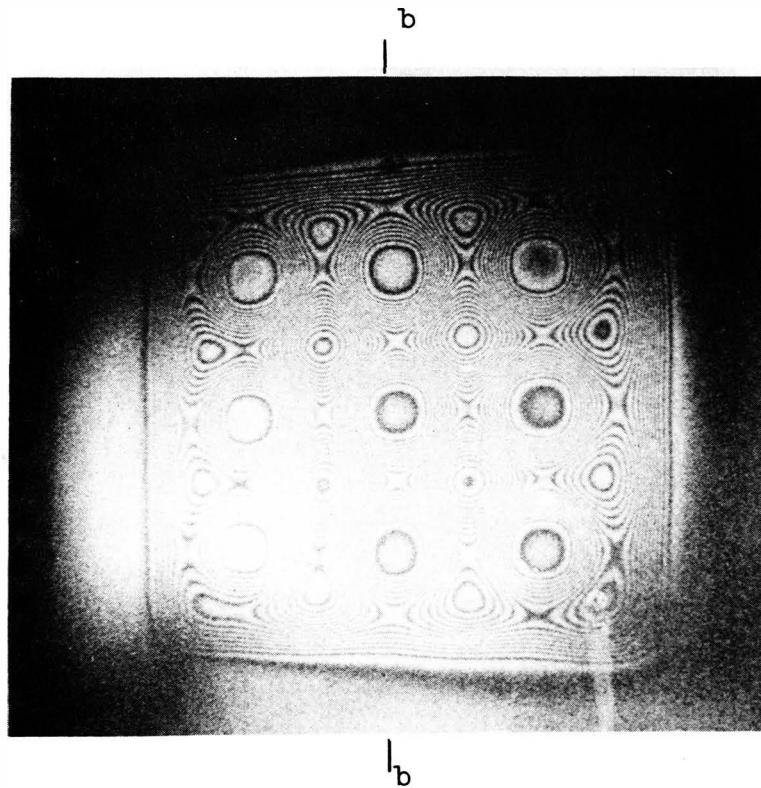
Figure V.5. 9 Pillar Model - 1.732 psi Applied.
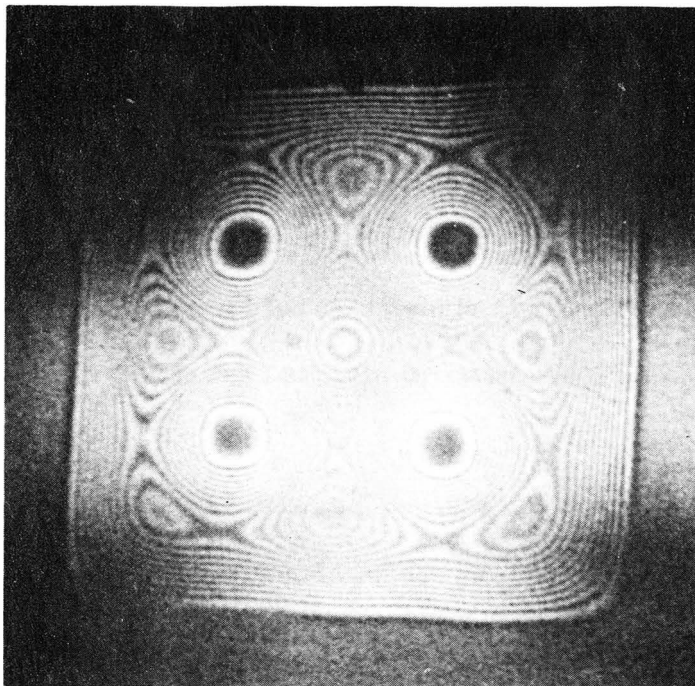
Figure V.6. 4 Pillar Model - 0.433 psi Applied.
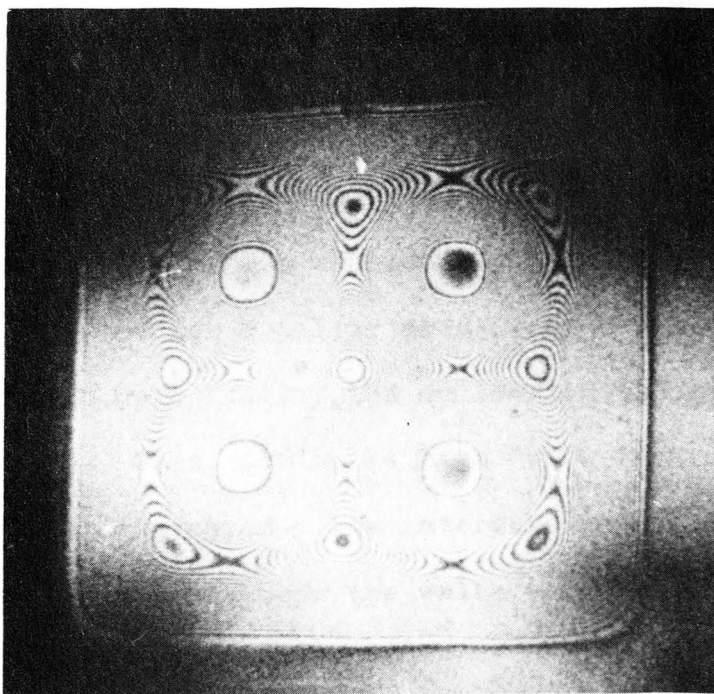
Figure V.7. 4 Pillar Model - 0.866 psi Applied.

the fringe pattern recorded the deflection distortion that resulted
(Figures V.8 and V.9).

B.   Results and Analysis

The direction of deflection is toward the camera, opposite to
the real condition of roof deflection or subsidence, but the magnitude
should be equivalent.

The fringe value was calculated by use of Equation II.32. Between
two fringes the deflection perpendicular to the plate was 22.5
micro-inches/fringe. The pressure on the model for 1 foot of water
level change is 0.433 psi. Using the double exposure method 4
holograms were taken for each of the 16, 9 and 4 pillar models for a
1, 2, 3 and 4 feet of water level change respectively. Using real
time holography, 4 fringe patterns were determined; one made for
failure of the pillar without any load, and the other three were made
by raising the water level 2, 4 and 6 inches respectively after the
pillar had failed (Figures V.8 and V.9).

Deflection profiles (cross section a-a in Figure V.4 and b-b in
Figure V.5) are plotted for 9 pillar model with the loading of 0.433
psi and 1.732 psi (Figure V.10). The deflection is proportionally
distributed to load. When loading is high deflection at the edges
of the pillars were compressed. The intervals between the pillars
were equal. But deflections near the walls were less than those in
the middle of the cavity.

The maximum amount of deflection was determined and compared
with the load on each pillar condition (number of pillars) as shown in
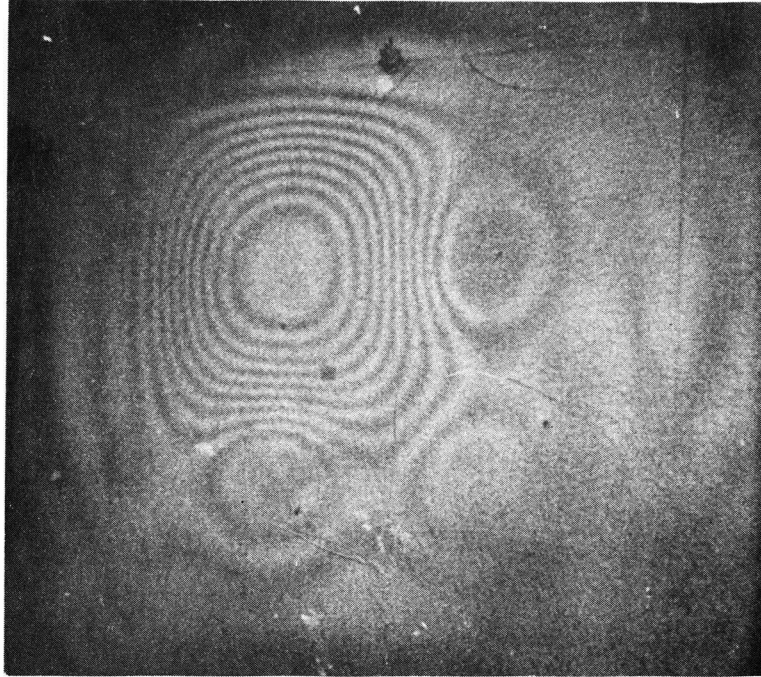
Figure V.8.   4 Pillar Model, 1 Pillar Failed - 0.072 psi
             Applied (Real Time Method Used).

c —   — c
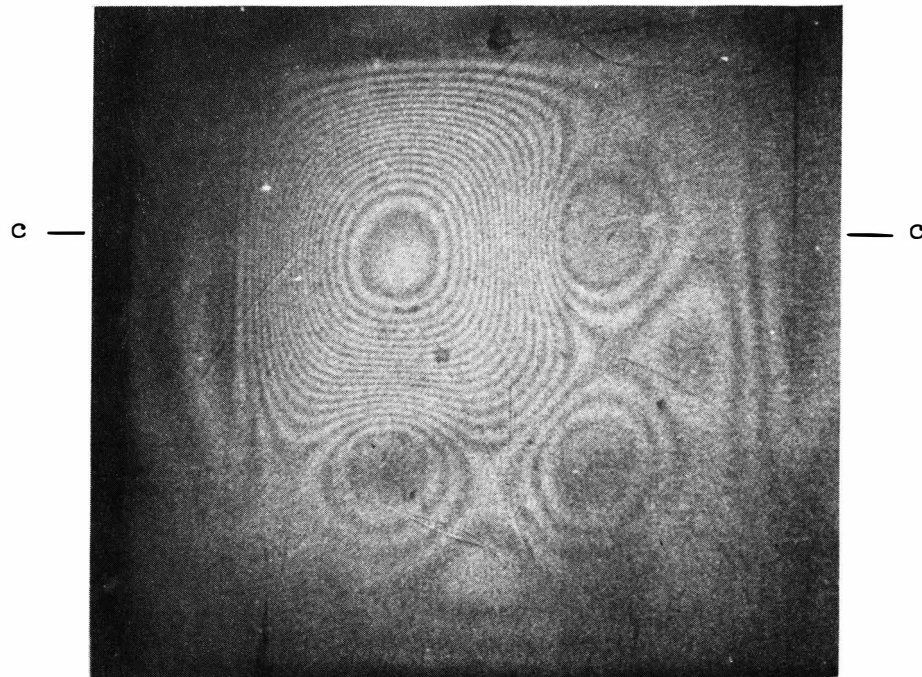
Figure V.9.   4 Pillar Model, 1 Pillar Failed - 0.144 psi
             Applied (Real Time Method Used).
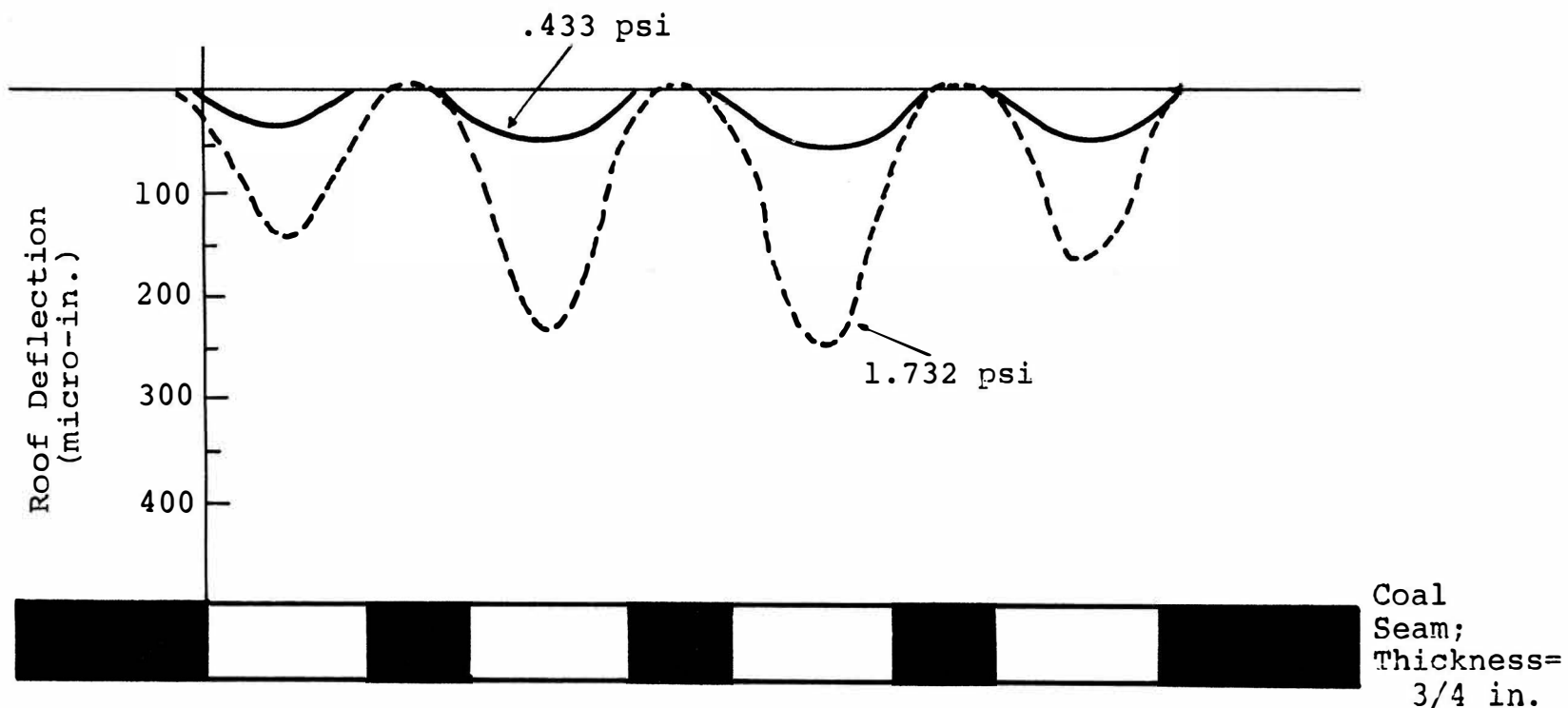
Figure V.10.   Deflection Profiles of the 9 Pillar Model.

Figure V.11.   Maximum deflection was proportionally increased with stress for each pillar condition.   Slopes were higher when the number of pillars was smaller.

The relationship between the number of pillars and maximum deflection under constant loading are shown in Figure V.12.   The greater number of pillars the model has the smaller the roof deflection was made as it was expected.   But the shape of the curves showed that the rate of change of deflection is higher when the number of pillars is lower and vice versa.

As the model roof was made of a thin elastic material, the model simulated the elastic character of the mine roof deflection or subsidence on a thin overburden in the condition of a uniform loading. If was found that model has potential application for simulation of deflections and subsidence of complicated mine conditions to help mine design and to understand and predict the environmental impact due to mine failures.

The pillar failure model proved the ability of the system to adequately simulate and monitor pillar failure, and real time holographic method can successfully be used for such models.

In Figure V.13 two deflection profiles of the 4 pillar model are plotted.   The distance between the pillars were equal.   But the deflection in the middle of the cavity is a little (about 20 percent). And the deflection profile with a pillar failure (cross section of c-c in Figure V.9) is shown in the same graph.

The examples of the deflection pattern by pillar failure showed that maximum deflection increased 5 times more than the condition
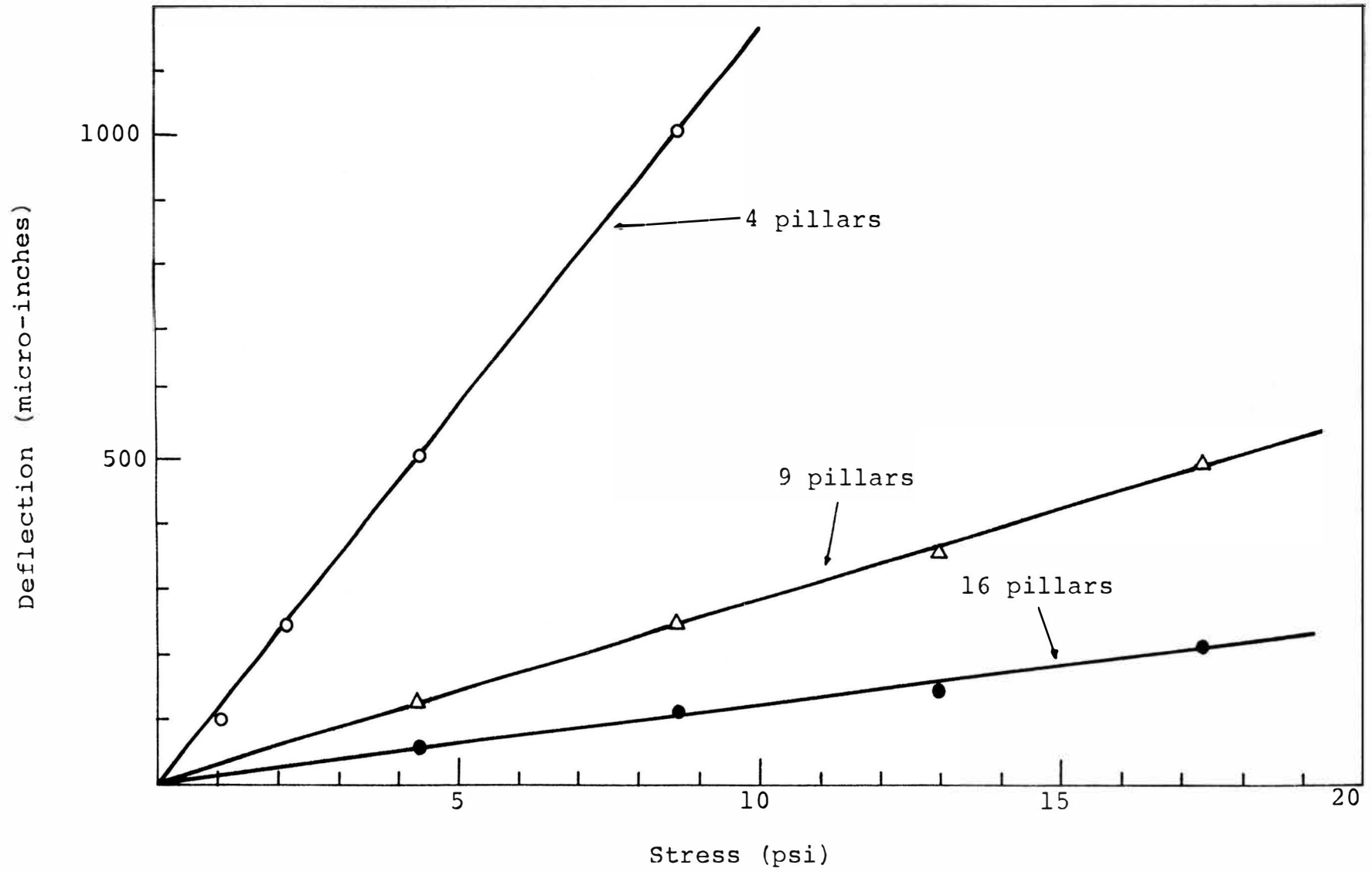
Figure V.11.   Stress vs. Deflection.
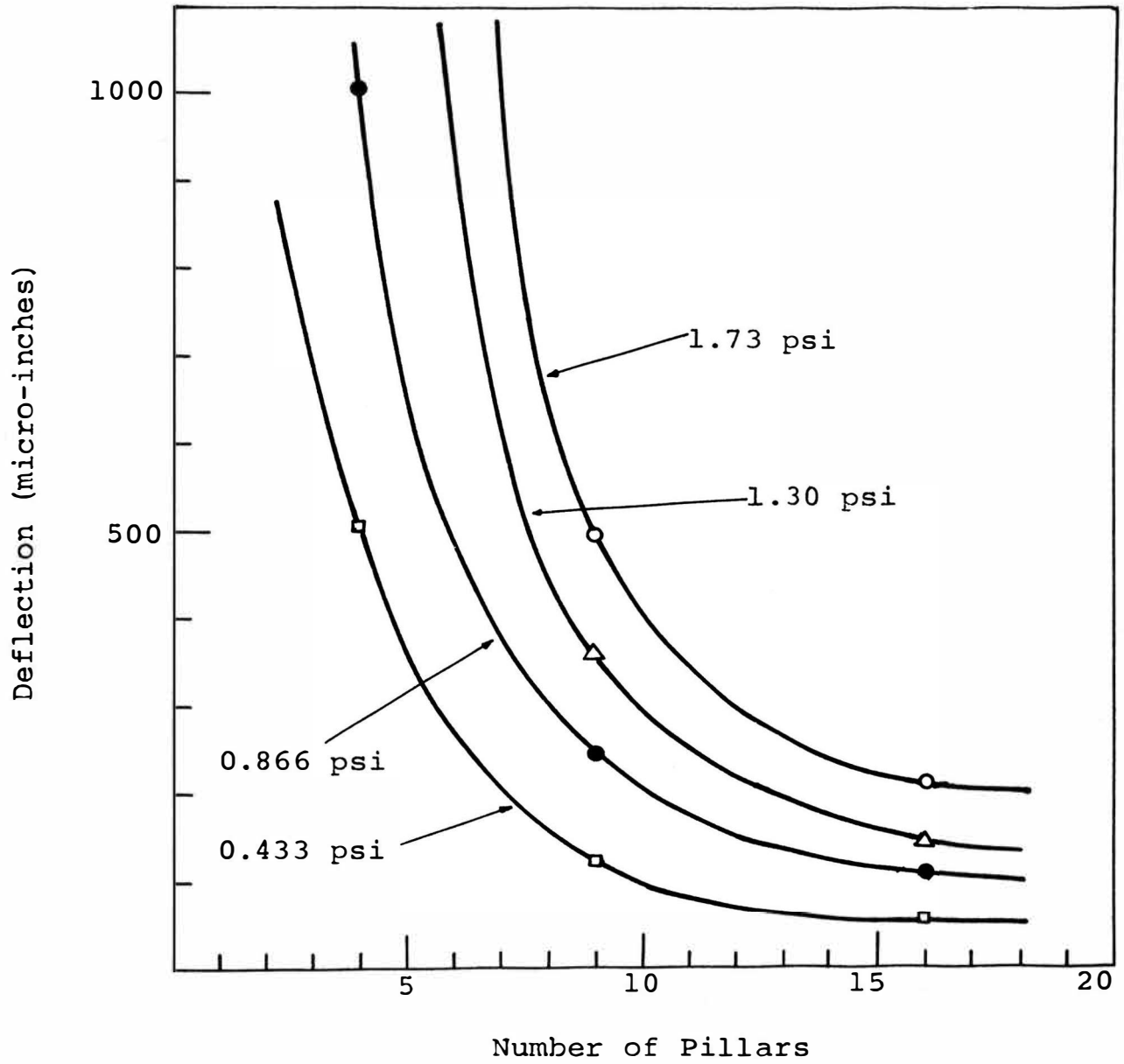
Figure V.12.   Number of Pillars vs. Deflection
under Constant Loading.
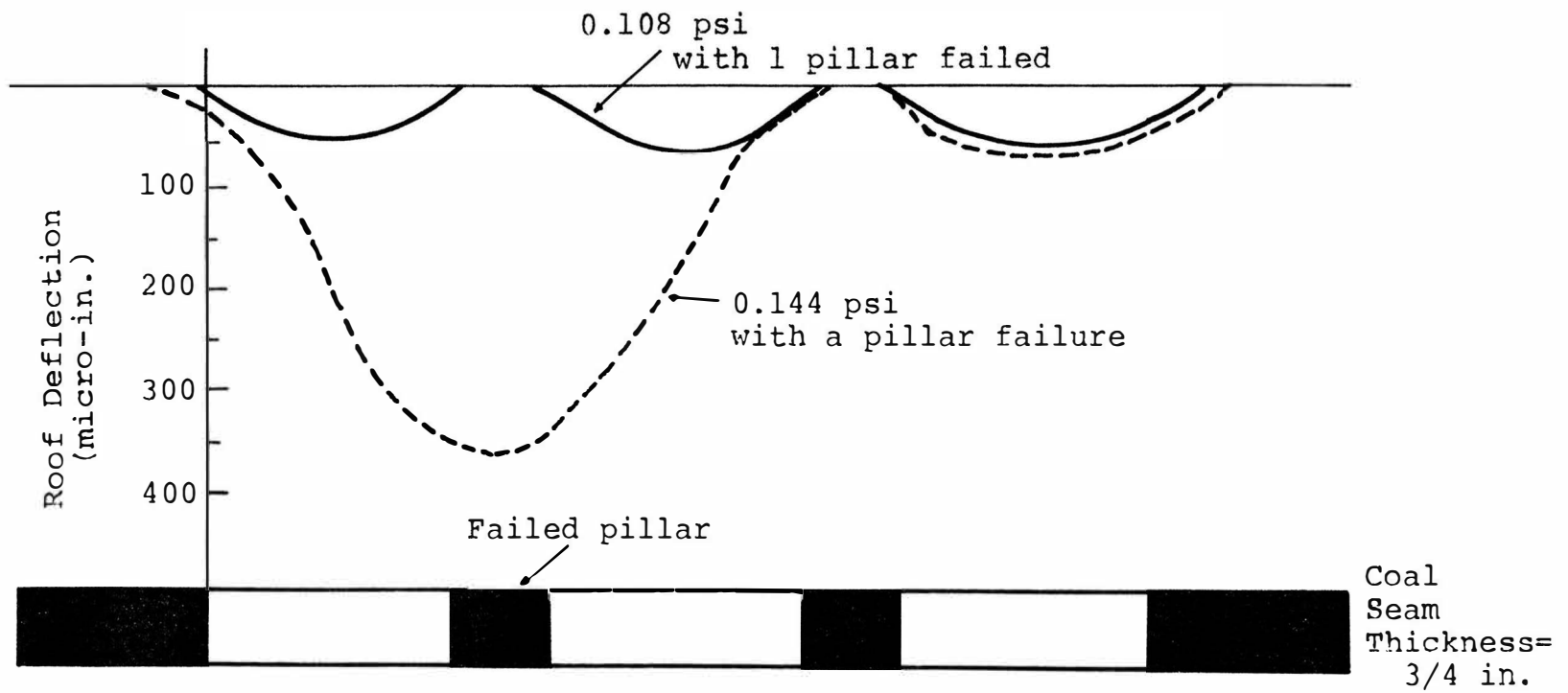
Figure V.13. Deflection Profiles of the 4 Pillar Model.

with pillar failure for the 4 pillar model.

Stress distribution can be calculated using the deflection distribution and stress-strain relationships given by elastic theory. Quantitative data will provide more consistent relationships between deflection or subsidence, number of pillars, dimensions of the model and material values.

The advantages of the method are

1) It can be applied to inelastic materials

2) Less time consuming

3) Accurate experimental method

4) Simulations can be made for more complicated mine conditions.

VI.   UNDERGROUND SIMPLE CAVITY MODELS: LONGWALL AND STOPE MINE MODELS

Simple self loading models were constructed to simulate subsidence by longwall and stope mining operations. By virtue of the accuracy of holographic interferometry and the ability to measure very small displacements, self loading models were found practical as a means of studying subsidence phenomena.

Both sand, gelatin and mixtures of sand, gelatin and a commercially available confectionary were used as model material. Gelatin acted as an elastic material and sand modeled a brittle material. Time dependent deformable material was obtained by a combination of the three materials.

Quantitative data were obtained from prints of the holograms and analyzed using the university computer and statistical analysis. Subsidence profiles were obtained for the three different materials, and various cavity depths and the profiles were compared with those predicted by the theories and experimental analysis which has been developed to date. Among the factors affecting subsidence studied were the subsidence area, the amount of maximum subsidence, the depth to the cavity, the cavity height, the cavity width, the modulus of elasticity of the model material and the effects of sequential cavity development and time.

A.   Simple Cavity Models

A square frame was built to hold the model material. A steel plate was placed in the box, and attached to a micrometer screwfeed located under the base of the box (Figure VI.1). The cavity was
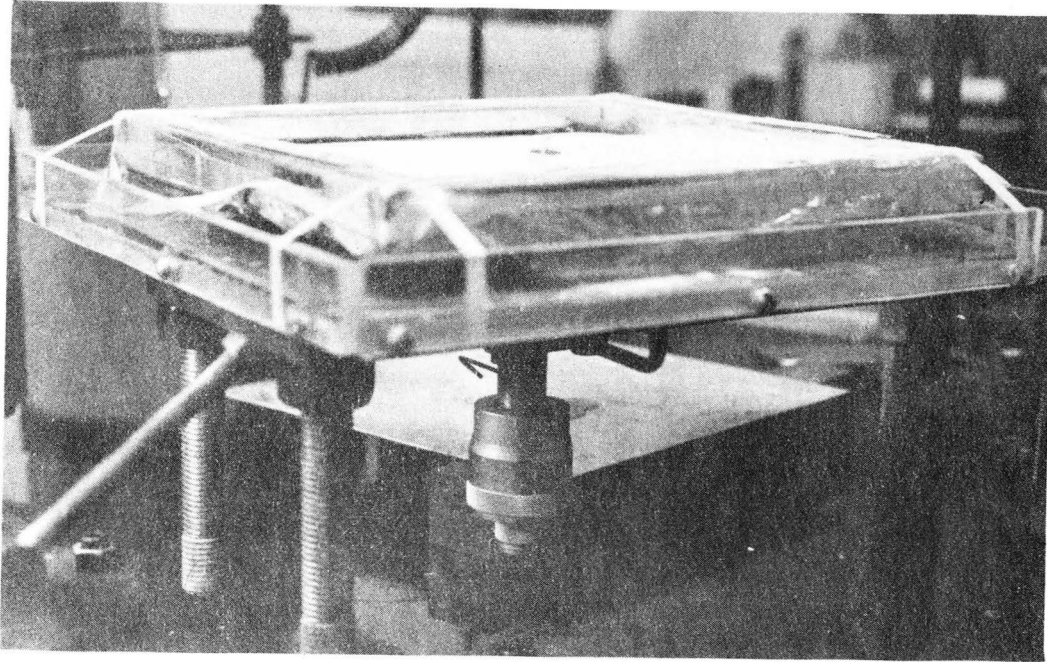
(a)
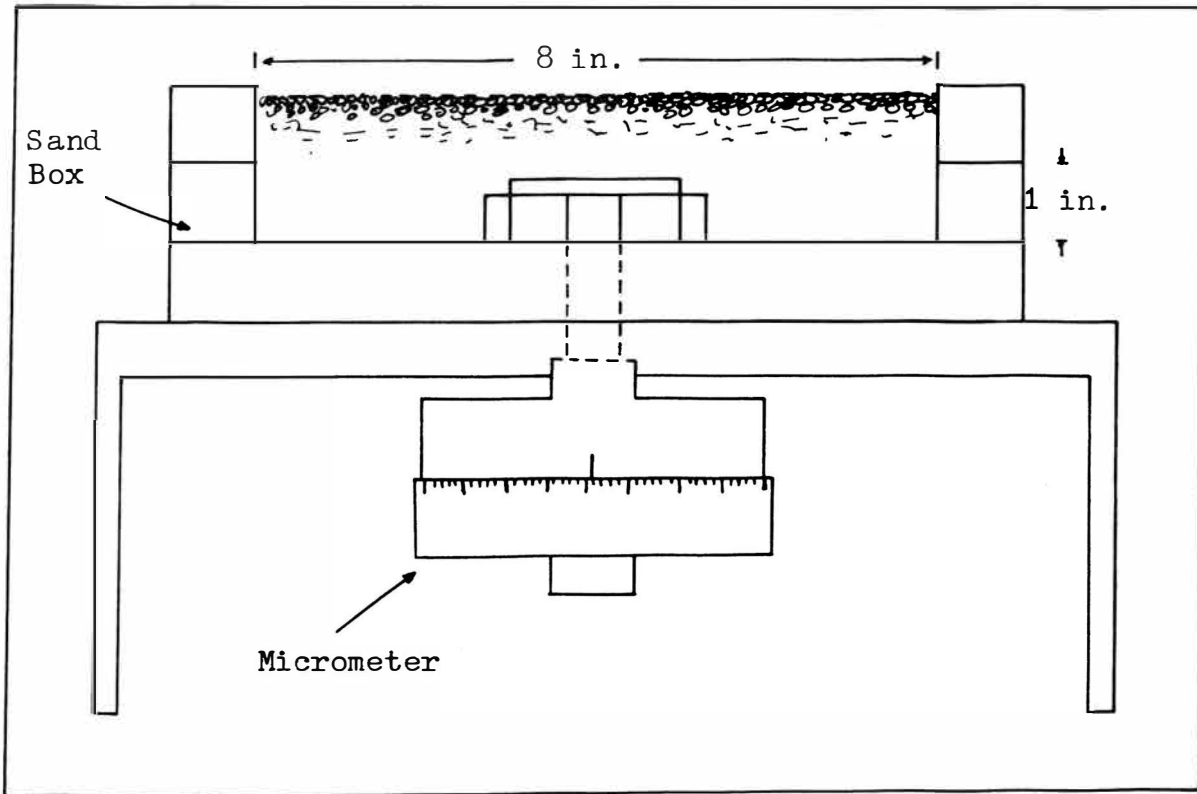
(b)

Figure VI.1. Simple Cavity Model.

created by turning the micrometer and lowering the plate after the box had been filled with the model material. Various cavity sizes were obtained by changing the plate size, and the cavity height was controlled within an accuracy of 20 micro-inches. The direction of the plate was adjustable to an inclination of 30° from the horizontal line by changing the position of the micrometer, and thus creating inclined cavities.

The subsidence contours were generated on a rough surface, but even when the fringe numbers were large the fringes were defined with sufficient clarity for accurate identification. In order to obtain such clarity, however, fine aluminum powder was springkled on the model surface to improve reflectivity and fringe resolution. Two sizes of frame were used in the tests. The first measured 6 x 6 1/2 x 3 inches, and the second consisted of 8 x 8 x 1 inches squares and the depth of the overburden could be increased by stacking up the squares. Several sizes of cavity area were created; 6 x 1 inches, 0.5 x 3.5 inches, 2 x 2 inches and 2 x 0.5 inches.

B.   Evaluation of the Model Material

Rock is a naturally occurring composite material. A simple equivalence does not exist for rock due to the anisotropy and discontinuity of its structure, and therefore a perfect model material simulating the character of rock cannot be obtained. The composite nature of rock has been investigated only superficially, primarily because of the irregular geometry and macroscopic heterogeneity of rock. Furthermore, rock typically contains many different kinds of

geologic feature such as fractures, faults, folds, joints and bedding each of which may be filled with clay or organic material.

Jaeger and Cook (94) defined a material in a ductile state, or ductile, as a material which can sustain permanent deformation without losing its ability to resist load, and a material is said to be in a brittle state, or brittle, under conditions in which its ability to resist load decreased with increasing deformation. In Figure VI.2, in the region of OA and AB the behavior is approximately elastic, in the region of BC it is ductile and in the region of CD is brittle.

Sand and gelatin were used as model materials. Gelatin exhibited elastic behavior in the load range applied and since loose sand has almost zero strength it approaches the limit of brittle behavior. The two materials thus defined the limits of the range of failure of rock. Whether rock behaves in an elastic, ductile, brittle or combination response, the behavior will lie in the range between pure elastic and limiting brittleness.

A special uniaxial testing device was devised to obtain the modulus of elasticity of the gelatin (Figure VI.3). Because of the low load values and the large deformation obtained, an elastic balance (sensitivity: 0.01 gm) and a micrometer (sensitivity: 1/10,000 inches) were used. The relationship derived between modulus of elasticity and gelatin content is shown in Figure VI.4. While determining the modulus of elasticity, the relative movement of the pan was subtracted from the measured movement of the micrometer to give model deformation.

The quartz sand used had a size distribution shown in Table 3.
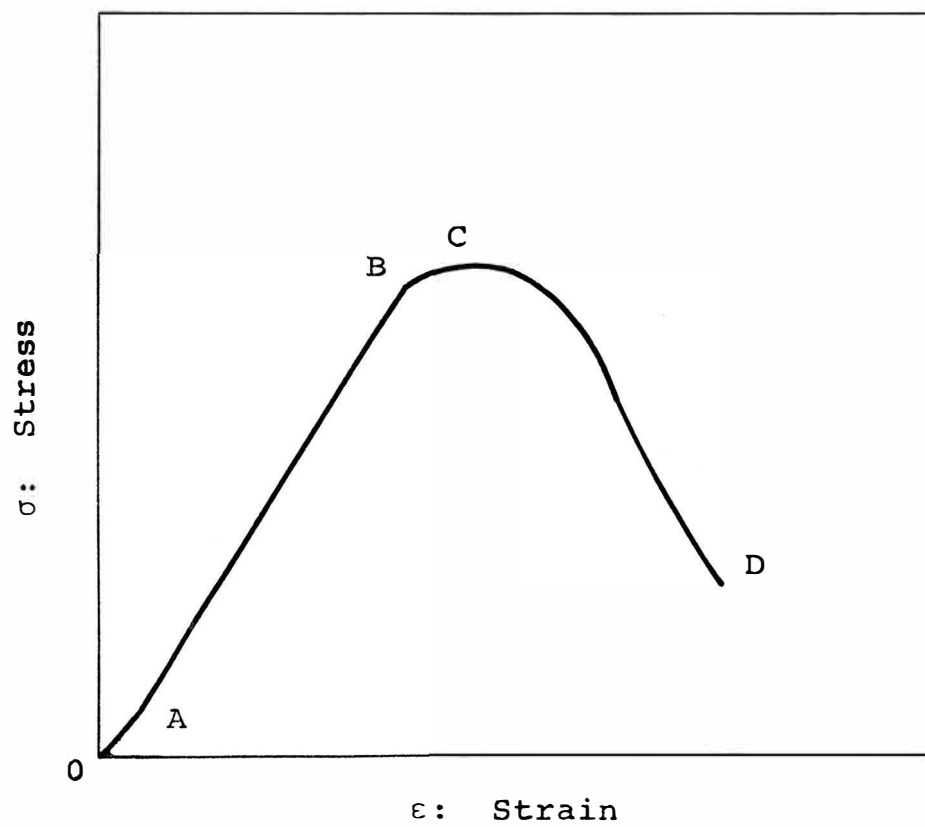
Figure VI.2. The Complete Stress - Strain
Curve for Rock (91).
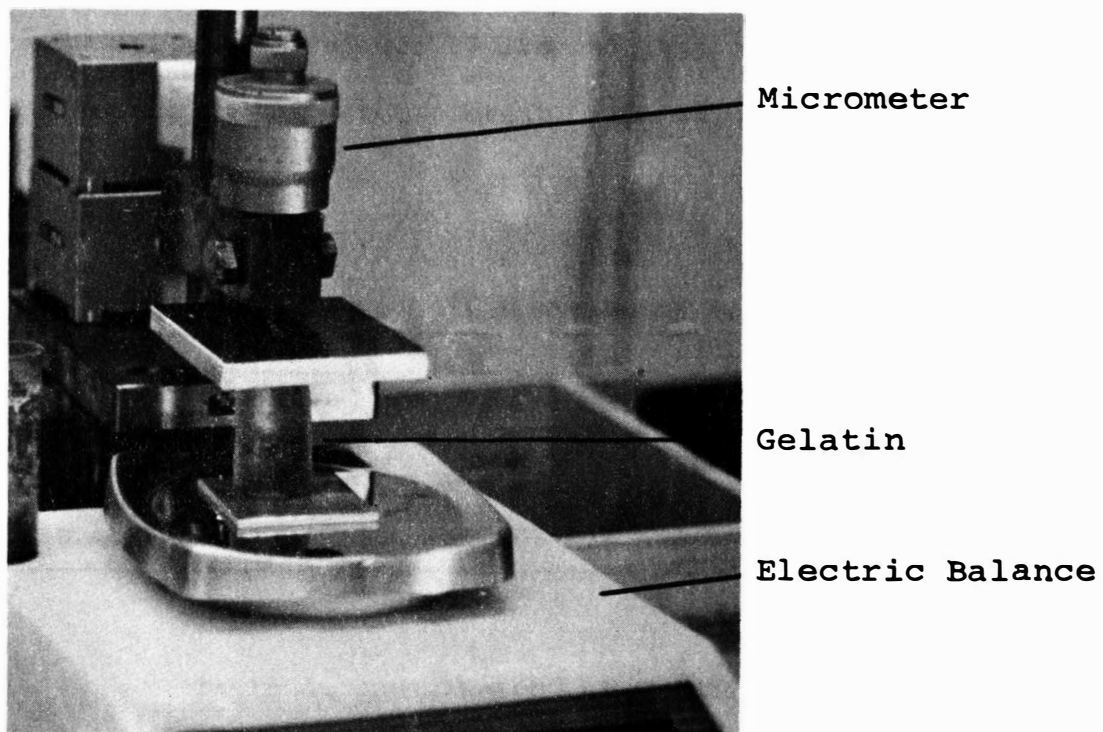
Figure VI.3.   Uniaxial Testing Device for Gelatin.
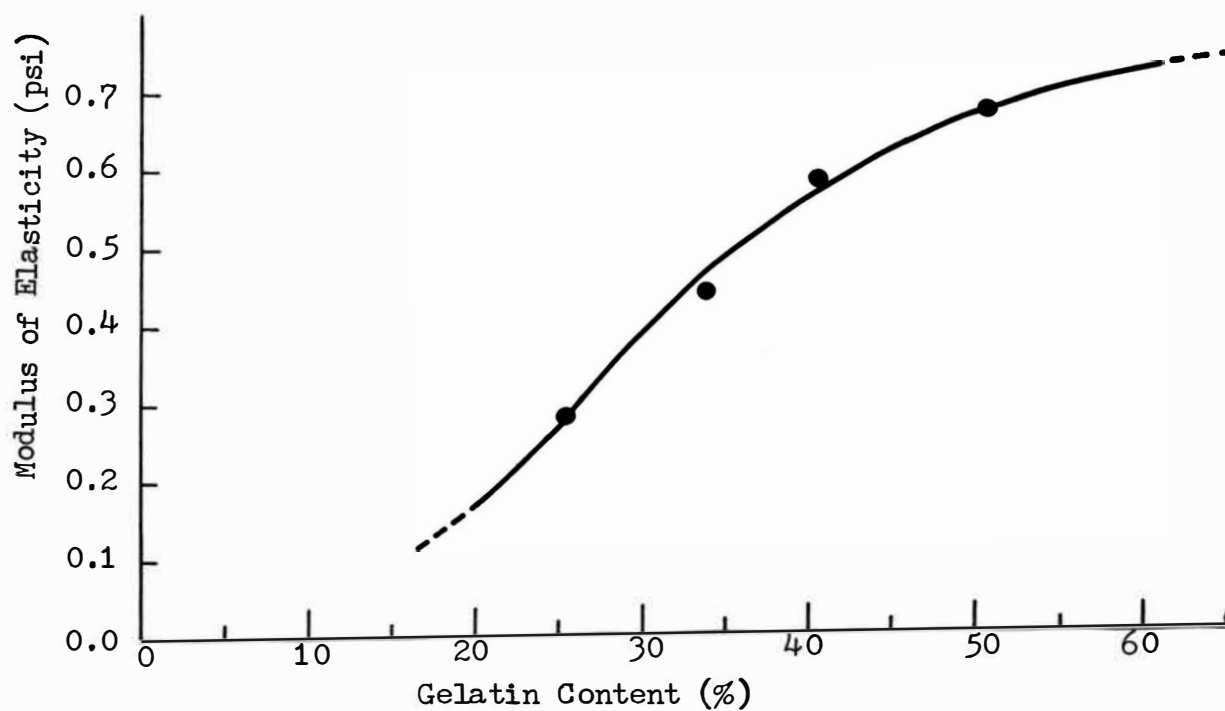
Figure VI.4.   Gelatin Content vs. Modulus of Elasticity.

The specific weight of sand was 97 lbs/cu. ft., and that of gelatin varied, according to the water content, from 64.46 to 74.75 lbs/cu. ft. as shown in Table 4.

Table 3.   Size Distribution of Sand.

Larger than 20 (meshes)	20-30	30-40	40-60	60-80	80-140	140-200	Smaller than 200
.04%	0.41%	6.43%	39.47%	31.20%	18.62%	1.69%	2.04%

Table 4.   Unit Weight of Gelatin.

Gelatin Content in 1 liter of Water (oz.)	6	12	24	36
Unit Weight (lbs/cu. ft.)	64.46	66.52	70.64	74.75

C.   Subsidence Area

In this section, observations were made of the subsidence shape, the shape of the subsidence boundary and the change in pattern of the subsidence contours. The cross sectional observations are discussed in the next section (Section E).

Most of the subsidence measurements were made using square or rectangular cavities since a typical longwall mine opening is a square or rectangular shape. The first observation made was that under certain conditions the corners of the cavities became rounded. Figure VI.5 is an oblique view of subsidence over a 2 x 2 inch square cavity at a depth of 1.5 inches in sand.

Where the cavity was rectangular, e.g., 0.5 x 3.5 inches, and at low depths of 1/4 inches or 1/2 inches in gelatin, all the contours on the longer sides were straight and the corners were rounded (Figures VI.6 and VI.7). But as the depth to the cavity increased to 1 inch, the contours became more rounded (Figure VI.8). Examples with sand are shown in Figures VI.9, VI.10 and VI.11 with contour lines rounded as depth increased from 1 to 3 inches. With increasing cavity depth the degree of rounding increased, and finally the surface depression became completely round.

These results agreed with the field data taken from a mine in southwestern Pennsylvania (88). Panel geometry was 455 ft. deep by 500 ft. wide by 68 ft. long, and surface subsidence over the corner of the panel became smoothly curved around the square corner.

The subsidence area will increase as the depth of the cavity increases (Figure VI.6 - VI.8 and Figures VI.9 - VI.11). The change in subsidence width with depth was studied. From 3 to 6 holograms were taken for each cavity depth while changing the cavity height. Several different depths were examined with both gelatin and sand models, and two sizes of cavity, 1 inch and 0.5 inches.

Relationships were established between subsidence width and cavity depth for gelatin with a cavity width of 0.5 inches and 1 inch, and sand with a cavity width of 1 inch (Figure VI.12). For a 1 inch wide cavity in sand it was possible to study cavity depth of up to 5 inches before the subsidence width exceeded the dimensions of the model surface, and mostly subsidence was less than 5% of the cavity height. It was only possible to study depths up to 1.5 inches for the gelatin
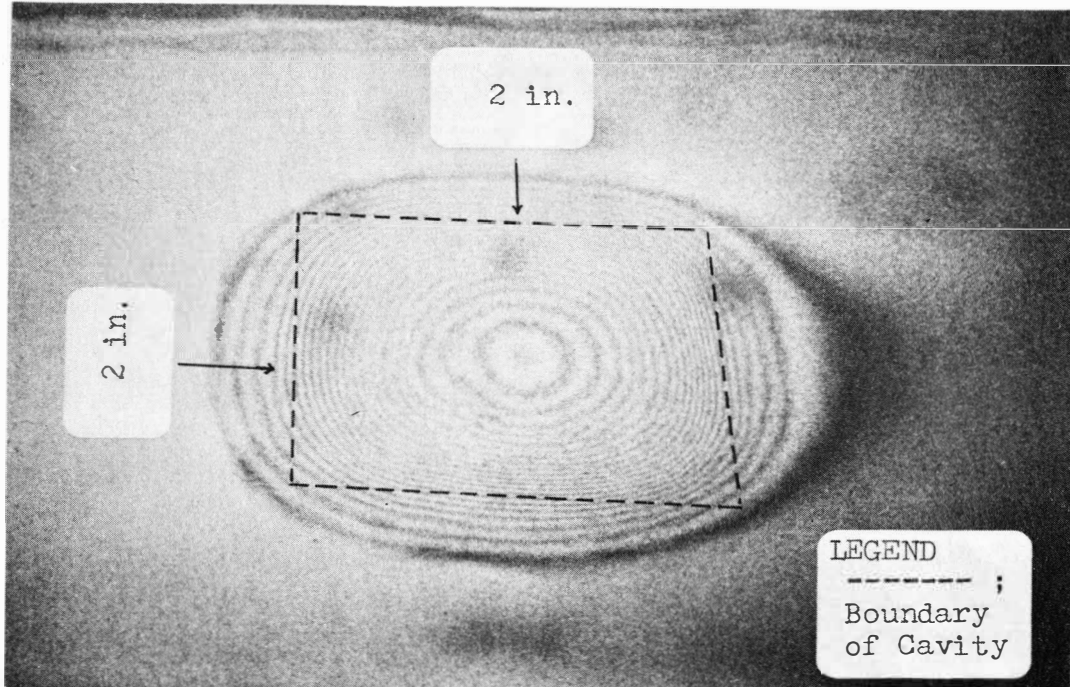
Figure VI.5.   Subsidence Contours on Sand Surface
                d=1.5 in., Cavity Size=2x2 in.x350 micro-in.
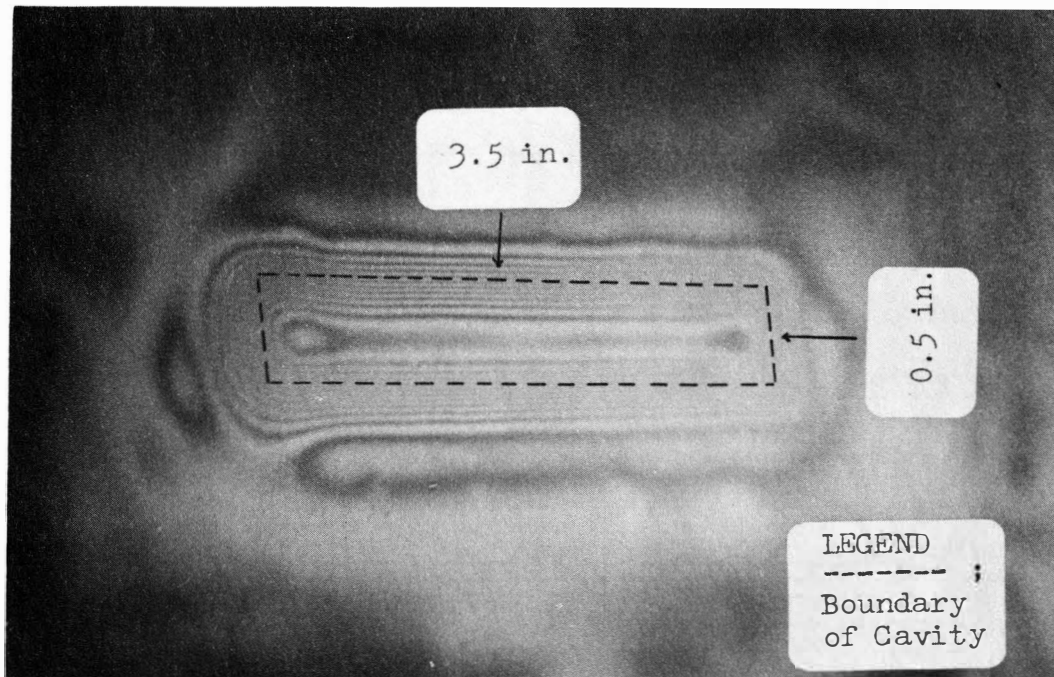
Figure VI.6.   Subsidence Contours on Gelatin d=0.25 in.,
                Cavity Size=0.5 in.x3.5 in.x200 micro-in.
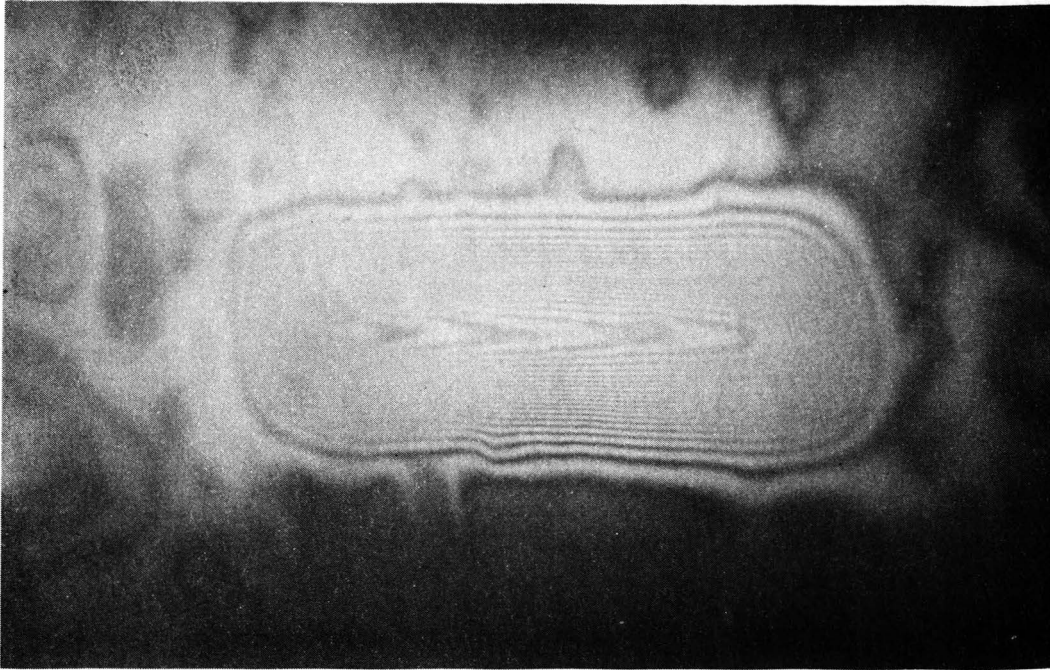
Figure VI.7.   Subsidence Contours on Gelatin d=0.5 in.,
                Cavity Size=0.5 in.x3.5 in.x400 micro-in.

Figure VI.8.   Subsidence Contours on Gelatin d=1 in.,
                Cavity Size=0.5 in.x3.5 in.x400 micro-in.
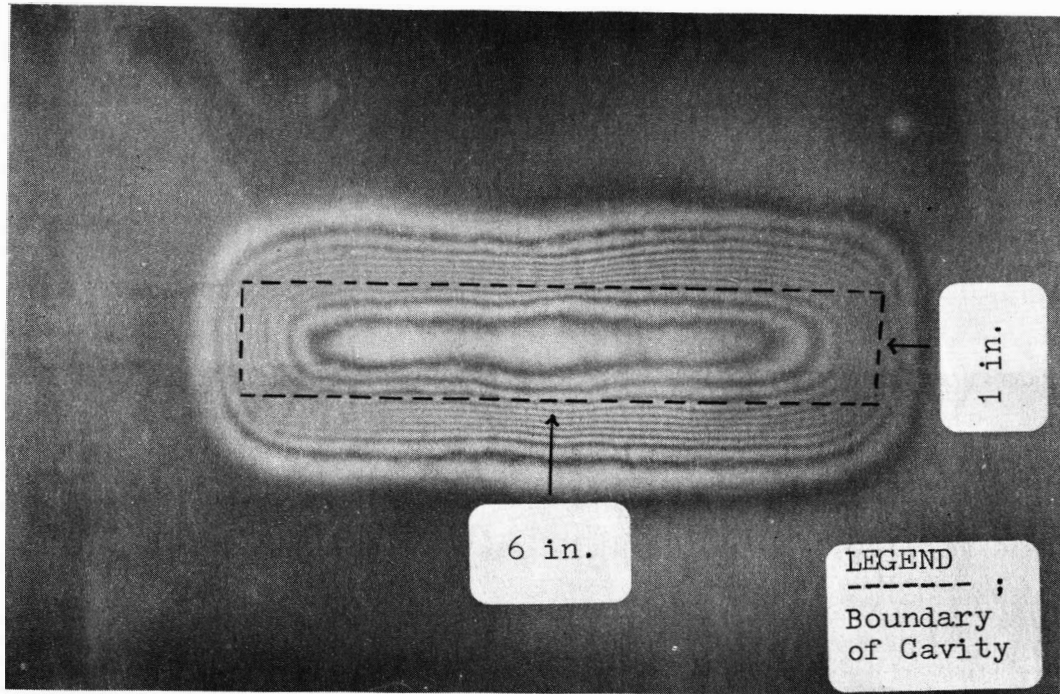
Figure VI.9.   Subsidence Contours on Sand d=0.5 in.,
                Cavity Size=1 in.x6 in.x500 micro-in.

Figure VI.10.   Subsidence Contours on Sand d=3 in.,
                Cavity Size=1 in.x6 in.x300 micro-in.
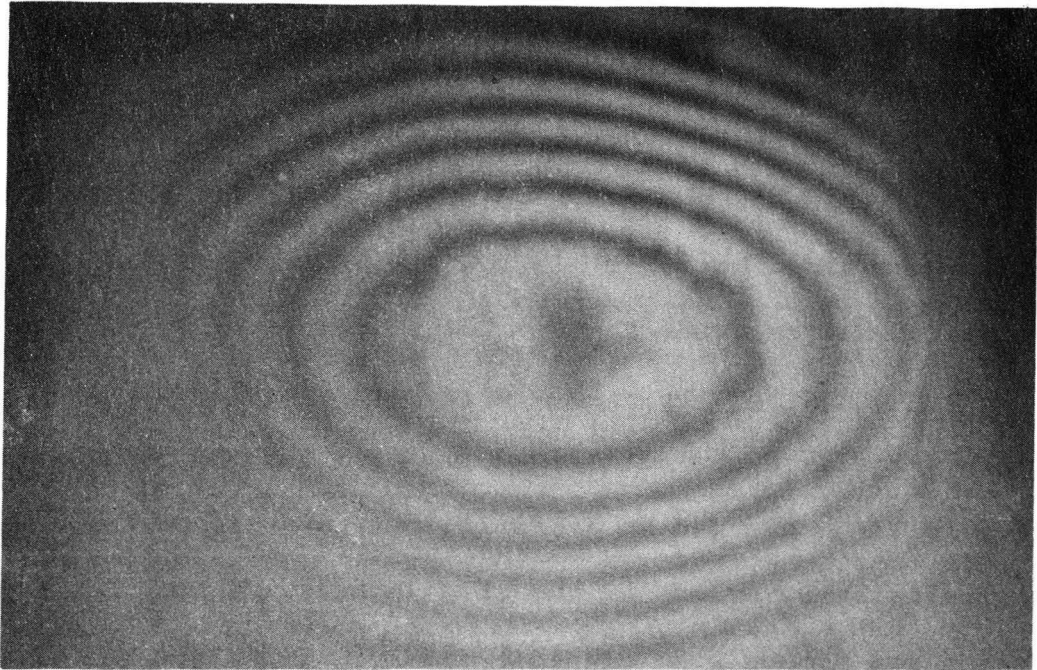
Figure VI.11. Subsidence Contours on Sand d=5 in.,
            Cavity Size=1 in.x6 in.x500 micro-in.

since beyond that depth no surface movement was detected.

For these results an important conclusion can be drawn. For sand, subsidence was not sufficiently detectable when the width/depth ratio of cavity was less than 0.2, and for gelatin where the ratio was less than 0.67. It can therefore be assumed that subsidence can be detected in rocks when width/depth ratio of cavity is larger than 0.67 and will not show any detectable subsidence when width/depth ratio is smaller than 0.2. Although the stiffness and modulus will affect the width/depth ratio which initiate detectable subsidence in elastic material. It seems to be that if rocks are more brittle and loose the number (width/depth) will be closer to 0.2, and if they are more elastic the number will be higher, closer to 0.67.

Two examples support this argument. The curve relating width/depth ratio and subsidence/seam thickness of British coalfields (90) start at a width/depth ratio of 0.3, and in the curve relating width/depth ratio and angle draw by Marr (15) the data points are shown from a width/depth ratio of 0.2.

This approach will be very useful to predict the condition of detectable mine subsidence.

Both the curves for gelatin and for sand when the cavity width is 1 inch (Figure VI.12) show that the relationship between depth and subsidence width is linear, when depth is more than 0.7 inches for gelatin and 0.85 inches for sand. The slopes are almost the same and the subsidence widths for both materials were within 4% of each other for a depth of 1.5 inches. The curves below the straight portions indicated a more rapid increase in the subsidence area and while almost
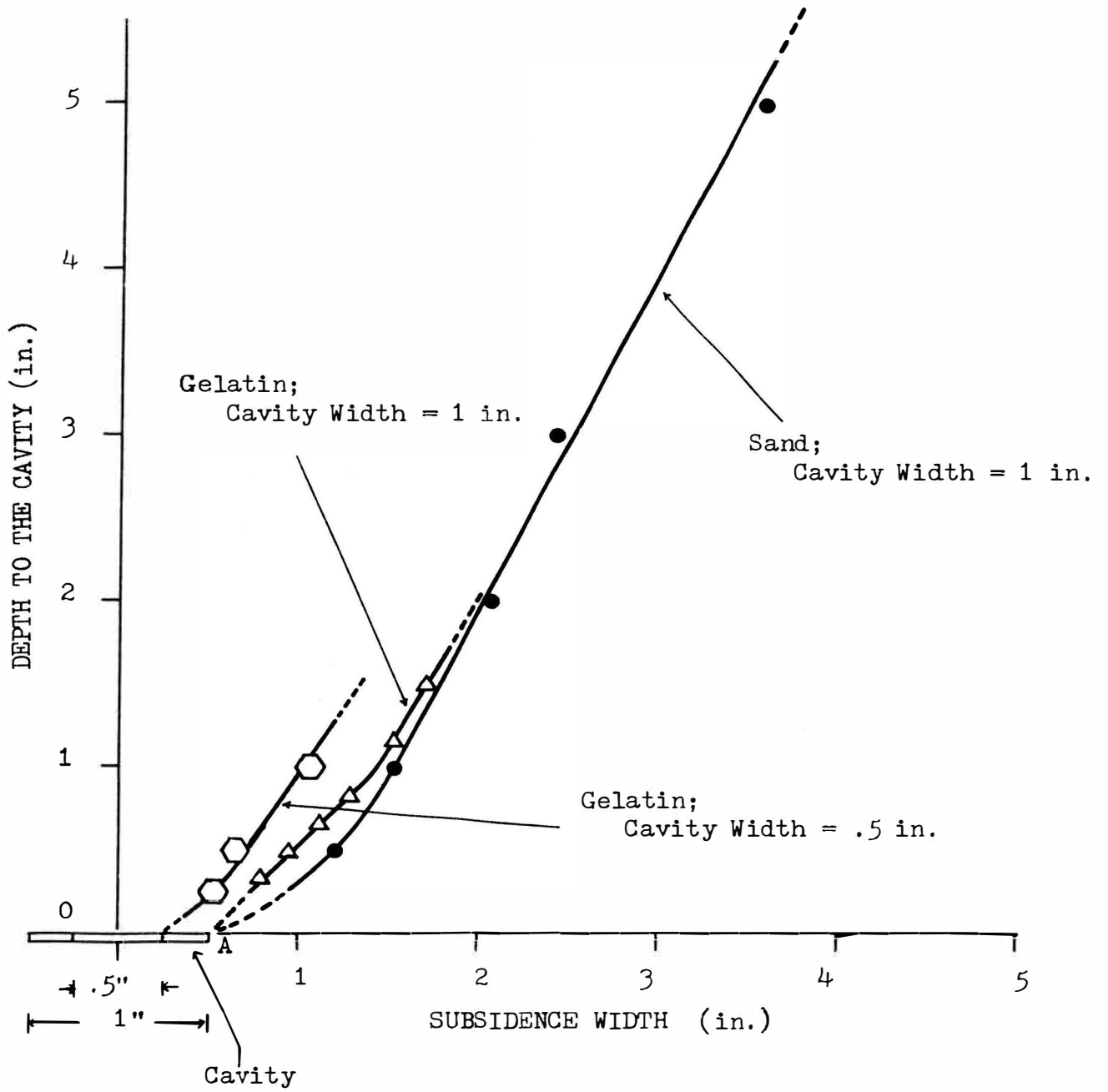
Figure VI.12.   Subsidence Width vs. Depth to the Cavity.

a straight line for gelatin an upturning curve was found for sand.

According to the National Coal Board when the width/depth ratio is 1.3 critical subsidence develops (19,81,90). As shown in Figure II.7 maximum subsidence develops when the width/depth ratio reaches 1.3. For a cavity width of 1 inch, this would indicate a critical depth of 0.77 inches for critical subsidence. As mentioned above a linear relationship was initiated between 0.7 and 0.85 inches of depth. This means that the subsidence width increases more rapidly with depth until critical subsidence is established, and subsidence width increases linearly with depth above the critical depth.

The results can be used for estimating width/depth ratio of the cavity for initiating subsidence and the subsidence area due to mine opening.

The curve obtained from the gelatin model when the cavity width was 0.5 inches showed similar behavior. The transition point was low because the critical depth was small due to the smaller cavity width.

D. Angle of Draw

A study of the values obtained for the angle of draw was conducted at the same time as the subsidence area was studied because the two factors are interrelated. In Figure VI.13 the angle of draw is defined as the angle between the vertical line from the edge of the cavity (A) and the extension from the point A to the boundary of the subsidence area. Figure VI.13 shows that the angle of draw decreases with increase in depth. For gelatin, the angle of draw is constant (51) until the depth reaches the critical width/depth condition. For sand
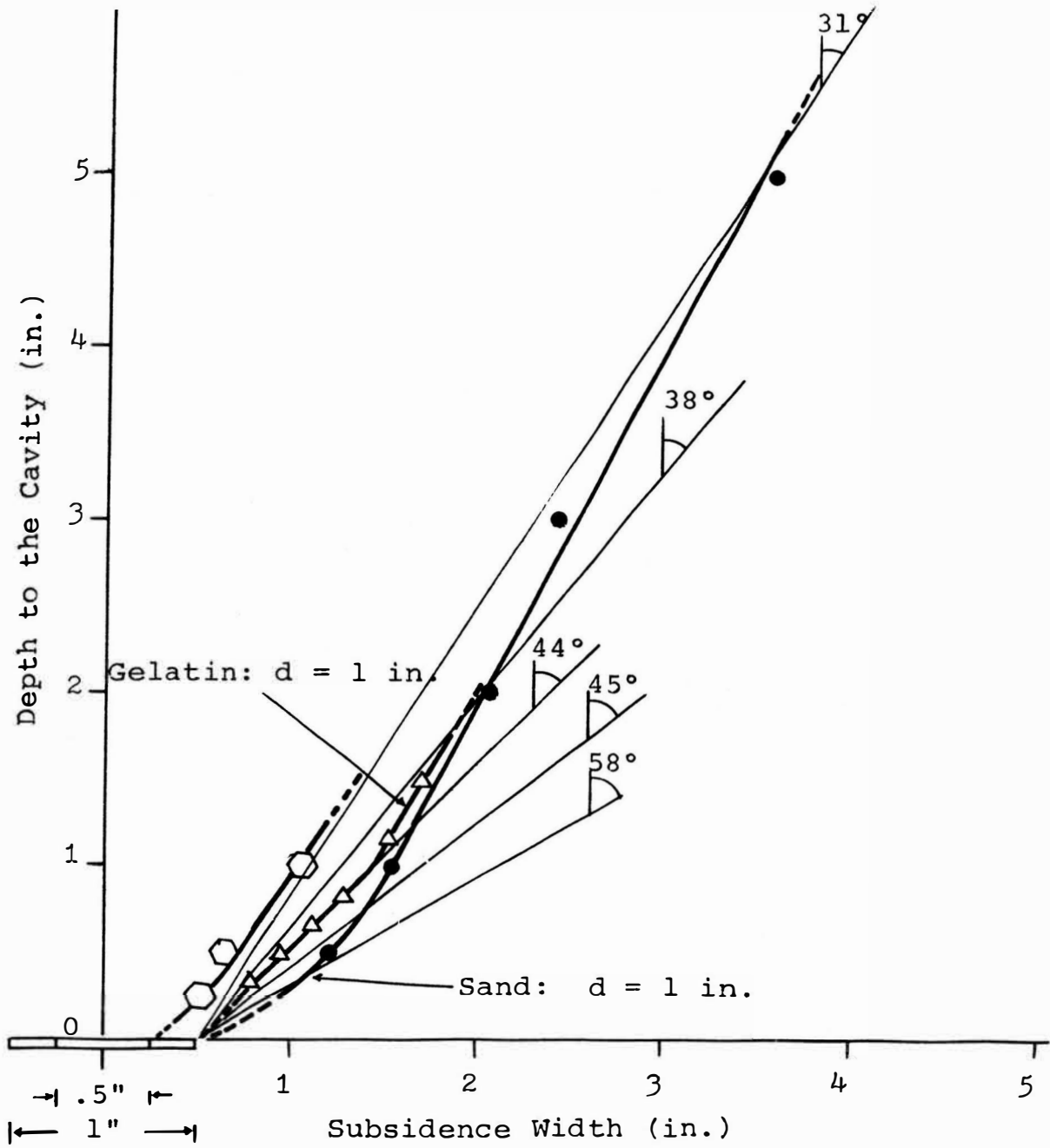
Figure VI.13.   Angle of Draw vs. Depth to the Cavity.

it decreased from around 58°, and at a depth of 2 inches the angle of draw became about 31°. For the critical subsidence point gelatin had a 44° angle of draw and sand 45°, and the average value of 44.5°, agrees with data from the United Kingdom and other coalfields.

In summary, the angle of draw varies with cavity width/depth ratio. Angle of draw decreases from 31° to 58° as the width/depth ratio decreases to 0.5. When rock is more brittle, the angle of draw will be higher all the conditions being equal.

E. Profile Study of Horizontal Cavities

Subsidence profile studies have been conducted by many engineers and scientists, and various profile equations have been propounded. But as yet, no comprehensive theory has been obtained.

In this section subsidence profile equations discussed in Chapter II are computed for a single set of conditions and plotted on the same graph. The subsidence profile data obtained from the simple cavity models were analyzed and were compared with these theoretical profiles.

1. Generalization of the Profile Functions

The calculated values of subsidence factors (K_s) for the equations are given in Table 5. The equations fall into several categories.

Several equations have the form (profile type I: Figure VI.14)

$$s = f(S_{max}, x, B, d)$$

Table 5. Calculated Values of Subsidence Factors by Different Theories.

$\dfrac{x}{B'}$, $\dfrac{x}{w'}$, $\dfrac{x}{2r}$	Eq. II.6	Eq. II.7	Eq. II.9	Eq. II.10	Eq. II.15	Eq. II.16	Eq. II.20	Eq. II.23	Knothe's (91)	Bahl's (91) ($\delta = 35°$)
1.0	1.80	0.00	0.00	0.00	4.73	4.32	0.00	0.00	0.61	0.00
0.9	2.66	0.07	0.00	0.94	-	5.87	0.23	0.05	1.20	0.80
0.8	3.93	2.45	0.24	3.61	8.295	7.85	0.78	0.48	2.25	2.34
0.7	5.73	5.45	0.30	7.70	-	10.33	2.62	1.79	3.97	4.53
0.6	8.32	9.55	0.91	12.96	14.14	13.39	5.46	4.38	6.63	7.38
0.5	11.92	14.65	2.14	19.14	-	17.08	9.68	8.47	10.51	10.96
0.4	16.80	20.61	4.25	26.01	23.07	21.45	15.27	12.87	15.80	15.39
0.3	23.15	27.30	7.45	33.35	-	26.52	22.10	21.64	22.60	20.85
0.2	31.00	34.55	11.94	40.96	35.30	32.27	29.93	30.30	30.80	27.64
0.1	40.13	42.18	17.79	48.65	-	38.66	38.46	39.90	40.11	36.44
0.0	50.00	50.00	25.00	56.25	49.75	45.59	47.33	50.00	50.00	50.00
-0.1	59.87	57.82	33.43	63.60	64.12	52.93	56.22	60.10	59.89	63.56
-0.2	69.00	65.45	42.84	70.56	76.04	60.49	64.79	69.70	69.19	72.36
-0.3	76.85	72.70	52.85	77.00	84.34	68.06	72.76	78.36	77.40	79.15
-0.4	83.20	79.39	63.03	82.81	89.02	75.37	79.93	87.13	84.20	84.61
-0.5	88.08	85.36	72.86	87.87	90.52	82.17	86.10	91.53	89.49	89.04
-0.6	91.68	90.45	81.81	92.16	89.02	88.19	91.18	95.62	93.37	92.62
-0.7	94.27	94.55	89.40	95.55	-	93.17	95.10	98.21	96.03	95.47
-0.8	96.08	97.55	95.17	98.01	-	96.91	97.86	99.52	97.75	97.66
-0.9	97.34	99.38	98.77	99.50	-	99.22	99.47	99.95	98.80	99.20
-1.0	98.20	100.00	100.00	100.00	-	100.00	100.00	100.00	99.39	100.00

where

        B is critical radius (refer to Figure VI.14)

        d is distance between the inflection point and the

            ribside.

When the expressions are considered for the condition B = W (profile type II: Figure VI.15) then

$$s = f(S_{max}, x, W, h)$$

where

        W is the half of the cavity width.

and when B or W are neglected (profile type III: Figure VI.16)

$$s = f(S_{max}, x, r)$$

Thus these three categories can be compared for one particular generalized condition and one particular system in order to contrast the profiles predicted by the different subsidence equations (Figure VI.17).

2. Construction of Subsidence Profiles Using Theoretical
    Equations and Data Obtained from Field Measurement

Figure VI.19 shows subsidence profiles calculated using equations discussed in Chapter II. Ten different profiles were constructed. Because Equation II.8 and II.9 are similar, only Equation II.9 was used since most of the experimental data from
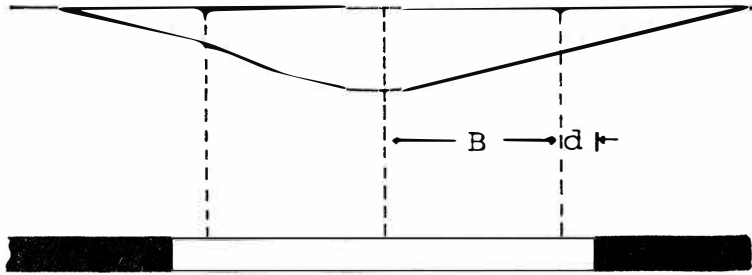
Figure VI.14.   Category I.
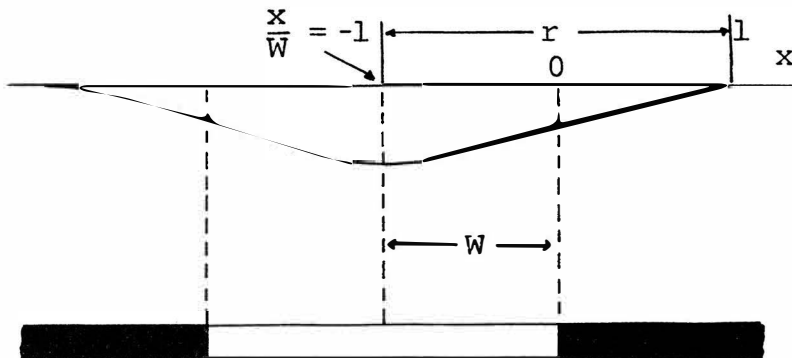
Figure VI.15.   Category II.
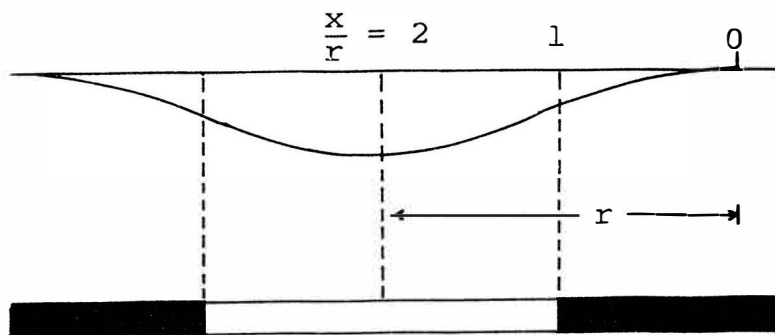
Figure VI.16.   Category III.

$$\frac{x}{r} = 2 \qquad\qquad 1 \qquad\qquad 0$$

$$\frac{x}{B} = -1 \qquad\qquad 0 \qquad\qquad 1$$

← B or W →
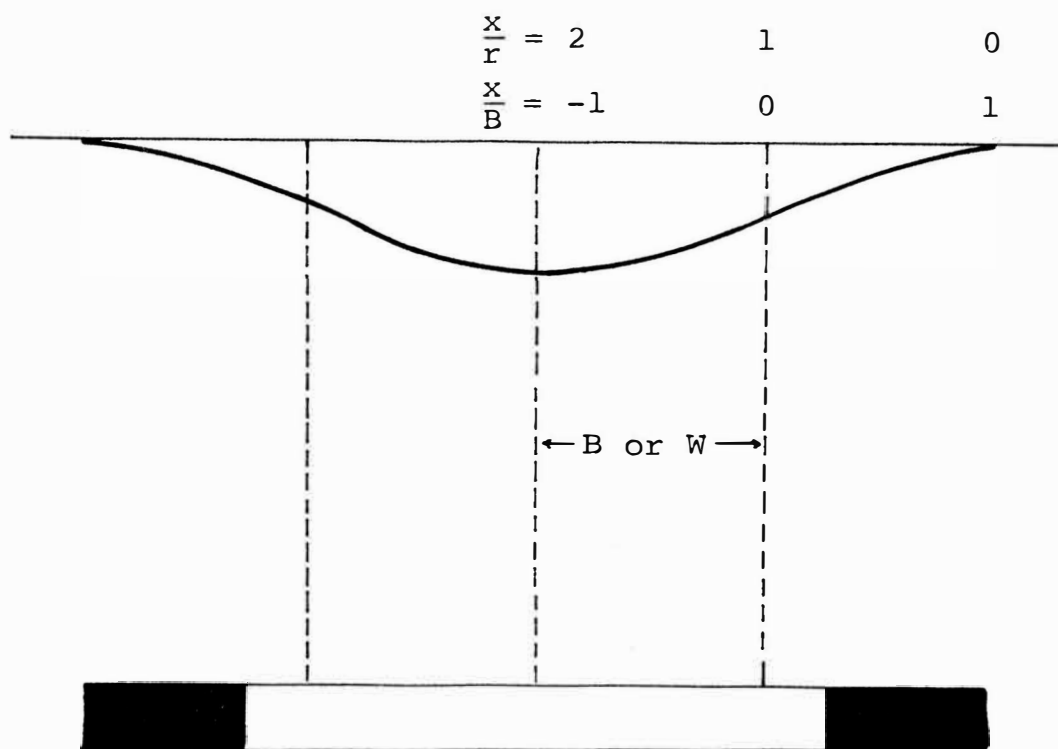
Figure VI.17.   Generalized Subsidence Category.

the research project were taken from the models which have n = 1/3. Subsidence profile data using Knothe's equation and Bal's equation were taken from Reference 91. Bal's data was computed with the angle of draw of 35°, as it was found that an angle of draw of 30-50° is common (refer to Chapter II, Section A-4).

Several profiles from field measurements obtained in the United Kingdom (88,92), U.S.A. (93) and U.S.S.R. (89) are shown.

3. Analysis of Experimental Data

Eighteen subsidence profiles were obtained using sand model and 20 subsidence profiles were obtained using gelatin models. The double exposure holographic method was used for all profile studies. The interference images were recorded from the holograms using a 35 mm camera in the same manner as with conventional photography. Each printed image was used to construct a subsidence profile.

The profiles were constructed in the same way as profiles are constructed from a contour map (Figure VI.18). The size of the plate used in the tests was 1 x 6 inches, so the cavity area made was 1 x 6 inches. Each fringe indicated a vertical displacement of 14.715 ± 0.007 micro-inches from the edge to the center of the subsidence area according to the incident angle of the laser light on the model surface. A best fit curve was constructed through the data points. The profiles obtained were expanded to the size of the generalized diagram of subsidence profiles (Figure VI.19). For this the subsidence length in the x direction was magnified

1 inch   b   6 inches

Cavity   a

a ——————————————————————————————— b

Subsidence
Profile
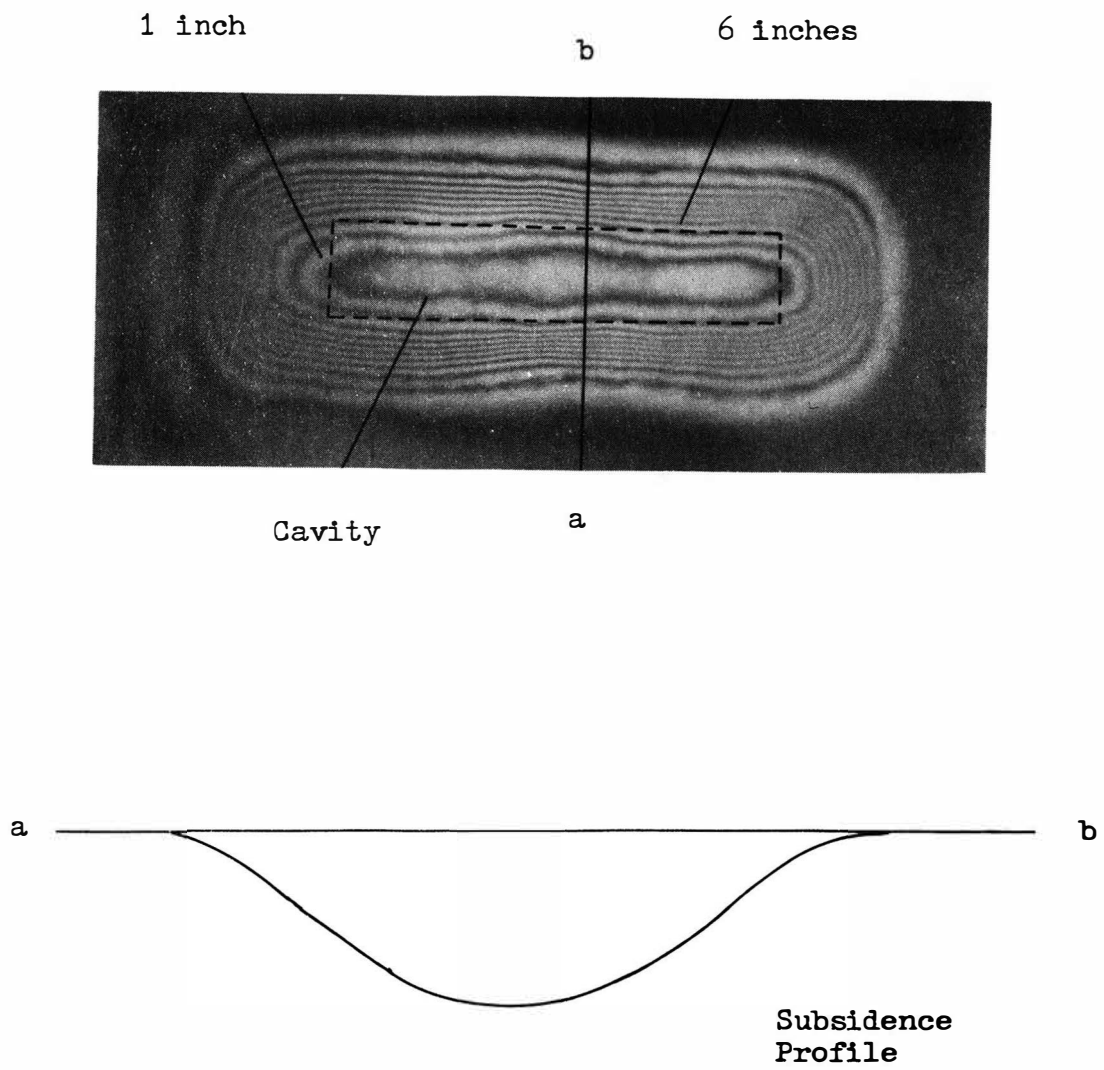
Figure VI.18. Construction of a Subsidence Profile.

Figure VI.19. Subsidence Profiles of Theoretical
and Field Measured Data.

by a factor of 2 and the subsidence was computed as percentage of total subsidence.

The average subsidence profile and the effect of change in cavity depth for the gelatin and sand models are shown in Figures VI.20 and VI.21. As shown in Figure VI.20, when cavity depths are small in sand the slopes of the profile are more gentle near the center of the depression (x = -1) than those of greater depth. For gelatin model the change of subsidence profiles was clearly related to depth, although variation was less than that obtained with sand. The effects of change in depth contrasted with that obtained where sand was used.

The closest value to the critical depth (0.77 in. for 1 in. width) is that of depth = 1/2 inches for sand and gelatin model. These are both supercritical and they define the behavior beyond critical subsidence. As was discussed in Section B of this chapter, the behavior of rock should lie in the range defined by these two bounding conditions. If overlying rocks show greater brittleness the subsidence profile curve will lie closer to that of sand, and where rock has a more elastic character it will lie closer to the profile of gelatin.

In the comparison of experimental profiles with those of theoretical and field data (compared Figures VI.19 and VI.22), average profiles with a depth of 0.5 inches for gelatin lie close to the National Coal Board field data and the profile based on Equation II.9, which was based on field data from the Donets coal field. The average profile when depth = 1/2 inches for sand lies
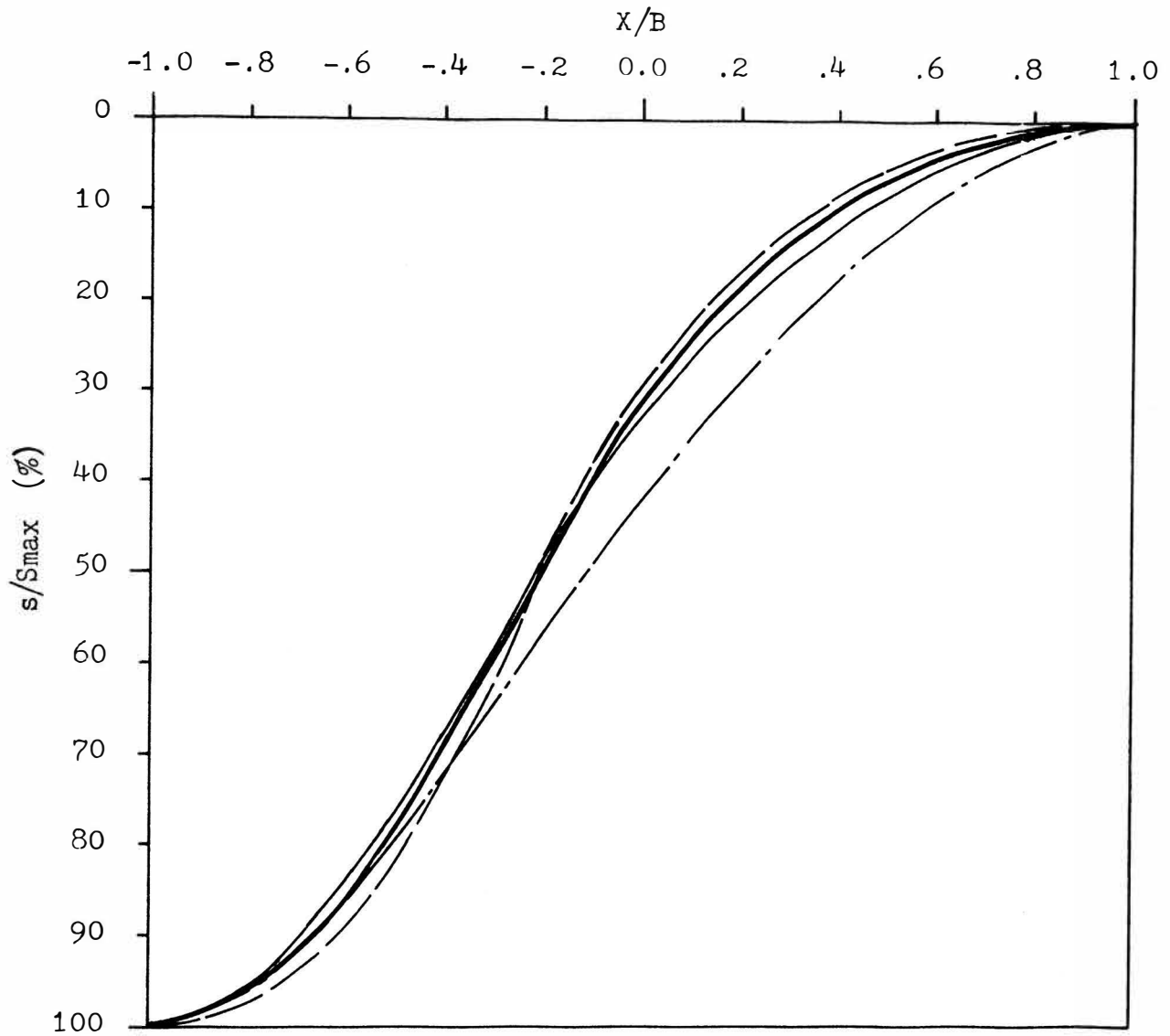
Figure VI.20. Average Subsidence Profile and Average
Profiles for Different Depth
for Gelatin Model.
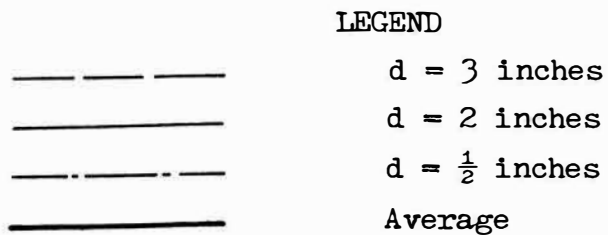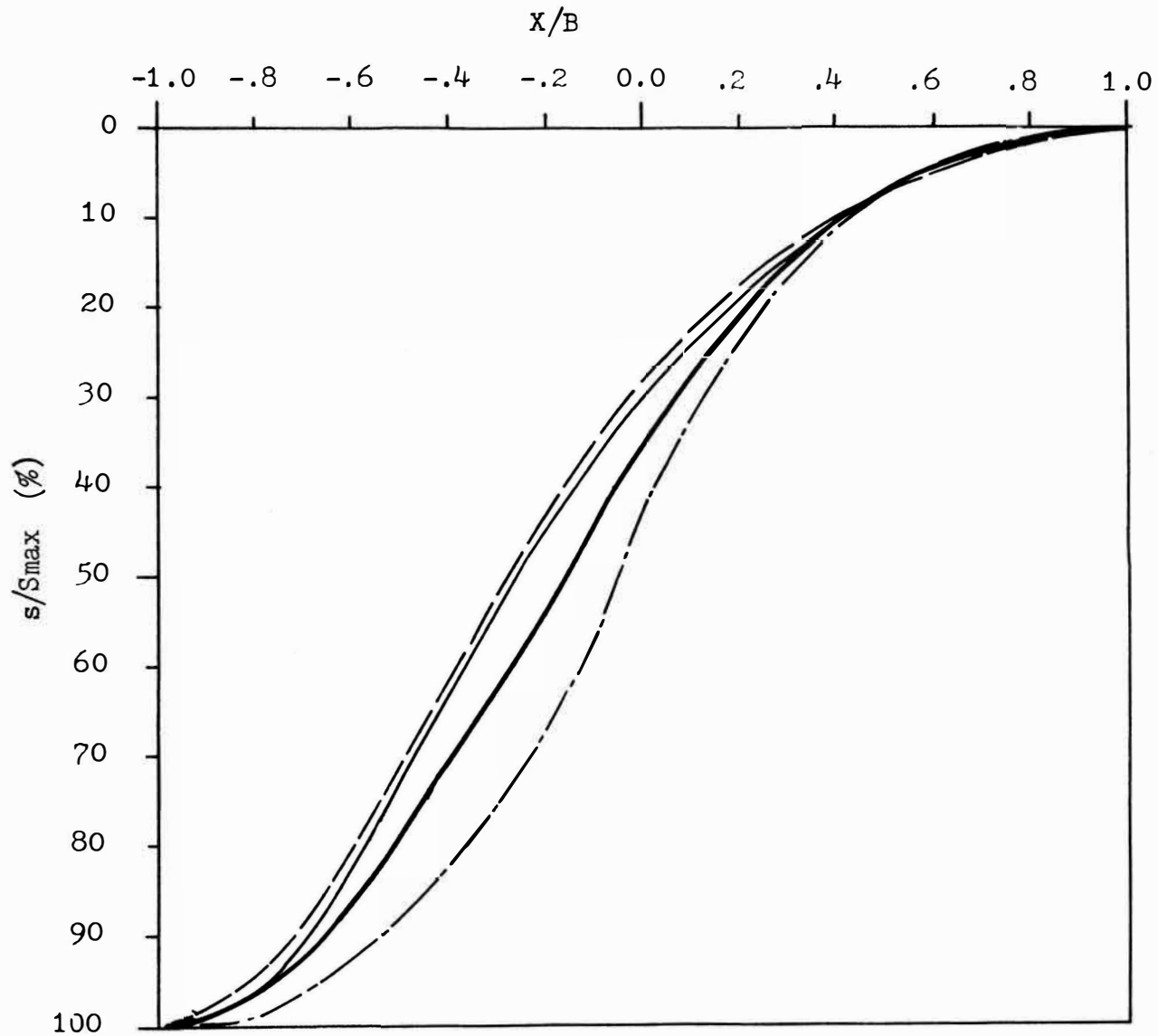
Figure VI.21.   Average Subsidence Profile and
Average Profiles for Different
Depth for Sand Model.

Figure VI.22. Average Profiles.

closer to other theoretical curves and almost agrees with the average profile curve of data from the Donets coalfield. The profile measured over Illinois coal mines lies between the average profile curves of gelatin and sand when the depth was 0.5 inches. Therefore, the experimental results agree with both field and theoretical subsidence profiles by establishing the range of behavior of rocks.

F. Subsidence Over Inclined Cavities

The removable plate used in the model to simulate the coal seam is adjustable up to an inclination of 30° from the horizontal, achieved by changing the position of the micrometer. This facility was used to obtain holograms at 10 and 20° of inclination (Figures VI.23 and VI.24 show typical subsidence contours).

Gelatin was used for the experiment. Depth to the center of the cavity was 0.5 inches in each case and the size of the cavity measured 1.05 x 2.4 inches. The corners of the rectangular cavities are indicated by black points.

The subsidence area increased on the dip side in both cases, and for 20° inclination the subsidence area was wider than that of the 10° inclination.

Subsidence profiles are plotted using the data obtained from Figures VI.23 and VI.24 (Figure VI.25). To compare the profiles, another profile taken from the 20° cavity with a 30 micro-inches cavity height was used to construct the profile of 500 micro-inches cavity height by superimposing the results on the profile made with
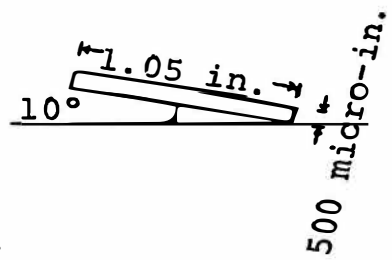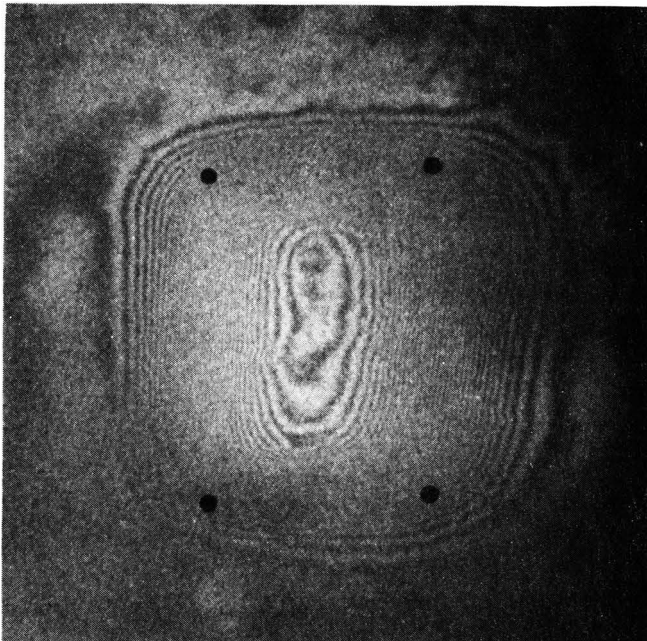
● : Corner of the Cavity

Figure VI.23. Subsidence Over an Inclined Seam (10° Slope).
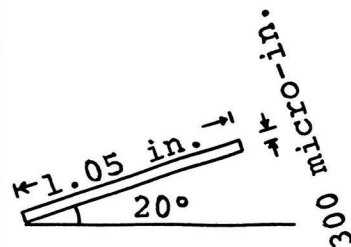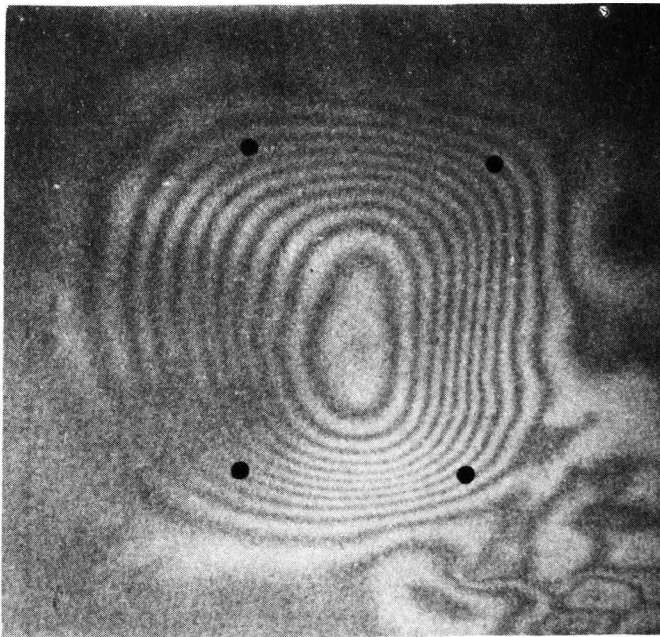
● : Corner of the Cavity

Figure VI.24. Subsidence Over an Inclined Seam (20° Slope).
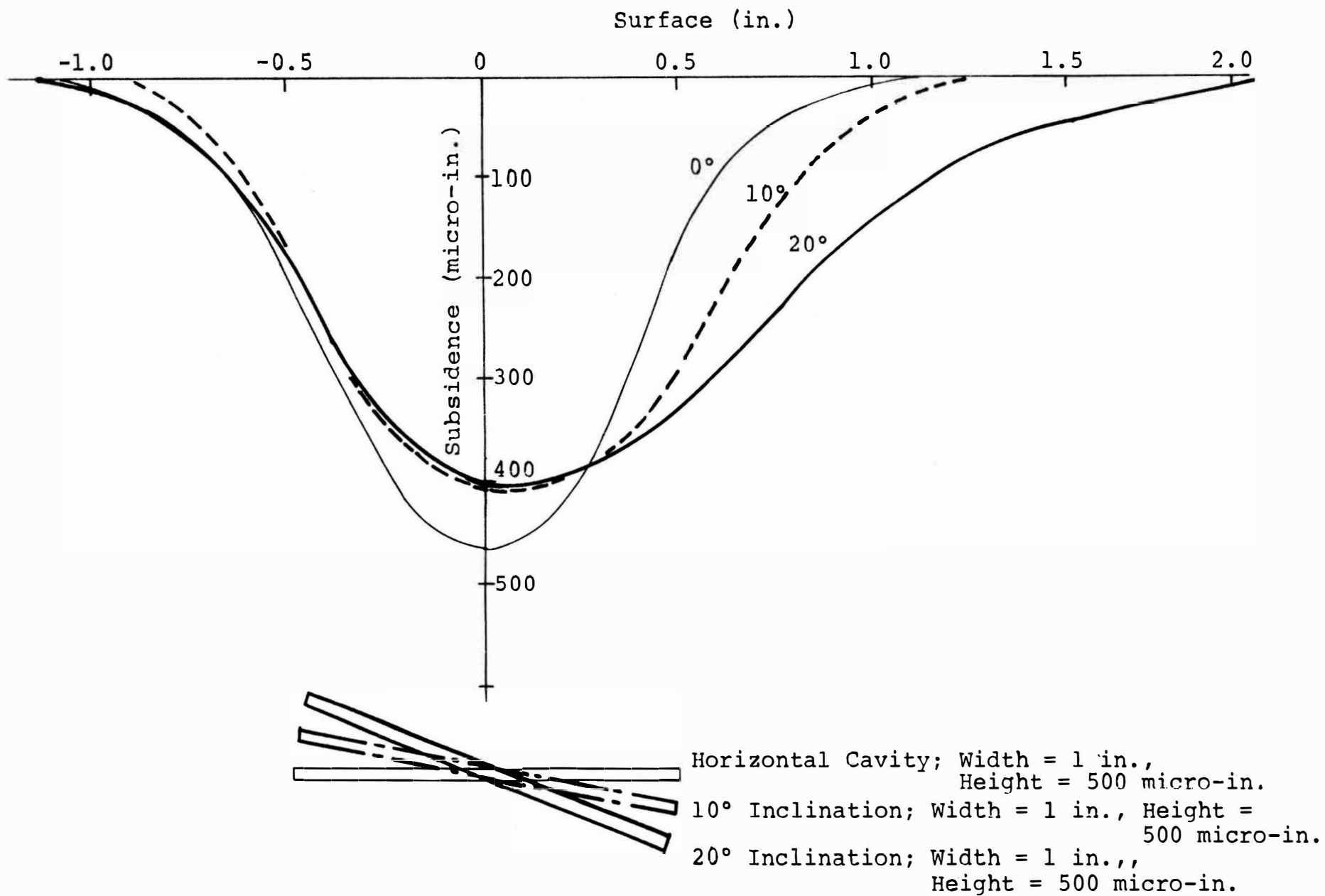
Figure VI.25.   Subsidence Profiles over Inclined Cavities.

the 200 micro-inches cavity shown in Figure VI.24. The method was based on the sequential overlapping method of subsidence (refer to Chapter II, Section A-5). In this way the cavity heights were considered as the same for each inclined cavity and could be compared with the average profile obtained from gelatin for depth of 1/2 inches. The orientation and dimension of the various cavities are shown.

The profiles on the left isde (rise direction) varied less than those of the right side (dip direction). Subsidence area increased to the dip side with inclination of the cavity. There was approximately 50% increase in the subsidence area when the inclination increased to 20° from the horizontal.

Luise's formula is not available for use in this case because it applies only when seam inclination is more than 30°. Also Statham's formula is not applicable as both angles of draw to the dip side and rise side decrease when the angle of draw of the horizontal seam is more than 24°.

The calculated angles of draw by O'Donohue's formula and those taken from the Figure II.10 were compared with the experimental data. They agreed each other to the extent that the angle of draw to the dip side is larger than that to the rise. To evaluate the experimental data and the O'Donohue's formula the medians of each set of angles of draw to the dip side and to the rise and their variations from the median were calculated (Table 6). The differences were 10° for 10° of seam inclination and 18° for 20° of seam inclination based on British field data (Figure II.12). From the O'Donohue's formula the difference is 3.3° for 10° of inclination and 6.6° for 20° of inclination, and

Table 6. Comparison of Angles of Draw of Inclined Cavities.

Inclination	Experiment		O'Donohue's Formula		British Coalfield (Figure II.12)	
	Median	Variation	Median	Variation	Median	Variation
θ_r	38.2	9.4°	39.67°	3.3°	25°	10°
10°	47.6°		43°		3.5°	
θ_d	56.0		46.33°	3.3°	45°	10°
θ_r	52.0	10 °	36.34°	6.6°	17°	18°
20°	62 °		43°		35	
θ_d	71.3	9.3°	39.67°	6.6°	53°	18°

thus the experimental results showed closer agreement with the field data than did O'Donohue's formula.

G. Subsidence - Cavity Width/Depth Ratio

Holograms were produced using 5 different depths for sand and 9 different depths for gelatin. A 1 x 6 inch cavity size was used for the both materials and both 1 x 6 inches and 0.5 x 3.5 inch cavity sizes were used for the gelatin models.

Subsidence development with increase in cavity height was studied for different width/depth ratios. The different cavity height and the subsidence values were plotted for sand and gelatin (Figures VI.26 and VI.27). As the relative width of the cavity increased so the depth of subsidence achieved also increased. And for the constant cavity width, subsidence increased with cavity height.

Using the data, the relationship between subsidence/cavity height and width/depth ratio could be established. The results were compared with the data obtained from British coal mines by the National Coal Board (19,90). Figure VI.28 shows that greater subsidence occurred for the higher width/depth ratio. Data obtained from the gelatin tests correlated well with the field data.

Maximum subsidence for the 1 inch cavity developed when the width/ depth ratio increased to 2. This does not agree with data for the other three curves. However, while error might involved, the maximum subsidence is comparable with the National Coal Board data. NCB curve agreed with the curve taken by the gelatin model except the final subsidence/cavity height, which is between the two curves from both
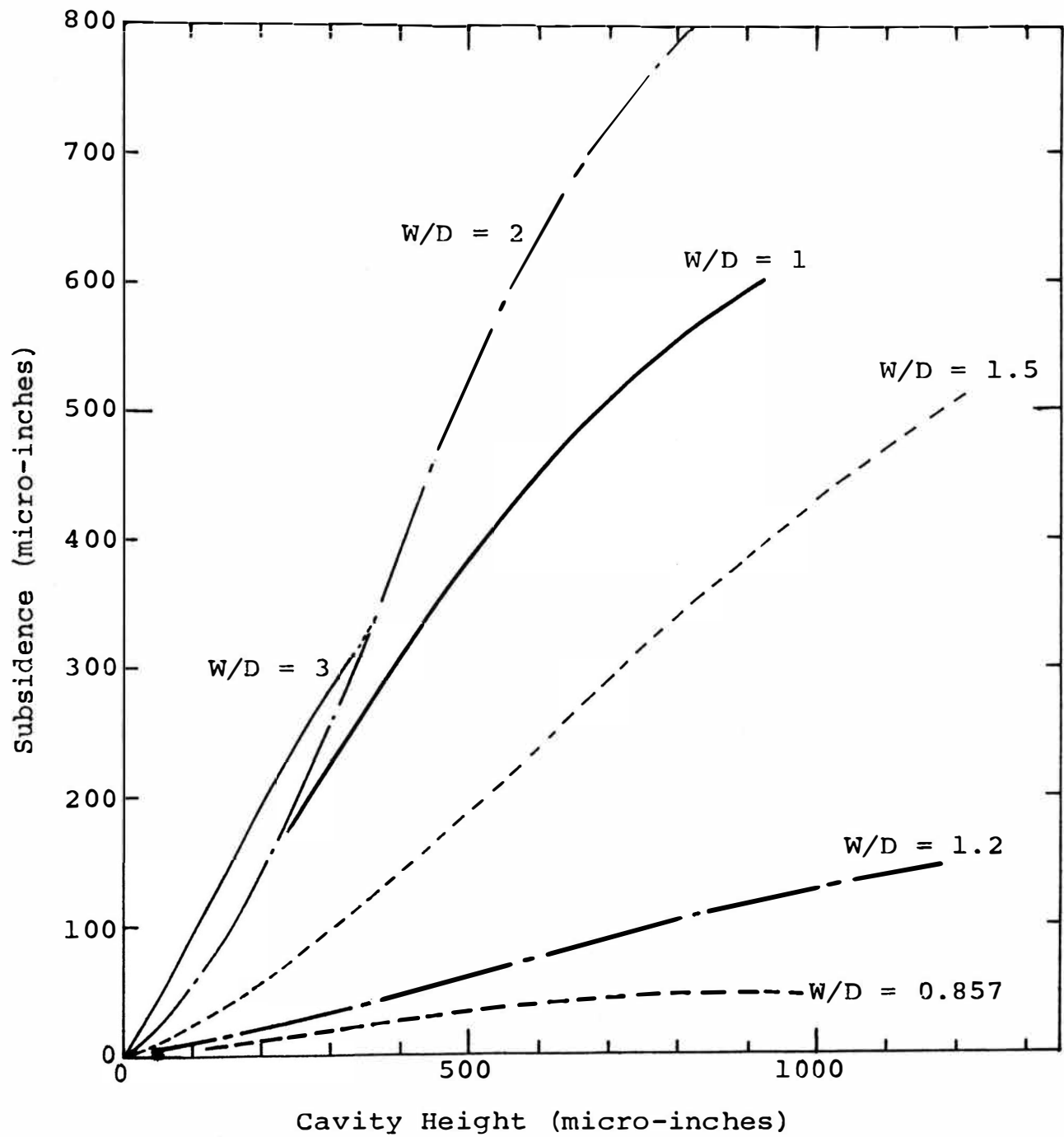
Figure VI.26.   Subsidence vs. Cavity Height for Gelatin.
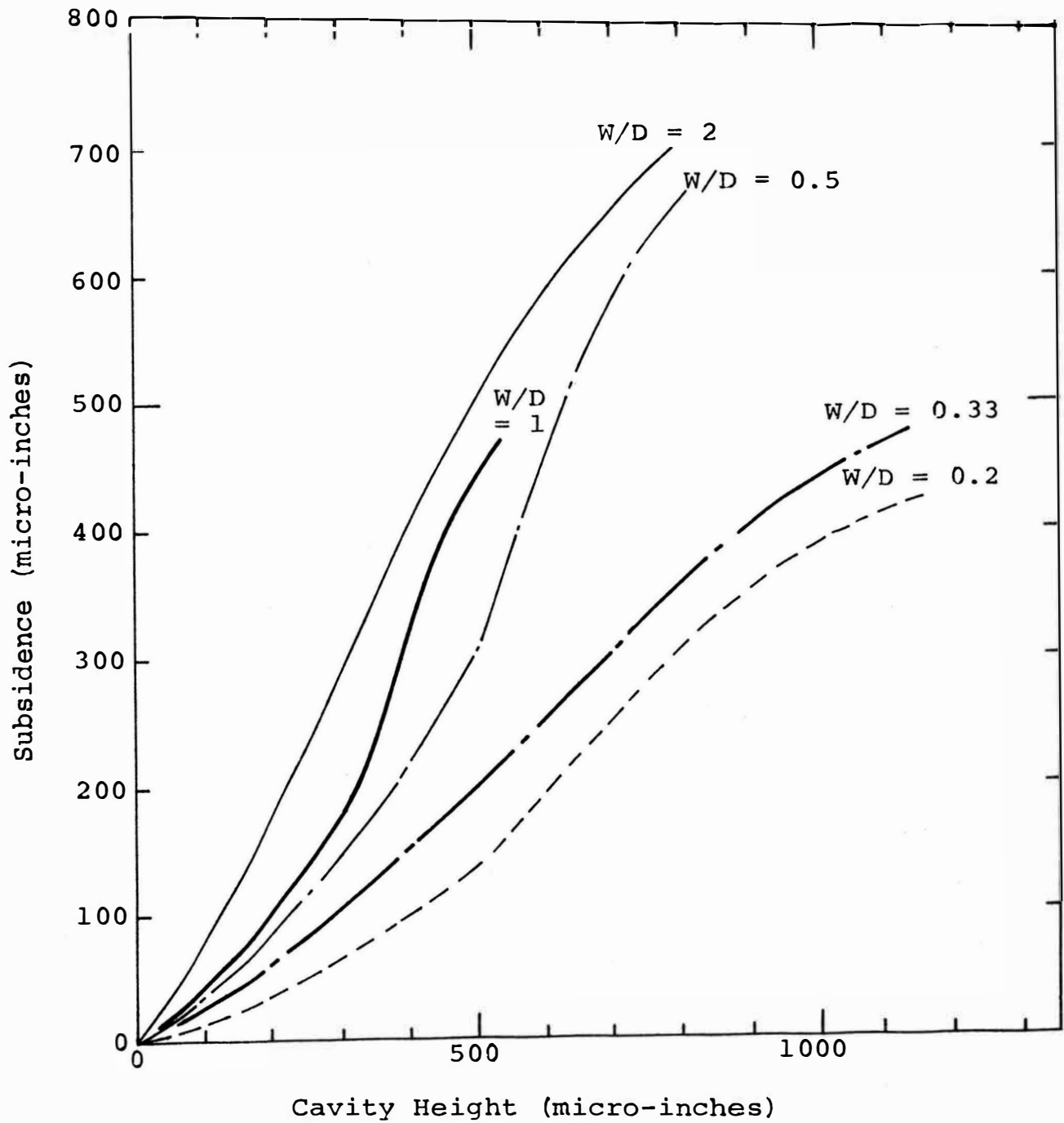
Figure VI.27. Subsidence vs. Cavity Height for Sand.
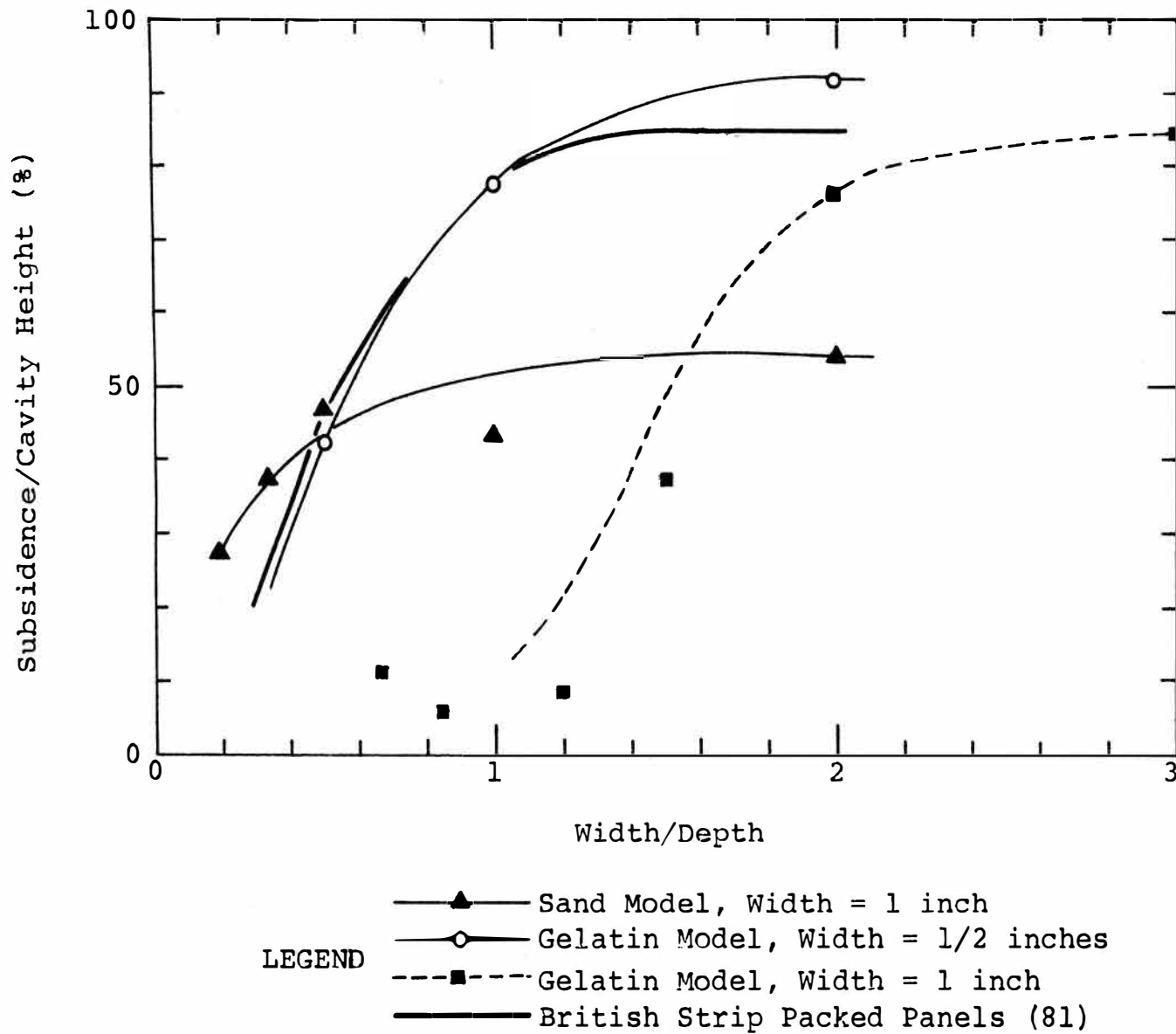
Figure VI.28. Subsidence/Cavity Height vs. Width/Depth.

sand and gelatin (d = 1/2 inches).

H.   Subsidence - Modulus of Elasticity of Gelatin

The relationship between the modulus of elasticity of the material and the subsidence factor (subsidence/cavity height or seam thickness) has been studied. The modulus of elasticity of gelatin was obtained as a function of the concentration of gelatin as described in Section B.

The maximum subsidence values for the various gelatins were normalized relative to height and the values obtained compared to the change in modulus of elasticity (Figure VI.29). A linear relationship was observed. These results may be directly applied to analysis of field data.

I.   Pilot Studies of Some Geologic Factors and Surface Structures

1.   Inclusions

Holograms were taken of model deformation with an inclusion incorporated into the simple cavity model. This experiment was conducted on the 20° inclined cavity model described in Section E. Gelatin was used as the model material.

Figure VI.30 shows a typical subsidence pattern developed with the hard inclusion, the position of which is shown by the dotted line. The inclusion measured 3/8 x 1/4 inches and 1/8 inches thick, and was located at the edge of the cavity. The depth to the center of the cavity was 0.5 inches and to the inclusion was 0.25 inches. The inclusion was constructed from a mixture of
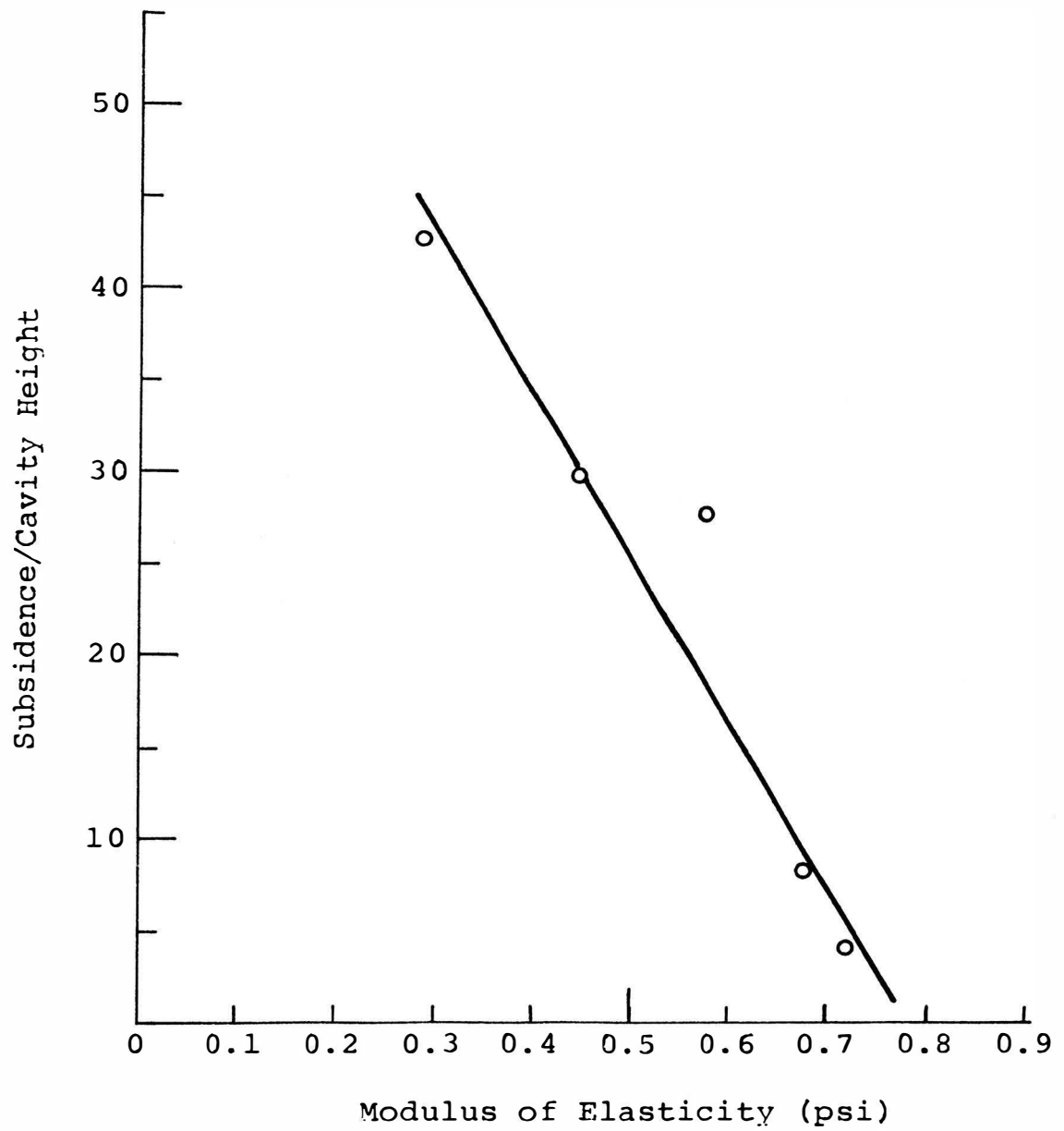
Figure VI.29.   Modulus of Elasticity vs.
              Subsidence/Cavity Height.

gelatin and fine sand. The strength was not measured, but was a hard lens relative to the surrounding medium.

Without the inclusion the subsidence pattern is illustrated in Figure VI.24. Fringes on the cavity side should parallel the edge of the cavity, but the fringes curved around the inclusion and the fringe interval near the inclusion became larger with the inclusion (Figure VI.30). Thus the subsidence profile became more gentle over the inclusion and consequently the slope to the center of the cavity became a little steeper as the total maximum subsidence remained unchanged. The area affected by subsidence was increased due to the influence of the inclusion, and the area affected was larger than that of the inclusion.

Several holograms were taken using different cavity dimensions but with the same inclusion present. No change in the area or pattern of subsidence except in that the number of fringes increased with the cavity height was found to occur.

2. Faults

An artificial fault was created in a gelatin model which contained a cavity. The size of the cavity was 0.5 x 3/5 inches, the depth to the cavity was 0.5 inches, and the height of the cavity was 200 micro-inches. The fault was created by a cut made across the cavity in the gelatin. The resulting fault line and subsidence contours are shown in Figure VI.31.

Stress concentration on the corners was observed where the edges of the cavity and the fault meet. There was an increase of
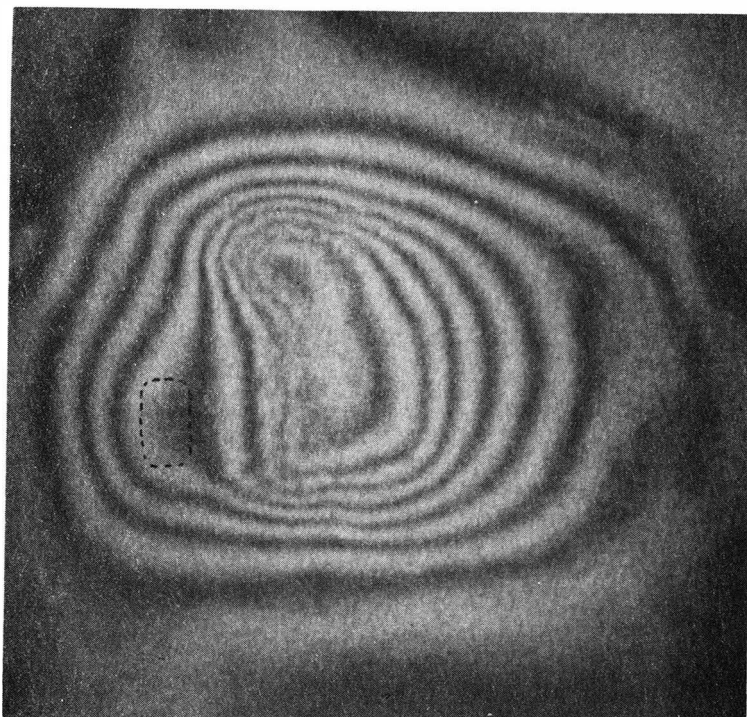
: Inclusion 3/8x1/4 inches

Figure VI.30.   Subsidence Affected by a Inclusion.

2 or 3 fringes in indicated displacement and the subsidence area increased, extending along the fault. Since the deflection between two fringes is 17.78 micro-inches, the subsidence at the center of the cavity increased from 142.2 micro-inches (71.7% of the cavity height) to 195.5 micro-inches (97.8% of the cavity height).

Several more holograms were taken for two or three fault systems and with different cavity heights, but it was decided that systematic research would be required to produce consistent results.

3. Surface Structures

Surface structures affect subsidence, but little is known of the mechanism by which this occurs. A pilot study was made to develop a technique for model investigation.

A 10 gm weight was laid on the edge of the subsidence area made by a 0.5 x 3.5 inches cavity in gelatin (Figure VI.32). The depth of the cavity was 0.5 inches and the height of the cavity was 400 micro-inches.

Comparing the left half of the subsidence contours where there was no building to the subsidence area on the right side with the building, subsidence was increased beyond the weight, curving around it. Subsidence width was increased by about 80% maximum relative to that without the weight.

However, it is clear that the modelling method works for the simulation of surface structures and their effect to subsidence.
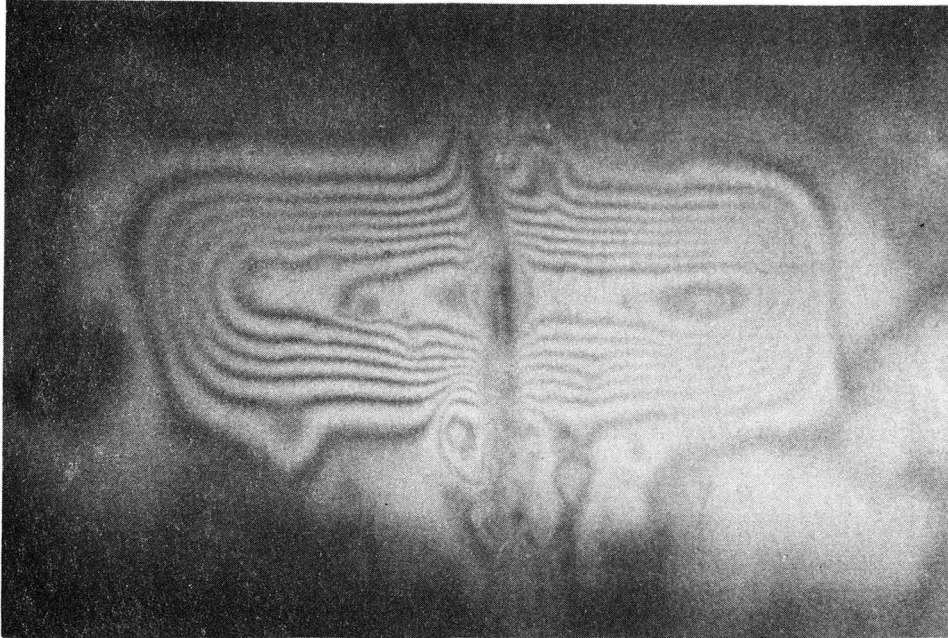
Figure VI.31.   Effect of a Fault Presence
              on Ground Subsidence.
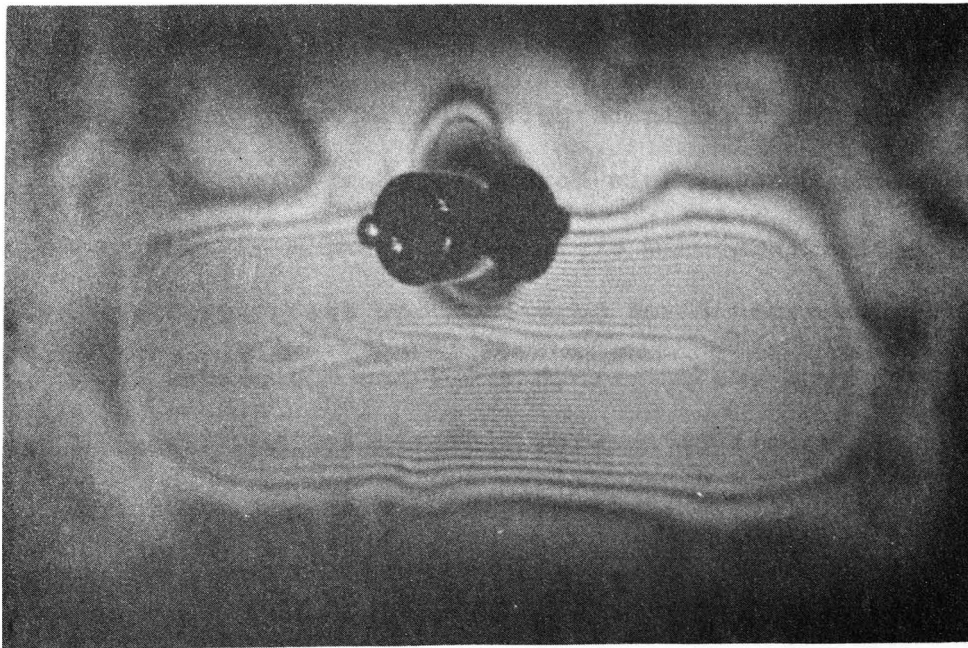
Figure VI.32.   Effect of a Surface Structure
              to Subsidence Pattern.

J. Time Dependent Study

A pilot study of time dependent subsidence phenomena was conducted using the simple cavity model. A model material was composed from fine sand, gelatin and a commercially available confectionary (*) in the following weight proportions,

sand : confectionary : gelatin : water =

1.9 :   1   :   1.6   : 7.9

The cavity measured 1.5 x 1.5 inches and the height was controlled by lowering a plate to a maximum distance of 3,000 micro-inches.

The double exposure method was used for each measurement of the subsidence development. The holographic system was sufficiently stable to that double exposure holograms could be taken at intervals of 75 minutes. The experiment was conducted overnight to avoid system vibration from any traffic in the vicinity.

For the initial stage of the hologram production, the interval between the double exposures was several minutes, and this was increased over the experiment to a final value of 75 minutes (Table 4).

Subsidence development was monitored for 5 hours and 50 minutes. The final total subsidence was 1,520 micro-inches, approximately half the cavity height. The relationship between developed time and resulting subsidence is shown in Figure VI.35. The subsidence holograms were not developed until the experiment was terminated because vibration caused by surrounding traffic made the holographic system

_____

*Marketed under the brand name "Jell-O Pudding".

too unstable to allow double exposure holograms to be made over a time interval of two hours between exposures. The curve obtained is similar to data from other model studies and field measurements (refer to Chapter II, Section A-6).

The relative proportion of the model material can be varied to control the time dependent characteristics. Real time holography can also be used, providing the system is sufficiently stable.

Table 7. Measured Data of the Time Dependent Subsidence.

Time (min.)	Accum. Time (min.)	Subsidence Accum. (micro-in.)	Subsidence (micro-in.)	Subsi./Cav. Ht. (%)
0.0	0.0	0.0	0.0	0.0
1.5	1.5	14.222	14.222	0.47
5.0	6.5	30.223	44.445	1.48
13.0	19.5	53.334	97.779	3.26
30.0	49.5	160.002	257.781	8.59
75.0	124.5	462.228	720.009	24.07
75.0	199.5	266.670	986.679	33.89
75.0	274.5	248.892	1235.571	41.19
7.50	349.5	284.438	1251.019	50.70
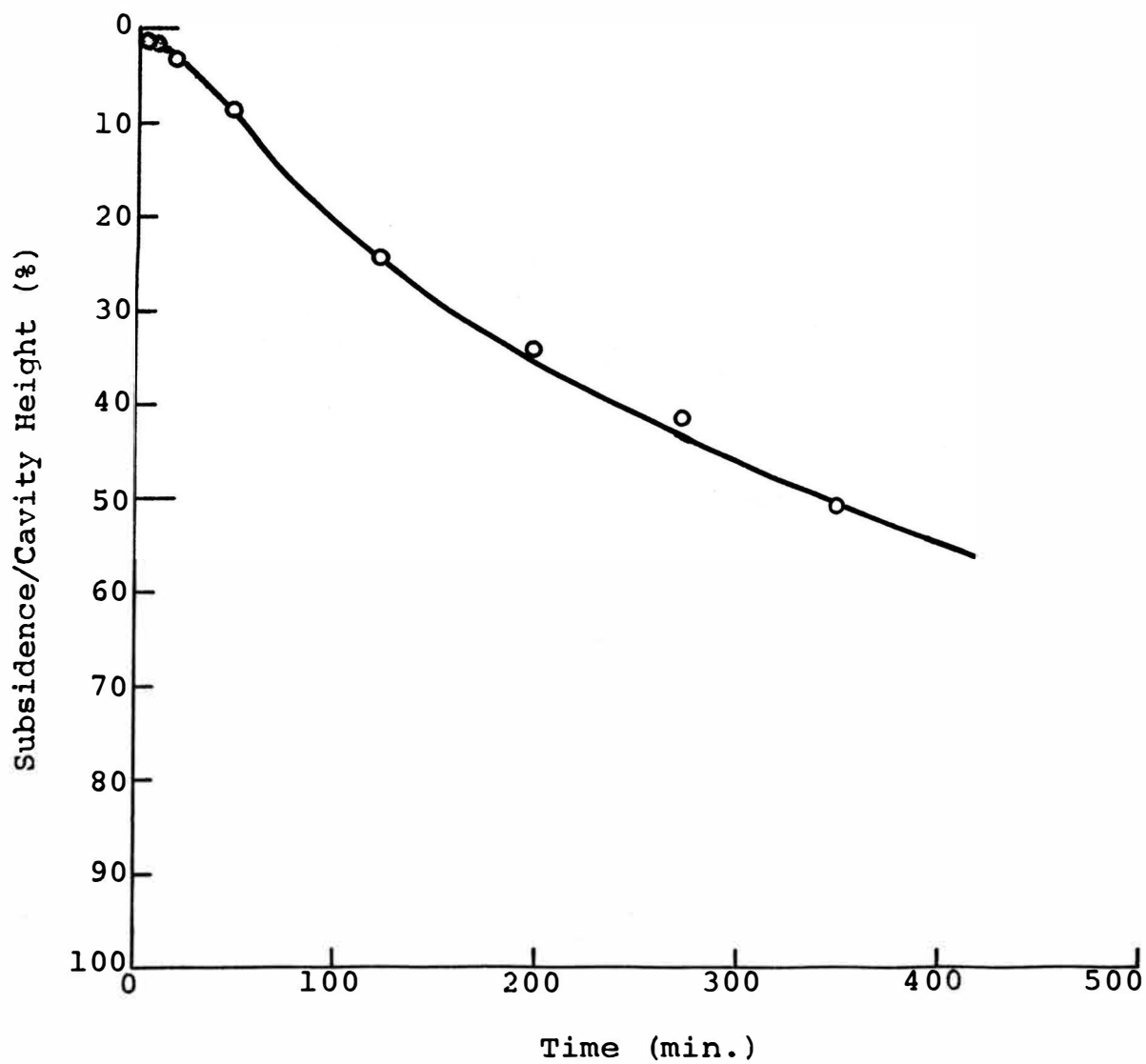
Figure VI.33. Time vs. Subsidence/Cavity Height.

VII. SEQUENTIAL LONGWALL MINE MODELS

Two different sequential longwall mine models were developed to simulate the subsidence development over expanding cavities. The first model was developed using the same box and micrometer as used for the simple cavity model (Figure VII.1).

Eight rectangular steel plates were located on the bottom plate connected to the micrometer. The size of each plate was 0.25 x 1.5 x 0.5 inches and the area of the bottom plate was 1 x 2.25 inches. The eight plates were each held with set screws on both sides of each plate. The tips of the set screws were sharpened to make the contact surface as small as possible so as not to disturb the plates. To make the cavity open sequentially, the bottom plate was moved downward the desired amount and each set of set screws was loosened in turn.

It was expected that the plates would drop by their own weight. It was found that some plates did not drop fully because of friction exerted between the plates. Lubrication oil was therefore applied between the plates and strings connected on both sides of each plate to pull it downward after the set screws were loosened. A weight (20 gm) was also connected to each. Several holograms were taken using the model, but it was found that the plates did not fully drop and the cavity developed irregularly.

The trouble seemed to be that the weight of the plate was insufficient. The plates were too thin for additional weight, and so the strings were pulled by hand. The results were not encouraging. The plates did not drop evenly and distorted the bottom plate due to the uneven load applied. One example of the ground movement pattern

is shown in Figure VII.2. The cavity measured 1.5 x 0.5 inches. The bottom plate was moved downward 500 micro-inches, but distorted.

Two separate ground movement contours were made. The pattern in the front half of the picture is the pattern of heaved ground movement and the other is the pattern of subsidence. The width of the plate was located in the center of the model floor.

The second model is the retraction model. As shown in Figure VII.3 a thin plastic (1,400 micro-inches thick) was inserted in the model material in the box. The plate was connected to a micrometer which withdrew the plate without distortion.

In the pulling out action the model was disturbed by friction forces from the plastic plate. As an example Figure VII.4 is shown. The plate has been pulled out 0.205 inches, i.e., the width of the cavity was 0.205 inches. Sand was used for the experiment and the depth to the cavity was 1.5 inches. A disturbance is shown in the right side of the subsidence area. The left half side of the subsidence pattern is similar to the other subsidence contours generated by the simple cavity models. The amount of the disturbance was about 50% of the maximum subsidence. A remedy was required to remove the friction between the plate and sand.

Two pieces of flexible plastic paper were placed, one on each side of the sliding plate. This generated subsidence patterns successfully with very little disturbance as in the example shown in Figure VII.5. In the example illustrated the cavity was 0.025 inches under a gelatin overburden. A minor disturbance is shown on the right side of the subsidence pattern, but the left half can be successfully used to compute subsidence.
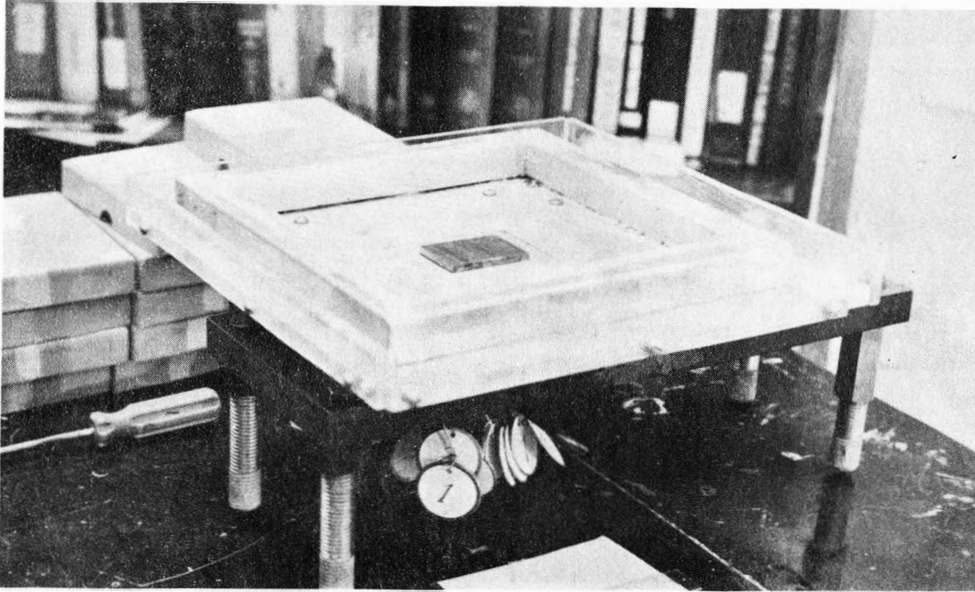
Figure VII.1. Sequential Longwall Mine Model.
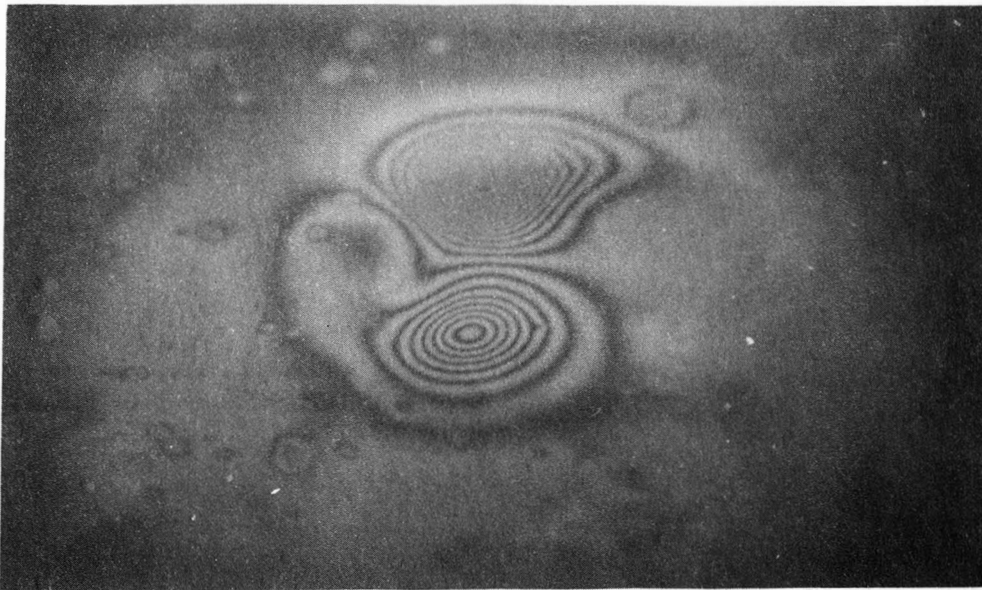
Figure VII.2. Subsidence Pattern Made by the Sequential Longwall Mine Model.
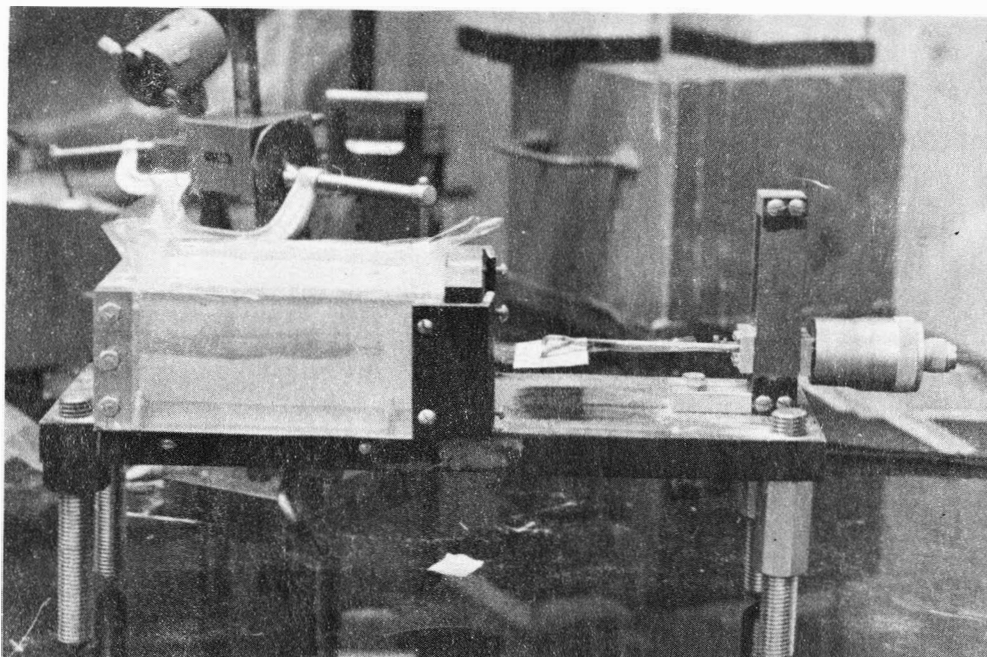
Figure VII.3.   Retraction Cavity Model.
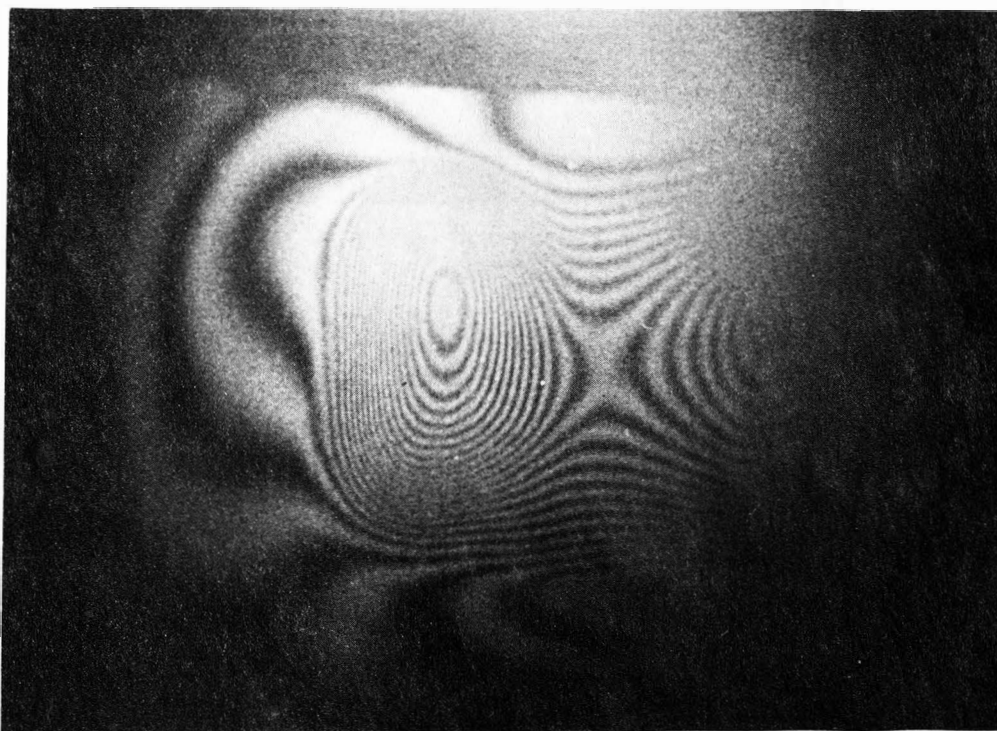
Figure VII.4.   Disturbed Subsidence Pattern Made
by the Retraction Cavity Model.
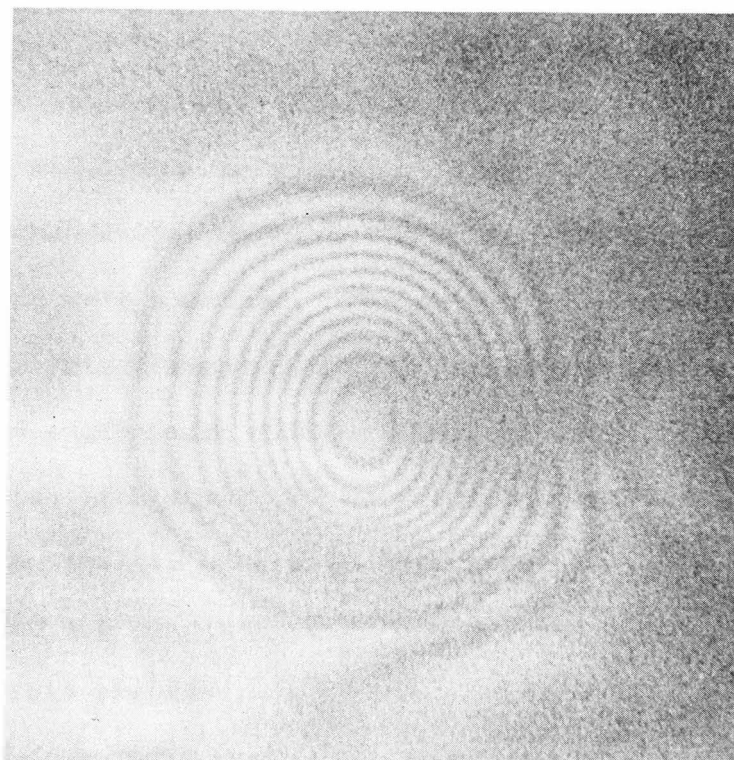
Figure VII.5.   Subsidence Pattern Obtained
                from the Retraction Model.

VIII. SUMMARY AND CONCLUSIONS

The primary objective of this research has been to examine the possibility of using the holographic interferometric technique to model ground movement with a concurrent objective of studying some of the controlling parameters of this subsidence phenomena.

Literature was reviewed in three different areas; subsidence, holography and modelling techniques. In the subsidence literature study various theories explaining the subsidence mechanism and effects of other factors were examined. The method of fringe interpreation for holographic interferometry was described and the possible applications to engineering fields discussed. The application of various modelling techniques for geomechanics and the methods of interpreting the results were also described.

The results and conclusions of the research program are summarized in this chapter.

A. The Holographic Systems and Calibration

Two different types of holographic systems were developed. One was made for the calibration model and the water pressure model, and the other for the simple cavity models and sequential longwall mine models. The holographic technique was improved to make clear holograms.

A calibration was conducted to ensure the accuracy of the holographic system to within 3% of the theoretical value.

B. Electromagnetic Models

Two types of electromagnetic models simulating from and pillar mining were developed. The results obtained did not provide sufficient data for study because of the difficulty in obtaining consistent data and this model technique was discontinued due to the length of time required to make accurate models. But the ability to simulate the gravitational force on room and pillar mine models using an electromagnet was demonstrated.

C. Water Pressure Room and Pillar Mine Models

Water loaded room and pillar mine models were constructed using plexiglass to provide sufficient load for roof deflection or subsidence of thin roof of underground mines.

Deflection profiles were plotted for 9 pillar model. The distributed deflection was proportional to the load. The edge of the pillars were compressed. The interval between pillars were equal, but deflection in the control cavity was larger than those to the sides.

Deflection patterns due to a pillar failure of 4 pillar model was plotted and compared with the pattern of the model without a pillar failure. Deflection increased 5 times above the failed pillar over that without pillar failure.

Deflection of the models with different pillar numbers was measured using the holographic double exposure method and deflection for a pillar failure monitored using real time holographic method. The relationship between the maximum deflection and stress was obtained. The maximum deflection was proportional to stress for each

model. Slopes were higher when the number of pillars was smaller. Also the relationship between the number of pillars and maximum deflection under constant loading was obtained.

The results were consistent and the holograms were clear even though the holographic system lost light intensity because of the use of collimators.

Real time holography worked successfully as a means of recording the changing fringes.

Water pressure room and pillar mine models in combination of holographic interferometry have the following advantages,

1) Ease of model construction

2) Possibility of quantitative data production

3) Accuracy of results

4) Inexpensiveness

5) Simulations can be made for the more complicated mine conditions.

D. Underground Simple Cavity Models

Self loading simple cavity models were constructed to simulate subsidence by longwall and stope mining operations. These models were used for the most important part of the program because they were used to study subsidence phenomena for various factors and they can simulate the subsidence phenomena of prototype the most accurately in the models developed.

The importance of the simple cavity models are as follows,

1) Self loading method was used to provide an equivalent load-
   ing condition to that of mines in the field.

2) By virtue of the holographic method granular material
   could be used to generate subsidence franges successfully.

3) Important factors affecting the subsidence phenomena were
   studied.

Sand and gelatin were used as model materials except for the time
dependent study. Both materials were used to define the range from
elasticity to brittleness between which the character of rock lies.
The modulus of elasticity of gelatin was obtained using a special
uniaxial testing device, and the relationship between modulus of
elasticity and the gelatin content obtained.

The mixture of sand, gelatin and a commercially available
confectionary was used as a time dependent model material. It simu-
lated the time dependent subsidence phenomena, and indicated that
this model material could be used for further time dependent study.
The proportion of the three components can be controlled to give the
required time dependent characteristics.

The conclusion drawn from results obtained from the simple cavity
models are listed as follows,

1) Rectangular or square cavities were made, but the subsidence
   patterns showed that the corners of the subsidence area
   became rounded. The deeper a cavity the more this occurred
   until finally the subsidence area became circular.

2) Subsidence area increased linearly with depth after critical subsidence width was reached. Before critical subsidence occurs the increase in the area is more rapid with depth.

3) For sand, which acts as a brittle material, subsidence was detectable when the cavity width/depth ratio was more than 0.2. For gelatin, which acts as an elastic material, it was detectable when the ratio was more than 0.67. The examples of field data agreed with the model behavior.

4) Angle of draw varied from 31° to 58° as the cavity width/ depth ratio increased. The average value was 44.5°. The more brittle the rock is the higher the angle of draw will be all other conditions being equal.

5) Rock has the character of elasticity and brittleness, so the behavior of rock should lie within the range defined by the two bounding conditions which were obtained from gelatin and sand. In the comparison of experimental profiles with those of theoretical and field data the following observations were made.

   a. Average profiles of the gelatin model which had a cavity near the critical depth lay close to the National Coal Board field data and the theoretical equation based on field measurements in the Donets coalfield.

   b. The average profile of sand with the depth nearest to the critical depth lies closer to other theoretical curves and almost agrees with the average profile curve of data from the Donets coalfield.

    c. The profile measured over Illinois coal mines lies between the average profile curves of gelatin and sand with the depth nearest to the critical depth. Therefore the experimental results agree with both field and theoretical subsidence profiles and establish a range of rocks.

6) Subsidence contours were made by inclined cavities ($10°$ and $20°$ from the horizontal line). As it was expected the subsidence area increased to the dip side of the cavity. It was found that a simple cavity model can be used for a systematic profile study for inclined cavities.

7) The relationship between subsidence factor (subsidence/cavity height) and cavity width/depth ratio was studied. Various width/depth ratios and subsidence values were obtained. Analyzed data obtained from the gelatin tests correlated well with the National Coal Board field data, and the final subsidence factor taken by the National Coal Board lay between those of gelatin and sand.

8) The subsidence factor was found to be linearly related to the modulus of elasticity of the gelatin model.

9) From pilot studies simulating some geologic factors, time factor and surface structures, the following conclusions were drawn.

    a. The subsidence profile became more gentle over an inclusion and consequently the gradient to the center of the cavity became a little steeper as the total maximum subsidence

remained unchanged. The area affected by subsidence was increased due to the influence of the inclusion.

b. An artificial fault was created in the gelatin model which contained a cavity. Stress concentration on the corners was observed where the edges of the cavity and the fault meet. At the center of the cavity about 27% increase in subsidence was due to the fault.

c. A surface structure in the subsidence area was modelled by using a weight laid in the vicinity of the subsidence area. An 80% increase of subsidence was experienced.

d. The material developed for time dependent study was used and successfully simulated time dependent subsidence development.

E. Sequential Longwall Mine Models

Two different sequential longwall mine models were developed to simulate the subsidence development over growing cavities. One was using square plates to make sequentially developing cavities by dropping them one by one, and the other a retreating model which has a square thin film withdrawn to make a continuous cavity.

The first required greater caution to eliminate distortion of the plates, but the second (retraction model) was successful and produced the unit subsidence pattern.

IX. RECOMMENDATIONS OF THE FUTURE RESEARCH

A. Time Dependent Study

The model material to simulate time dependent phenomena was only recently developed. The pilot study showed that the viscoelastic material can simulate the time dependent phenomena of subsidence. Real time holographic method can be used to detect the fringe change continuously from the beginning of subsidence development. The relationships between time and subsidence development can be systematically studied. Also the time dependent effect of different material can be investigated.

Time dependent sequential study can be made using the retreating model and real time holography.

B. Subsidence Development with Different Model Materials

Changes in particle size distribution of the sand will vary the internal friction angle of the sand, which in turn will change the failure phenomenon controlling the subsidence. Also a more systematic evaluation can be made of the effects that changes in the gelatin properties have on surface movement.

C. Vertical Stress Measurement Combined with the Holographic Technique

Pressure transducers can be installed on the bottom of the model material to measure the change in the vertical stress distribution as subsidence develops.

D. Geologic Simulations

The feasibility of simulating geologic formations and irregularities have been successfully studied in the pilot studies. More systematic studies are proposed as follows.

1. Faults

The orientations of fault directions and dips can be simulated in the gelatin model, and multi fault systems can be simulated and analyzed.

2. Layered Roof Systems

Layered room systems can be simulated. This investigation will verify the subsidence mechanisms. The physical properties of each layer can be simulated.

3. Inclusions

More systematic study can be made using inclusions of different material value and different shapes and dimensions.

E. Simulation to the Prototype

Models can be made to simulate real mine conditions, and predicted subsidence can be compared with subsidence data obtained in the field. Sufficient data are available in the literature for a mine to be simulated. Time dependent data can be obtained. A model can be made to simulate the mine structure and the overlying geologic formations.

BIBLIOGRAPHY

1. Ray, D. L. "The Nation's Energy Future - A Report to Richard M. Nixon, President of the United States," Dec. 1, 1973.

2. Scott, J. J. "Research and Development Priorities for Underground Coal Mines-Illinois Basin," report on U. S. Bureau of Mines Contract No. H0242034, April 25, 1974, 13 pages.

3. Holland, C. T. "Design of Pillars for Overburden Support," Min. Cong. J., March, 1962, pp. 24-28, 32.

4. Woodruff, S. D. Methods of Working Coal and Metal Mines, Pergamon Press, V3, 1966.

5. Whittaker, B. N. "An Appraisal of Strata Control Practice," Trans. Inst. Min. Met., V83, 1974, pp. 85-95.

6. Gray, R. E. and Meyers, J. F. "Mine Subsidence and Support Methods in Pittsburgh Area," Soil Mech. and Foundation Division, ASCE, SM4, July, 1970.

7. Parisean, W. G. and Dahl, H. D. "Mine Subsidence and Model Analysis," Society of Mining Engineers, AIME, Transactions, Vol. 241 (Dec., 1968).

8. Nelson, A. and Nelson, K. D. Dictionary of Applied Geology - Mining and Civil Engineering, London, George Newness Limited, 1969.

9. Adler, L. "Roof Control in Longwall Mining," Mining Congress Journal, 1968.

10. Denkhaus, H. G. "Critical Review of Strata Movement Theories and Their Application to Practical Problems," Journal of the South African Institute of Mining and Metallurgy, March, 1964.

11. Terzaghi, K. Theoretical Soil Mechanics, John Wiley and Sonc, Inc., New York, 1943.

12. Kim, C. S. "An Approximate Method to Calculate the Height of Final Caved Dome in Goaf," Journal of Korean Mining Association, Vol. 10 (1973).

13. Wiggill, R. B. "The Effects of Different Support Methods on Strata Behavior Around Stopping Excavations," Journal of the South African Institute of Mining and Metallurgy, Vol. 63 (1963).

14. Singh, T. N. and Singh, B. "Angle of Draw in Mine Subsidence," Journal of Mines, Metals and Fuels, July, 1968.

BIBLIOGRAPHY (cont.)

15. Marr, J. E. "A New Approach to the Estimation of Mining Subsidence," _Transactions of the Institution of Mining Engineers_, Vol. III (1959).

16. _American Institute of Mining Engng_, Subsidence Committee Report, 1926.

17. Brauner, G. _Subsidence Due to Underground Mining, Part 1_, U. S. Bureau of Mines, I.C. 8571, (1973).

18. Mabry, R. E. "An Evaluation of Mine Subsidence Potential," _New Horizon of Rock Mechanics_, ASCE, 1972.

19. Orchard, R. J. and Allen, W. S. "Longwall Partial Extraction Systems," _The Mining Engineers, AIME_, June, 1970.

20. Rellensman, O. and Wagoner, E. "The Effect on Railways of the Ground Movements Due to Mining," _Proc. European Cong. Ground Movement_, Leeds, 1957.

21. Kumar, R. and Singh, B. "Mine Subsidence Investigations over a Longwall Working and the Prediction of Subsidence Parameters for Indian Mines," _Int. J. Rock Mech. Min. Sci._, Vol. 10, 1973.

22. Whetton, J. T. and King, H. J. "The Time Factor in Mining Subsidence," _Proc. of Int. Symposium on Mining Research_, Rolla, Mo., 1961.

23. Wardell, K. and Webster, N. E. "Some Surface Observations and Their Relationship to Movement Underground," _European Cong. Ground Movement_, Leeds, 1957.

24. Deere, D. U., et al. Design of Tunnel Liners and Support Systems, U. S. Dept. of Commerce, PB 183799, 1969.

25. Popski, S. and Lama, R. D. "Subsidence in the Near Vicinity of a Longwall Face," _Int. J. Rock Mech. Min. Sci._, Vol. 10, 1973.

26. General Institute of Mining Surveying, "The Movements of the Rock Masses and of the Surface in the Main Coalfields of the Soviet Union," _Ugletekhizdt_, Moscow, 1958.

27. Knothe, S. "Observations of Surface Movements Under Influence of Mining and Their Theoretical Interpretation," _Proc. European Cong. Ground Movement_, Leeds, 1957.

28. King, H. J. and Whetton, J. T. "Mechanics of Mine Subsidence," _Proc. of Int. Symposium on Mining Research_, Rolla, Mo., 1961.

BIBLIOGRAPHY (cont.)

29. Hoffman, H. "The Effects of Direction of Working and Rate of Advance on the Scale-Deformation of a Self-Loaded Stratified Model of a Large Body of Ground," Proc. Int. Conf. Strata Control, New York, 1964.

30. Schumidt, B. "Prediction of Settlements Due to Tunneling in Soil," 1974 Rapid Excavation and Tunneling Conference, San Francisco, June 24-27, 1974.

31. Borecki, M. and Chudek, M. Mechanika Gorotworu, Wydawnictwo, Slask, Katowice, 1972 (in Polish).

32. Smith, H. M. Principles of Holography, Wiley-Interscience, 1968.

33. Leith, E. N. and Upatnieks, J. "Wave Front Reconstruction with Continuous-Tone Objects," J. Opt. Soc. Amer., Vol. 53, 1963.

34. Meyer-arendt, J. R. Introduction to Classical and Modern Optics, Prentice Hall, 1972.

35. Summers, D. A., Park, D. W. and Aughenbaugh, N. B. "The Application of Laser Holographic Interferometry to Analysis of Ground Movement Above Underground Openings," 20th International Instrumentation Symposium, Instru. Soc. America, May, 1974.

36. Collier, R. J. and Burckhardt, C. B. Optical Holography, Academic Press, 1971.

37. Wilson, A. D. and Lee, C. H. "Holographic and Analytic Study of a Semiclamped Rectangular Plate Supported by Struts," Exp. Mech., Vol. II, N5, 1971.

38. Sampson, R. C. "Holographic-Interferometry Applications in Experimental Mechanics," Exp. Mech., Vol. 10, 1970.

39. Dudderar, T. D. "Applications of Holography to Fracture Mechanics," Exp. Mech., Vol. 9, N6, 1969.

40. Burchett, O. J. and Irwin, J. L. "Using Laser Holography for Nondestructive Testing," Mechanical Engineering, March, 1971.

41. Yamaguchi, I. and Saito, H. "Application of Holographic Interferometry to the Measurement of Poisson's Ratio," Japanese J. Applied Physics, Vol. 8, N6, 1969.

42. Aprahamian, R. and Evenson, D. A. "Application of Pulsed Holographic Interferometry to the Measurement of Propagating Transverse Waves in Beams," Exp. Mech., Vol. II, N7, 1971.

BIBLIOGRAPHY (cont.)

43. O'Regan and Dudderar, T. D. "A New Holographic Interferometer for Stress Analysis," Exp. Mech., Vol. 11, N6, 1971.

44. Dhir, S. K. and Peterson, H. A. "An Application of Holography to Complete Stress Analysis of Photoelastic Models," Exp. Mech., Vol. 11, N12, 1971.

45. Holloway, D. C. and Johnson, R. H. "Advances in Holographic Photoelasticity," Exp. Mech., Vol. 11, N2, 1971.

46. Salamon, M. D. G. "Elastic Analysis of Displacements and Stress Induced by Mining of Seam or Reef Deposits," Journal of the South African Institute of Mining and Metallurgy, Vol. 64 (1964).

47. Nishida, M. and Saito, H. "A New Interferometric Method of Two-dimensional Stress Analysis," Exp. Mech., Vol. 4, N12, 1964.

48. Hovanesian, J. D., Bricic, V. and Powell, R. L. "A New Experimental Stress-Optic Method: Stress-Holo-Interferometry," Exp. Mech., Vol. 8, N8, 1968.

49. Aronson, R. "What Good is Holography," Machine Design, Jan., 1969.

50. Morgan Grampian, Inc. "Acoustical Holograms Seek Out Flaws and Voids in Materials," Product Engineering, Jan., 1972.

51. Neely, V. I. "Acoustical Holography," Society of Automotive Engineers Transactions, 1972.

52. Hildbrand, B. P. "Current and Potential Applications of Holography," Proc. Symposium, Engineering Applications of Holography, L. A., California, 1972.

53. Brenden, B. B., Neely, V. I. and Garlick, G. F. "Acoustical Prospecting from Diamond Drill Holes," The Colorado Mining Association, 73rd National Western Mining Conference, Denver, Colorado, 1970.

54. Erf, R. K., Waters, J. P., Aas, H. G. and Michael, F. "Inspection of Aerospace Materials," Proc. Symposium, Engineering Applications of Holography, L. A., California, 1972.

55. Larson, R. W., Zelenkam, J. S. and Johansen, E. L. "Microwave Hologram Radar Imagery," Proc. Symposium, Engineering Applications of Holography, L. A., California, 1972.

BIBLIOGRAPHY (cont.)

56. Mikhail, E. M. "Hologrammetric Mensuration and Mapping System," Photogrammetric Engng., Vol. 37, N5, 1971.

57. Kurtz, M. K., Balasubramanian, N., Mikhail, E. M. and Stevenson, W. H. "Study of Potential Application of Holographic Techniques to Mapping," Final Report for Research Institute, Dept. of Army, 1971.

58. Hobbs, D. W. "Scale Model Studies of Strata Movement Around Mine Roadways," Int. J. Rock Mech. Min. Sci., Vol. 6, N4, 1969.

59. Adler, L. "Roof Control in Longwall Mining," Mining Congress J., March, 1968.

60. Harris, G. W. "A Sandbox Model Used to Examine the Stress Distribution Around a Simulated Longwall Coal-Face," Int. J. Rock Mech. Min. Sci., Vol. 11, 1974.

61. Daws, G. "Discussion," The Mining Engineer, J. of the Inst. of Mining Engineers, Oct., 1974, pp. 35-36.

62. Babcock, C. O. "Plates with Rows of Holes Considered as Anisotropic Soft Inclusion Models of Three Dimensional Room and Pillar Mining Systems," U. S. Bur. of Mines, RI 7436, 1970.

63. Serata, S. "Theory and Model of Underground Opening and Support System," 6th Symposium on Rock Mechanics, University of Missouri-Rolla, 1964.

64. Barr, C. A. "Creep Measurement in Deep Potash Mines vs. Theoretical Predictions," Proc. of the 7th Canadian Rock Mechanics Symposium, 1971.

65. Stephanson, O. "Stability of Single Openings in Horizontally Bedded Rock," Engng. Geology, Vol. 5, N1, 1971.

66. Zelonka, J. R., Kline, R. J. and Mitchell, D. W. "Structural Models for the Design of Mining Systems," U. S. Bur. of Mines, RI 7442, 1970.

67. Haas, C. J. and Clark, G. B. "Experimental Investigation of Small Scale Lined and Unlined Cylindrical Cavities in Rock-Like Materials," Technical Report No. AFWL-TR-70-58, Rock Mechanics and Explosive Research Center, University of Missouri-Rolla.

68. Scott, J. J. "Three-Dimensional Photoelastic Study of Stress Fields Around Room and Pillar Mine Openings," Trans. of Soc. of Min. Geol. Engrs. of AIME, March, 1964.

BIBLIOGRAPHY (cont.)

69. Wright, F. D. and Mirza, M. B. "Stress Distribution Around
        Vertical Crack in Mine Roof Beam," Trans. of the Soc. of Min.
        Engrs. of AIME, June, 1963.

70. Agarwal, R. K. "Photoelastic Analysis of Composite Model," Trans.
        of Soc. Min. Engrs. AIME, April, 1968.

71. Wilson, K. V. and Bohidar, N. K. "Stress Distribution in Short
        Columns, Photoelastic Test," Trans. of Soc. of Min. Geol.
        Engrs. of AIME, December, 1969.

72. Theocaris, P. S. and Koufopoulos, T. "Photoelastic Analysis of
        Shrinkage Microcracking in Concrete," Mag. Conc., March, 1969.

73. Ergun, I. "Stress Distribution in Jointed Media," Proc. 2nd Conf.
        Int. Soc. Rock Mech., Belgrade, 1970.

74. Brcic, V. and Nesovic, M. "Photoelastic Investigations of
        Discontinuous Rocks," Proc. 2nd Conf. Int. Soc. Rock Mech.,
        Belgrade, 1970.

75. Voight, B. and Pariseau, W. "State of Predictive Art in Subsidence
        Engineering," J. of the Soil Mech. and Foundations Div., ASCE,
        SM2, 1970.

76. Litwiniszyn, J. "The Theories and Model Research of Movement of
        Ground Masses," Proc. European Cong. on Ground Movement, Leeds,
        1957.

77. Sweet, A. L. and Boganoff, J. L. "Stochastic Model for Predicting
        Subsidence," J. of the Engineering Mech. Div., ASCE, Vol. 91,
        EM2, 1965.

78. Bodziony, J. and Smorlarsky, A. Z. "Experimental Investigations
        of Loose Bodies from the Aspect of the Theory of the
        Stochastic Medium," Bulletin De L'Academic Polonaise,
        Des Sciences, Vol. 8, 1960.

79. Bodziony, J., Litwiniszyn, J. and Smolarksi, A. "New Research
        into Rock Masses Treated as Media Characterized by Stochastic
        Equations," Third Int. Conf. on Strata Control, Paris, 1960.

80. Berry, D. S. "An Elastic Treatment of Ground Movement Due to
        Mining," J. of Mech. and Physics of Solids, Part 1, Vol. 8
        N4, 1969.

81. Zenc, M. "Comparison of Bal's and Knothe's Methods of Calculating
        Surface Movements Due to Underground Mining," Int. J. Rock
        Mech. Min. Sci., Vol. 6, 1969.

BIBLIOGRAPHY (cont.)

82. Berry, D. S. "A Theoretical Elastic Model of the Complete Region
        Affected by Mining a Thin Seam," Proc. Sixth Symposium on
        Rock Mech., University of Missouri-Rolla, 1964.

83. Berry, D. S. and Sales, T. "Elastic Treatment of Ground Movement
        Due to Mining," J. of Mech. and Physics of Solids, Part 2,
        Vol. 9, N1, 1961, Part 3, Vol. 10, 1962, Corrigendum, Vol. 11,
        N5, 1963.

84. Hacket, P. "An Elastic Analysis of Rock Movement Caused by
        Mining," Trans. Institution of Mining Engng., Vol. 118,
        Part 7.

85. Hackett, P. "Prediction of Rock Movement by Elastic Theory
        Compared with In-Situ Measurement," Rock Mech. and Engineering
        Geol., Supplementum 1, 1964.

86. Woodward, Clyde and Assoc. "Feasibility Investigation, Mining
        Subsidence Potential," Proposal to Nanticoke Power Plant,
        1969.

87. Inman, H. I. "A Viscoelastic Analysis of Mine Subsidence in
        Horizontal Laminated Strata," Thesis, University of
        Minnesota, 1965.

88. Dahl, H. D. "Two and Three Dimensional Elastic-Elastoplastic
        Analysis of Mine Subsidence," Fifth International Strata
        Control Conference, London, 1972.

89. General Institute of Mining Surveying. "The Moments of the Rock
        Masses and of the Surface in the Main Coalfields of the
        Soviet Union," Ugletekhizdt, Moscow (explained in 12), 1959.

90. National Coal Board, "Principles of Subsidence Engineering,"
        Production Dept. Information Bulletin 63/240, 1963.

91. Zenc, M. "Comparison of Bal's and Knothe's Methods of Calculating
        Surface Movements Due to Underground Mining," Int. J. Rock
        Mech. Min. Sci., Vol. 6, 1969.

92. Simes, D. J. and Jagger, F. E. "Strata Control in Mining
        Operations in a New Mine at South Bulli Colliery," Fifth
        International Strata Control Conference, London, 1972.

93. Herbert, C. A. and Rutledge, J. J. "Subsidence Due to Coal
        Mining in Illinois," U.S. Bur. of Mines, Bulletin 238, 1927.

94. Jaeger, J. C. and Cook, N. G. W., Fundamental of Rock Mechanics,
        Methuen & Co. Ltd., 1969.

VITA

Duk-Won Park was born on March 8, 1945, in Kyoung-Book, Korea. He received his primary and secondary education in Taegu, Koreau. He received a Bachelor of Science degree in Mining Engineering from Inha Institute of Technology (presently known as Inha University) in Incheon, Korea.

Additional educational training was obtained by Mr. Park at the Korean Army Engineering School while on active duty, as a Lieutenant, with the Korean Army.

He has been enrolled in the Graduate School of the University of Missouri-Rolla since January, 1970. He received a Master of Science degree in Geological Engineering in December, 1971, and advanced to candidacy for the Ph.D. degree thereafter.

Since May, 1971, he has been a Research Assistant working for the research project, "Investigation of Failure of Roofs in Coal Mines," and the thesis project.

He was married to the former Sun-Ja Kim on December 6, 1974.